



Universität für Bodenkultur Wien
University of Natural Resources
and Life Sciences, Vienna

Doctoral Dissertation

Bulk crystallization of recombinant proteins

submitted by

DI (FH) Hauke HÜTTMANN, MSc

in partial fulfilment of the requirements for the academic degree

Doktor der Bodenkultur (Dr.nat.techn.)

Vienna, November 2021

Supervisor:

Univ.Prof. Dipl.-Ing. Dr.nat.techn. Alois Jungbauer
Institute of Bioprocess Science and Engineering
Department of Biotechnology (DBT)

Affidavit

I hereby declare that I have authored this dissertation independently, and that I have not used any assistance other than that which is permitted. The work contained herein is my own except where explicitly stated otherwise. All ideas taken in wording or in basic content from unpublished sources or from published literature are duly identified and cited, and the precise references included. Any contribution from colleagues is explicitly stated in the authorship statement of the published papers.

I further declare that this dissertation has not been submitted, in whole or in part, in the same or a similar form, to any other educational institution as part of the requirements for an academic degree.

I hereby confirm that I am familiar with the standards of Scientific Integrity and with the guidelines of Good Scientific Practice, and that this work fully complies with these standards and guidelines.

Vienna, 05th November 2021

Hauke Hüttmann (*manu propria*)

Acknowledgements

Als erstes möchte ich mich bei meinem Betreuer Prof. Alois Jungbauer bedanken. Er stand mir zu jeder Zeit mit wissenschaftlichen Rat zur Seite und hat meinen Fokus geschärft eine Herausforderung immer aus verschiedenen Blickwinkeln zu betrachten, um eine Lösung herbeiführen zu können. Seine herausragende und breit gefächerte wissenschaftliche Kompetenz, sowie seine herzliche Art hat mich immer wieder motiviert und diese Arbeit erst ermöglicht.

Desweiteren möchte der Firma Boehringer Ingelheim RCV GmbH & Co KG ganz herzlich danken, dass sie es mir ermöglicht haben diese Arbeit in ihrem biopharmazeutischen Unternehmen durchführen zu können. Ganz herzlichen Dank gebührt dafür meinen Betreuern Wolfgang Buchinger und Matthias Berkemeyer, die immer Zeit für mich hatten und mir stets mit wertvollen Tipps zur Seite standen. Auch bei allen anderen Kollegen aus der Process Science möchte ich mich für ihre Unterstützung und das tolle und freundschaftliche Arbeitsumfeld bedanken.

Ich möchte mich auch bei meinen ehemaligen beiden Masteranden Yvonne Augustin und Stefan Haidinger für die wertvollen fachlichen und produktiven Diskussionen bedanken. Es hat wirklich Spaß gemacht eure Arbeiten zu betreuen.

Herzlichst bedanken möchte ich mich bei Hans Huber und meinen Kollegen von der Biomay AG, die mir den Rücken frei gehalten haben um diese Arbeit endlich vollenden zu können.

Meine Familie und Freunde haben mich überall die Jahre unterstützt und mit ihren unerschütterlichen Glauben an den Erfolg der Arbeit mich immer bestärkt, vielen lieben Dank dafür.

Ganz besonders bedanken möchte ich mich bei dir, Claudia, ohne deine Liebe und deinen Rückhalt wäre diese Arbeit niemals fertig geworden.

Table of content

| | |
|---|-----|
| Affidavit | I |
| Acknowledgements | II |
| Table of content..... | III |
| 1 Abstract..... | 1 |
| 2 Kurzfassung | 2 |
| 3 Introduction..... | 3 |
| 3.1 Advantages of protein crystallization in the biopharmaceutical industry | 3 |
| 3.2 Protein crystallization mechanisms | 4 |
| 3.2.1 Nucleation | 5 |
| 3.2.2 Crystal growth | 7 |
| 4 Objectives | 9 |
| 5 Results – Development of a preparative crystallization process as purification or formulation step for recombinant proteins..... | 10 |
| 5.1 Initial Screening to determine crystallization conditions | 11 |
| 5.1.1 Precipitants | 11 |
| 5.1.2 Appropriate screening techniques and methods..... | 12 |
| 5.2 Adjustment Screen..... | 14 |
| 5.3 Phase diagrams | 17 |
| 5.4 Process design..... | 19 |
| 5.4.1 Crystallization of process intermediates maintaining the nucleation zone | 19 |
| 5.4.2 Crystallization of process intermediates with loss of the nucleation zone..... | 22 |
| 5.4.3 Overcome co-precipitation of impurities in crystallization processes | 25 |
| 5.4.4 Optimization of pH and temperature..... | 27 |
| 5.4.5 Control of the degree of supersaturation in the process by fed batch processes | 28 |
| 5.5 Integrated Process..... | 29 |
| 5.6 Consideration for a Scale-up | 31 |
| 6 Discussion..... | 32 |
| 7 Conclusion | 36 |
| 8 References..... | 37 |
| 9 Publications..... | 46 |

1 Abstract

Bulk crystallization of biopharmaceutical proteins is a promising alternative to chromatographic separation techniques or traditional formulation processes. It is highly economical (low-cost operation), unlimited scalable and offers excellent selectivity. Furthermore protein crystals have been proven to be very stable and preserve proteins biological activity. Reduced viscosity and extended-release properties compared to liquid formulations leads to improved syringeability and injectability and facilitate the delivery to the patients.

We developed a general and practical approach to implement such crystallization processes for the biopharmaceutical industry using two recombinant proteins recombinant interferon gamma and a recombinant single chain antibody. The developed approach consist of 5 steps: (a) initial screening for crystallization conditions, (b) adjustment of crystallization conditions, (c) generation of phase diagrams as process map, (d) process design regarding impurities, seeding technique, influence of pH and temperature and (e) scale-up. Three dimensional crystals for both proteins were generated by microscale crystallization screening methods. Phase diagrams and solubility curves of the proteins with different precipitants were generated and compared regarding there suitability to enable a robust, time-effective and high-yielding crystallization process. Operating points were proven in a scale-up using a stirred beaker for both proteins. In case of recombinant interferon gamma the crystallization rate was driven by nucleation and the formation of three dimensional crystals were generated by Oswald ripening. It could also be shown that determined crystallization conditions could be applied for impure solution. In case of the single chain antibody an integrated process design was developed, combining protein extraction and protein crystallization using an aqueous two-phase system (sodium sulfate and polyethylene glycol 2000).

2 Kurzfassung

Proteinkristallisation ist eine vielversprechende Alternative zu herkömmlichen chromatografischen Trenntechniken oder traditionellen Formulierungsprozessen in der biopharmazeutischen Industrie. Sie ermöglicht kostengünstige, hochselektive und unlimitiert skalierbare Prozesse. Proteinkristalle sind sehr stabil und konservieren die biologisch aktive Wirkung des Proteins. Eine reduzierte Viskosität, sowie verlängerte Release-Eigenschaften erleichtern die Verabreichung an Patienten mittels Injektion.

In dieser Arbeit haben wir einen generischen, gesamtheitlichen und praktischen Ansatz entwickelt um industrielle Proteinkristallisationsprozesse zu implementieren am Beispiel von zwei rekombinanten Proteinen (Interferon gamma und einem einzelkettigen Antikörperfragment). Der Ansatz beinhaltet 5 Schritte: (a) Screening von Kristallisationsbedingungen, (b) Anpassungen der Bedingungen um 3-dimensionale Kristalle zu erhalten, (c) Erstellung von Phasendiagrammen als Prozesslandkarten, (d) Erstellen des Prozessdesigns unter Berücksichtigung von Verunreinigungen, Verwendung von Impfkristallen, pH Werten und Temperaturen, (e) Scale-Up. Dreidimensionale Kristalle konnten für beide Proteine im Mikromaßstab erzeugt werden. Phasendiagramme und Löslichkeitskurven der Proteine mit verschiedenen Fällungsmitteln wurden generiert und hinsichtlich Robustheit, Kristallisationseffizienz und Ausbeute verglichen. Geeignete Bedingungen wurden im Scale-up erfolgreich überprüft. Im Fall von rekombinantem Interferon gamma bestimmte die Nukleation den Kristallisationsprozess, die Bildung von dreidimensionalen Kristallen entstand durch die Oswald-Reifung. Gefundene Kristallisationsbedingungen konnten erfolgreich auch auf unreine Lösungen übertragen werden. Im Falle des Antikörperfragments wurde ein integriertes Prozessdesign entwickelt, das Proteinextraktion und Proteinkristallisation unter Verwendung eines wässrigen Zweiphasensystems (Natriumsulfat und Polyethylenglykol 2000) kombiniert.

3 Introduction

3.1 Advantages of protein crystallization in the biopharmaceutical industry

High titers in the upstream of production processes of biopharmaceuticals have shifted the bottleneck towards the downstream process. The purification of biopharmaceuticals is in general achieved by chromatography, but chromatographic separation steps are not unlimited scalable and chromatographic resins expensive. The increasing titers of the upstream processes enhance the pressure to find alternative, more economical, and unlimited scalable purification processes to chromatography (Gottschalk, 2005; Kelley, 2006; Low et al., 2007, Roque et al., 2020).

Crystallization processes met all these demands. It is highly selective, unlimited scalable and can be achieved in low-cost operation procedures using inexpensive ingredients (Etzel, 2006; Pechenov et al., 2007; Prince and Smith, 2004; Schmidt et al., 2005; Thömmes and Etzel, 2007; Vuolanto et al., 2003; Dos Santos et al. 2017). It was also shown that protein crystallization used as an formulation step has some advantages regarding stability and controlled slow release (Klyushnichenko, 2003; Pechenov et al., 2007; Shenoy et al. 2001; Elkordy et al., 2004). However, successful crystallization is dependent on many process parameters, as for instance pH, temperature, salt concentration, additives. Thus, protein crystallization was considered more an art than a science (Chayen, 2004; Filho et al., 2011). The focus within the last decades was set more on protein crystallization for structure determination than on preparative crystallization (Kim et al., 2011; Peters et al., 2005). The field of preparative or industrial crystallization nowadays can benefit from this extensive research. A lot of proteins related to different protein families were successful crystallized and data about initial crystallization conditions are provided in different data base like the Biological Macromolecule Crystallization Database (BMCD) (Gilliland, 1988).

3.2 Protein crystallization mechanisms

Protein crystallization is based on phase transition within supersaturated solutions representing a non-equilibrium state (McPherson, 2004). Supersaturation can be reached by increase of precipitant or protein concentration, variation of pH, temperature, or additive concentration (Chayen, 2004). In order to re-establish the equilibrium state, a solid state (crystals) is built within two distinct steps, nucleation and growth (Etzel, 2006). Protein solubility plays a significant role within this process and can be demonstrated via a phase diagram, as shown in Figure 1.1.

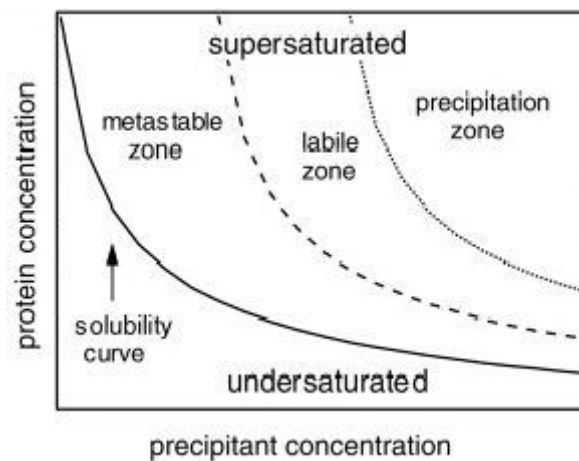


Figure 3.1: Typical phase diagram, the x-axis shows precipitant concentration, the y-axis represents the corresponding protein concentration; adopted from McPherson, 1999.

The solubility curve is formed by protein concentrations at certain precipitant concentrations where the system holds an equilibrium state. Thus, existing crystals can further exist (Asherie, 2004) but no new crystals can grow. In the undersaturated zone below the solubility curve, no crystals can form (nucleation), and existing crystals would dissolve. The metastable zone is characterized by growth of existing crystals, but without nucleation (Etzel, 2006) since the level of supersaturation is too low. Formation of crystals occurs in the labile zone where the supersaturation level is sufficient for spontaneous nucleation (Asherie, 2004; Haire, 2001; McPherson, 2004). At a high level of supersaturation, the precipitation zone is reached where amorphous precipitates instead of crystals are formed. However, due to dependency of nucleation and growth rate, crystal form can be influenced by the level of supersaturation (McPherson, 2004).

Determination of the overall crystallization rate and estimation of the behavior of nucleation and growth can be accomplished by the Avrami equation (Avrami, 2004).

$$X_t = 1 - e^{-kt^n} \quad (\text{Equation 1})$$

where X_t is the fraction of protein crystallized after time t , k is the crystallization rate constant and n is the Avrami Exponent. The Avrami exponent consists of two terms:

$$n = N + qC \quad (\text{Equation 2})$$

where N is the nucleation and is either 0 if all crystals are nucleated simultaneously at the beginning of the growth process or 1 if nuclei form at a constant rate. C is the dimensionality of crystal growth and is 1, 2, 3-dimensional and q describes the time dependence of growth: $q = 1$ for linear growth and $q = 0.5$ for diffusion limited growth.

3.2.1 Nucleation

The following chapters of Nucleation and Crystal Growth were also discussed in a similar way in two master theses under my supervision (Obermair, 2014; Haidinger, 2012).

Nucleation is a first-order phase transition process (McPherson, 2004) leading to an ordered solid state, the formation of crystalline intermediates of a non-equilibrium state has been created, enforcing protein molecules to aggregate. Nucleation occurs when nuclei are built out of the aggregates (Erdemir, 2009). Thus, this step represents the driving force for crystallization. Nucleation is divided into three types: homogenous nucleation, thus within a solution, heterogeneous nucleation, caused by solids within the crystallization bulk (seed crystals) or even caused by the walls of the vessels the solution is kept in or dust (Chayen, 2004), and secondary nucleation, where nucleation is caused by either breakage or attrition of existing crystals due to collisions or high shear forces (Etzel, 2006). The nucleation rate (B) is given by (Jacobsen et al., 1998):

$$B^0 = k_B * M_T^m * S^b \quad (\text{Equation 3})$$

where M_T gives the mass concentration of crystals, S is the degree of supersaturation, K_B is the Boltzmann constant. Other variables represent kinetic constants. Alternatively, the nucleation rate can be described by (Saikumar et al., 1998):

$$B^0 = k_n * \left(\frac{c - S}{S}\right)^a \quad (\text{Equation 4})$$

where s represents the equilibrium solubility, c the concentration of the solute in the solution and k_n a nucleation constant. The exponent a is the nucleation order. This equation was used for kinetic modelling by Saikumar et al. (Saikumar et al., 1998).

According to the classical nucleation theory, for the onset of nucleation an energy barrier must be overcome (Erdemir et al., 2009). This is given by the fact that a crystalline lattice shows a low entropy-state, causing the activation barrier. Thus, enthalpic conditions favoring crystal lattice formation have to be set. Cluster formation and deformation happens, as long as the increase of enthalpy is lower than the decrease of entropy within the system. When reaching a critical size, volume contribution is more influencing than surface contribution, enabling nucleation (Saridakis and Chayen, 2009), as depicted in Figure 1.2.

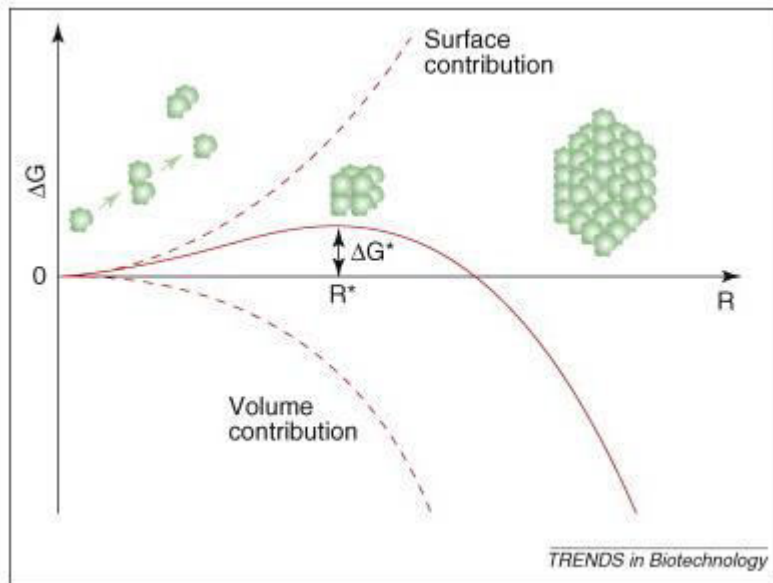


Figure 3.2: Energy barrier ΔG for nucleation; Gibbs free energy is dependent on aggregate size (R) (red unbroken line); broken lines show dependence on surface formation and bulk incorporation; R^* shows the size of a critical nucleus and ΔG^* the corresponding free energy; $R > R^*$ critical nucleus can convert into stable crystal; adopted from Saridakis and Chayen, 2009.

Thus, nucleation is dependent on the free-energy change, which was defined by Gibbs in the 19th century (Erdemir et al., 2009; Vekilov, 2010). The classical nucleation theory is often considered as a simplified version where nuclei are built within one step as soon as the energy barrier is overcome due to supersaturation, leading to the formation of aggregates, called critical nuclei (Erdemir et al., 2009). The two-step nucleation theory describes an intermediate step where subcritical clusters, thus metastable liquid particles containing a high concentration of protein are built and result in so called liquid-liquid phase separation, followed by an organization into an ordered structure (Erdemir et al., 2009; Haas and Drenth, 1999; Vekilov, 2010). The two-step mechanism with two small energy barriers is thought to be faster than a one-step mechanism, where within one step a high barrier has to be overcome (Haas and Drenth, 1999). Lomakin et al. showed via numerical simulations that dense liquid

clusters due to surface effects are more stable than crystalline structures, which can only form when reaching a critical size (Lomakin et al., 2003). However, according to Lomakin's findings, this is caused by the fact that when liquid particle clusters grow, fewer particles have surface contact with the bulk leading to a higher influence of the bulk conditions, which in turn enables crystalline structures. Moreover, the first step of building metastable dense clusters is thought to be fast, whereas the second step of formation of crystalline nuclei within the clusters seems to be rate determining (Vekilov, 2010). The effect of composition of the precipitant solution on the formation of dense liquid clusters was demonstrated via mathematical simulations, which showed a minimum in this area of the nucleation barrier curve (Chernov, 2003). In addition, Galkin and Vekilov demonstrated within their experiments using two different additives that nucleation could be influenced by precipitant solution (Galkin and Vekilov, 2000).

As stated, the process of nucleation is mainly based on the interactions between protein molecules. George et al. created a mathematical approach, referred to as the second virial coefficient B_{22} , representing the "crystallization slot" where due to appropriate conditions, crystallization can be promoted. Positive values for B_{22} indicate repulsive interactions between protein molecules, whereas negative values indicate attractive interactions, leading to crystallization within the slot of $-0.8 \leq B_{22} \leq -0.1$ (George and Wilson, 1994; Wanka and Peukert, 2006). Thus, the higher the repulsive forces (higher positive values of B_{22}), the better solubility of the protein is given, showing the correlation of solubility and the second virial coefficient. Wanka and Peukert depicted that B_{22} within this slot is dependent on pH, temperature as well as ionic strength, demonstrating the importance of these process parameters for crystallization (Wanka and Peukert, 2006).

3.2.2 Crystal growth

As for nucleation, the key factor for growth is given by the degree of supersaturation. The process of nucleation is followed by the process of crystal growth where particles add to the critical nuclei and form an ordered, stable three-dimensional crystal lattice (Russo et al., 2013). Resulting crystal shape is dependent on the conditions while growth is occurring, whereas the process seems to be based on random protein-protein interactions (Carugo and Argos, 1997). The growth process itself shows similarity to that of crystallization of small molecules. The process can be described by (Filho et al. 2011; Saikumar et al., 1998):

$$G = k_g \left(\frac{c - s}{s} \right)^b = k_g \times \Delta C^g \quad (\text{Equation 5})$$

where k_g is the specific growth constant, c represents the concentration of the solute in a solution and s the solubility at equilibrium state, which is also given as ΔC . The exponent g represents the growth order, which lies usually between 1 and 2 for soluble compounds and >2 for poorly soluble ones (Filho et al., 2011).

Since protein crystallization is based on intermolecular bonds of the macromolecules within a crystal it is mainly influenced by pH, temperature, and composition of the solution. Different molecular surfaces are thus accessible for integration, which leads to various crystal structures (Chernov, 2003). Therefore, the transport of building blocks is the limiting factor within unstirred vessels or under conditions of microgravity, where diffusion is altered (Jen and Merkle, 2001).

The resulting protein crystal is a solid material with orderly packed protein units within a defined lattice groups separated by channels containing mother liquor. The protein units are bound by hydrophobic interactions, H-bonds, and salt-bridges (Jen and Merkle, 2001).

4 Objectives

The aim of this work was to generate a general and practical approach to develop industrial crystallization processes either for the purification or formulation of biopharmaceutical proteins, using two recombinant proteins (recombinant interferon gamma and a single chain antibody). The approach should cover the crystallization process development procedure from screening for crystallization conditions, crystal optimization techniques with respect for the requirements of large scale biopharmaceutical productions, generation of phase diagrams for crystallization process characterization and to depict appropriate operating points, considering applicable process integration steps leading to a process design to achieve a scalable economic process regarding crystallization yield, purity, and process time.

One major aspect was to close the gap between crystallization processes used for the generation of crystals for X-ray diffraction analysis and crystallization processes for the generation of crystals suitable for large scale processes. For this purpose, already established work of the last decades in crystallization screening and optimization techniques were considered and adopted to achieve robust and scalable crystallization processes.

Another aim was to establish process maps in the smallest reliable scale, on which base process designs and operating points for future large scale processes could be defined. Given that process maps or phase diagrams comprise a lot of operating points, it is important to minimize the required amount of protein since in general it is limited at the start of process development. Furthermore, various aspects regarding the optimization of process design and influence of impurities were investigated. Process integration and other opportunities to enhance the process quality in respect to purity, yield, process time, and process control were considered.

5 Results – Development of a preparative crystallization process as purification or formulation step for recombinant proteins

Although crystallization processes are implemented in several enzyme purification processes and widely used in the chemical production of small molecules (Myerson and Toyokura, 1990), it is not a common purification technique in biopharmaceutical processes till now and the number of such processes like the crystallization of insulin is rare (Hekmat et al. 2015a; Dos Santos et al., 2017; Chen et al., 2021). This is due to the diversity and complex structure of biomacromolecules excluding a predictability of crystallization conditions and crystal properties (Lorber et al., 1993; McPherson, 1999; Lu et al., 2002). Furthermore, the high quality requirements on pharmaceutical processes and the limited knowledge about crystallization process development, control, and scale-up have hindered the break-through of this technique. Some approaches to develop and scale-up crystallization processes were shown for lysozyme, bovine serum albumin and alcohol dehydrogenase as model proteins using evaporative crystallizers (Hubbuch et al., 2019; Barros Groß and Kind, 2018; Kołodziej et al., 2018) and also for stirred vessels using ovalbumin (Judge et. al, 1995), lysozyme (Carbone and Etzel, 2006; Hekmat et al. 2007), lipase (Jacobsen et al., 1998, Hebel et al. 2013), cross-linked enzyme crystals (Lee et al., 2000), recombinant l-methionine γ -lyase (Takakura et al., 2006), an antibody Fab fragment of Canakinumab (Smejkal et al., 2013a), a single chain antibody (Huettmann et al., 2014) and two full length antibodies IgG4 (Zang et al., 2011) and IgG1 (Smejkal et al., 2013b). Nowadays also some new approaches arising using tubular crystallizers to facilitate continuous crystallization processes (Pu and Hadinoto, 2020; Hekmat 2017). However most of the approaches were done with pure protein and even with the shown approaches including impurities in the product solution there is still a lack for a general, systematic approach to implement crystallization processes as a purification step or as a formulation step in biopharmaceutical manufacturing processes. In this work a systematic and practical approach to implement a crystallization process at different steps in a biopharmaceutical manufacturing process was shown using two biopharmaceutical relevant proteins (recombinant Interferon gamma (rhINF- γ) and a single chain antibody).

The approach presented containing the following steps:

1. Screening of initial crystallization conditions
2. Optimization of crystalline state and crystal habit

3. Generation of phase diagrams as process map
4. Development of process design
 - a. Choice of operating point
 - b. Amplification of phase diagrams by pH or temperature
 - c. Crystallization of process intermediates without loss of the nucleation zone
 - d. Crystallization of process intermediates with loss of the nucleation zone
 - e. Control of the degree of supersaturation and the speed to achieve supersaturation
 - f. Application of an integrated processes
5. Scale up

5.1 Initial Screening to determine crystallization conditions

The aim of the initial screen is the investigation of different precipitants in combination with different pH values to crystallize the target product. In general, salts, polymers, organic solvents, and small weight polyalcohols are used as precipitants. Also, the successful use of non-ionic detergents as precipitants was reported (Mustafa et al., 1998).

5.1.1 Precipitants

In general, salts increase the solubility of proteins at low concentrations (salting in effect) but can strongly reduce protein solubility at higher concentrations (salting out effect) (Hofmeister, 1888). The salting out effect is caused by the competition of protein molecules and salt ions for water molecules since they have to be hydrated to stay in solution. The ability of salts to salt out or salt in proteins is classified in the Hofmeister series and salts are either kosmotrope or chaotrope. Chaotrope salts disorder the structure of water and force protein denaturing (Duong-Ly and Gabelli, 2014; Von Hippel and Wong, 1964).

Polymer precipitants like polyethylene glycol (PEG) are chemical inert and have non-denaturing properties to proteins. They reduce the solubility of proteins by sterically exclude proteins from their hydrate shell due to their large molecular weight. The reduction of the protein solubility has a linear dependence to the concentration of used PEG. PEG is manufactured in different length and the slope of the described linear dependence is reduced by lowering the length of used PEG (Atha and Ingham, 1981).

Organic solvents and small molecular weight polyalcohols lower the dielectric constant of the solution and enhance electrostatic interactions of the protein (Affleck et al., 1992; De Souza et al., 2007). Repulsive interactions lead to partial denaturing of the protein and create new surface areas which can lead to self-assembly of the protein (Zhou and Pang, 2018).

Detergents are amphiphilic and contain a hydrophobic alkyl chain with a hydrophilic head group (Neugebauer, 1990). Since the protein consist also of hydrophobic and hydrophilic parts they can interact and alter protein structure as well as change the solubility of proteins forcing protein self-assembly or build protein-detergent complexes (Breibeck and Rompel, 2019; McPherson et al., 1986; Privé, 2007).

The pH alters the protein net charge, and the isoelectric point (pI) is the pH at which the net charge is zero. The solubility of a protein is strongly reduced at its pI and was first considered as a promising pH for crystallization, but the majority of proteins have been crystallized at different pH values (Kantardjieff and Rupp, 2004; Kirkwood et al., 2015; McPherson and Cudney, 2014).

5.1.2 Appropriate screening techniques and methods

All these precipitants influence the solubility and / or structure of the protein in different ways, sometimes the best results was achieved with combinations of them. The optimal screening technique is either a complete random screen or, due to the high number of samples, an incomplete factorial design to achieve highest success (DeLucas et al., 2003; Rupp and Wang, 2004). Today commercially available initial protein screenings are sparse matrix screens. They comprise either the investigation of single precipitants or a variety of combinations of precipitants, e.g., PEGs and salts, based on previous success (Cudney et al., 1994; Jancarik and Kim, 1991; Luft et al., 2011).

There are several ways to reach supersaturation within crystallization experiments, given by the influence of pH, ionic strength, and temperature on protein solubility (Chayen, 2004; Gavira, 2016; Judge et al., 1999; Wanka and Peukert, 2006).

From a practical view and also the most widely used method is the vapor diffusion method (Matthews et al., 2009). In this case a small droplet (2-10 μ l) comprises the target protein and the mother liquor (precipitant solution) is slowly concentrated by vapor diffusion against a larger reservoir (500-1000 μ l) containing only the mother liquor in a sealed chamber. The difference in concentration between the droplet and the reservoir drives the system toward

equilibrium by diffusion through the vapor phase (Benvenuti and Mangani, 2007). Figure 2.1 shows the schematic course of action in a successful vapor diffusion experiment. The initial concentrations of protein (C_{ip}) and precipitant (C_i) in the droplet are in the undersaturated phase (A) and will rise into the supersaturation zone where crystallization can take place (B). Crystals will grow until the solubility limit is achieved at equilibrium (C) with the final soluble protein concentration (C_{fp}) and final precipitant concentration (C_f) (Chirgadze, 2001).

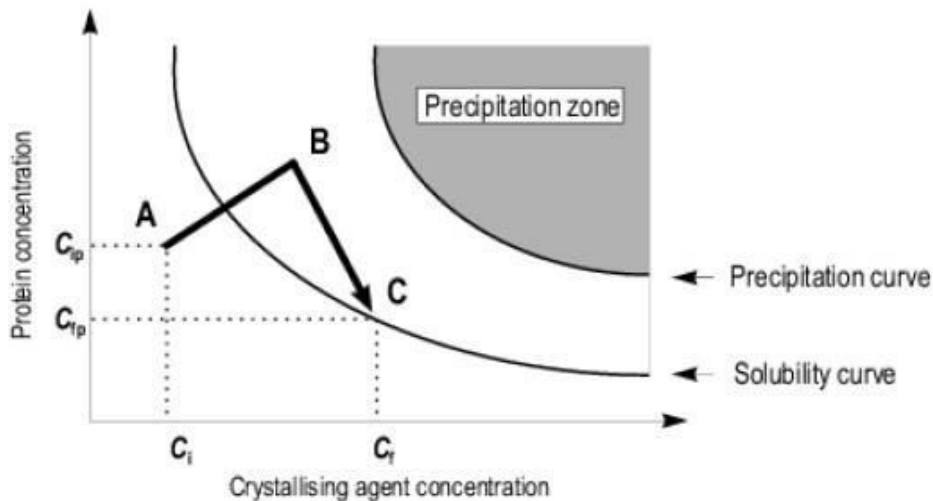


Figure 5.1: Schematic crystallization process using the vapor diffusion method. Starting with the initial concentration of protein (C_{ip}) and precipitant (C_i) in the undersaturated zone (A), slightly concentrated by vapor diffusion into the supersaturated zone where crystallization takes place (B) and crystal growth until the solubility limit is reached at equilibrium (C) with the final soluble protein concentration (C_{fp}) and precipitant concentration (C_f); adopted from Chirgadze, 2001.

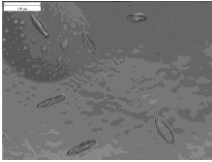
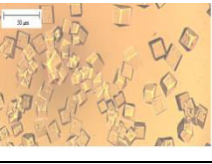
The droplet is either placed on a pedestal (sitting drop) or hanging from a siliconized glass cover slip (hanging drop) or is placed between two cover slips (sandwich drop) to reduce exposure to air.

In the initial screen, pure product (>95 %) is used to determine crystallization conditions and to exclude interferences with impurities. Given that in general at the starting point of a development process the amount of pure protein is limited initial screens are performed in nanoliter or microliter scale.

In this work the composition of the crystal screen I and II of Hampton Research as well as the JB Screen classic from Jena Bioscience was used as initial screen carried out as a vapor diffusion method (sitting drop) using Greiner Crystalquick 96 well plates. Compositions containing harmful ingredients were not tried.

Three hits for interferon gamma and one hit for the single chain antibody were found listed in Table 2.1.

Table 5.1: Overview of found crystals and crystallization conditions of the initial screening

| Microscopic image | Protein | Initial concentrations of the droplet | Time until crystals appeared | Morphology |
|---|-----------------------|--|------------------------------|--------------------------------|
|  | Interferon gamma | 2 g/l protein, 0.88 M ammonium phosphate pH 6.0 | 4 d | Ellipsoid |
|  | Interferon gamma | 2 g/l protein, 1 M sodium sulfate, 0.1 M ammonium acetate pH 6.0 | 24 h | Cubic |
|  | Interferon gamma | 2 g/l protein, 1 M ammonium sulfate, 0.1 M sodium acetate pH 6.0 | 24 h | Cubic |
|  | Single chain antibody | 2 g/l protein, 1 M sodium sulfate, 0.1 M Tris pH 8.5 | 24 h | Sea urchins, bundle of needles |

5.2 Adjustment Screen

The adjusted screen is used to optimize the crystal habit and achieve uniformity of crystals. For this purpose, the initial conditions will be defined further. The initial screen was performed using the vapor diffusion method hence the correct concentrations when crystallization occur are not known. To determine these distinct protein and precipitant concentrations a different screening method has to be used, the microbatch method. In case of the microbatch method the droplet containing protein and precipitant is placed at the bottom of a well of a 96-well plate and overlaid with oil (D'Arcy et al., 2004). Paraffin oil should be used for determination of distinct conditions since it is air-impermeable and will conserve the generated conditions in the droplet. In Figure 2.2 the possible processes using a microbatch method and a grid screen are shown.

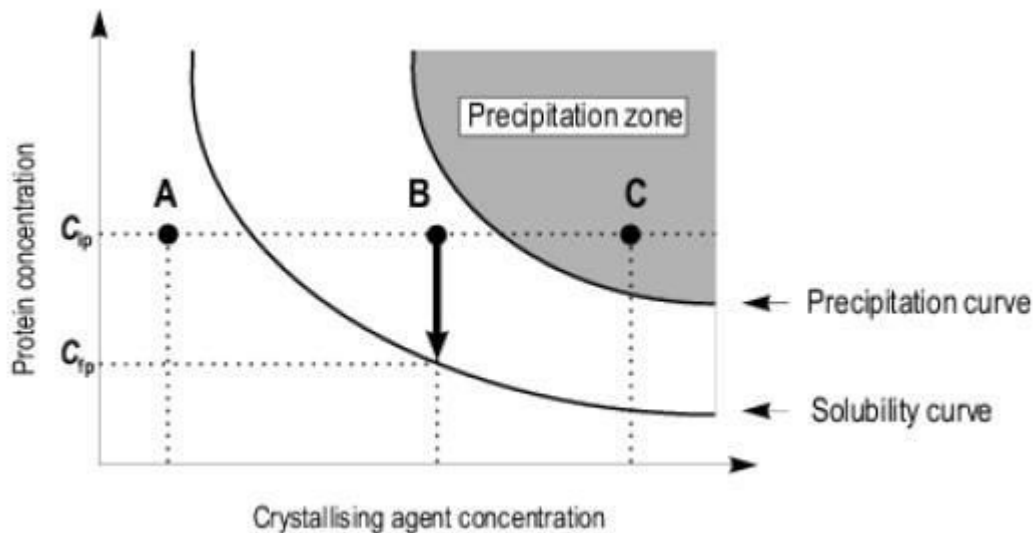


Figure 5.2: Schematic process using microbatch method and a grid screen. The points A, B and C are the initial adjusted conditions with the initial protein concentration C_{ip} . The point A is in the undersaturated phase and the drop will stay clear. In the case of B nucleation occurs and crystals will grow until the solubility limit is reached with a final soluble protein concentration of C_{ip} . In case of C precipitation will occur; adopted from Chirgadze, 2001.

First a grid screen (Cudney et al., 1994) should be performed with the used protein concentration and pH of the initial screen and varying the precipitant concentration. After distinct crystallization conditions are determined these conditions will be amplified by addition of additives and variation of the pH and buffer substances to investigate their impact on crystal habit and homogeneity. In general, as additives, all chemicals from the initial screen are used but also other ingredients, e.g., detergents can be tested (McPherson and Cudney, 2014).

As previously mentioned, over the last decades a lot of crystallization conditions for many proteins were identified (Kim et al., 2011; Luft et al., 2011) to determine the three-dimensional structure of proteins (Kim et al., 2011; Watson et al., 2011). These published results could be used as starting conditions for development of an industrial crystallization process, but the demands for large-scale crystallization are different than those for structure determination (Etzel, 2006; Kougoulus et al., 2006). An overview of the different demands is listed in Table 2.2 (Peters et al., 2005).

Table 2.2: Overview of requirements on crystals generated for structure determination and crystals generated for bulk crystallization, adapted from Peters et al., 2005

| Criterion | Crystals for structure determination | Crystals for industrial processes |
|----------------------------------|---|--|
| Excipient | Not important | Important (e.g., no toxic/hazardous compounds) |
| Excipient costs | Not important | Important |
| Crystal size | Very important (large) | Important (moderate) |
| Crystal lattice quality | Important (high resolution needed) | Not important |
| Crystallization yield | Not important | Very important (high yields) |
| Growth kinetics | Not important (days to months) | Very important (hours to days) |
| Process compatibility | Not important | Very important |
| Scalability of conditions | Not important | Very important |
| Redissolution conditions | Not important | Important |

Bulk crystallization demands inexpensive, pharmaceutically acceptable compounds, fast growth kinetics, and high crystallization yields. Crystal grid irregularities and a large single crystal habit are not as important as purity and scalability of the process (Peters et al., 2005).

The goal of the adjusted screen is to achieve 3-dimensional crystals of moderate size (>10 μm). The crystal habit should be uniform and other solid states like amorphous precipitates should be avoided. This would facilitate crystal harvest and demonstrate that the transition of the target protein from the soluble phase to the solid phase is homogenous. The 3-dimensional form of the crystals prevents them from breakage during stirring in the large scale and avoids second nucleation, which leads to a broad size distribution of the crystals (Kougoulus et al., 2006). Needle crystals are more sensitive to shear stress.

In case of the single chain antibody fragment, the found crystallization conditions from the initial screen resulted in heterogeneity of crystal forms (sea urchins and bundle of needles) and precipitates. An exchange of the buffer system to HEPES, but maintaining the pH, resulted in uniform needle crystals without precipitates. This condition was used for the next screening round and the addition of PEG-2000 resulted in 3-dimensional crystals shown in Figure 2.3 (Huettmann et al., 2014).

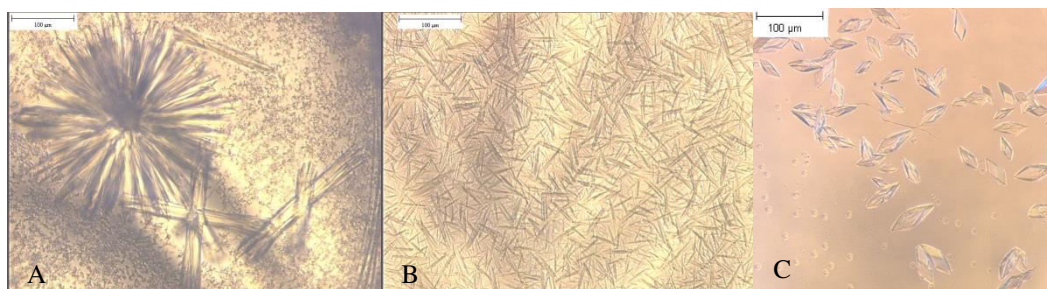


Figure 5.3: Results of the adjusted screen for the single chain antibody fragment. Starting conditions from the initial screen (A), exchange of Tris buffer with HEPES buffer (B) and HEPES buffer and PEG as additive; adopted from Huettmann et al., 2014 (C)

5.3 Phase diagrams

The generation of phase diagrams is the basis of robust and scalable crystallization processes (Klijn and Hubbuch 2020; Huettmann et al., 2015). Phase diagrams characterize the interaction of the protein of interest and the chosen precipitant under constant conditions. Different precipitants could result in different phase diagrams. Hence it is an advantage to generate several phase diagrams and compare them regarding process suitability. The requirement of an appropriate precipitant is to cause a broad crystallization zone. The solubility curve below the crystallization area should go against zero to assure high crystallization yields and a minimum of protein which will stay soluble in the mother liquor after the crystallization process. The amount of precipitant which has to be used to achieve crystallization conditions should be low to avoid high dilution rates of the used protein solution.

An economical way to obtain phase diagrams for large scale processes is the millibatch method. In this case, batch crystallization of approximately 1 ml volumes is performed under slight shaking. This method needs only limited starting material and at the same time mimics the stirred tank crystallization (Huettmann et al. 2014; Huettmann et al., 2015). This is an advantage compared to the microbatch method since the energy input due to stirring can alter a phase diagram (Hekmat, 2015a, Castro et al. 2016). In addition, the solubility curve after a distinct crystallization time can be determined, which enables the correct calculation of the crystallization yield. In Figure 2.4 a schematic picture of the method is shown. However, sometimes the available amount of pure protein is too low to use the millibatch method. In this case coarse phase diagrams can be generated using microbatch method and on demand further amplified by a solubility curve generated from a few single millibatch experiments.

The microbatch method can also be used to predetermine the relevant precipitant and protein concentrations for the millibatch method as shown in Figure 2.5.

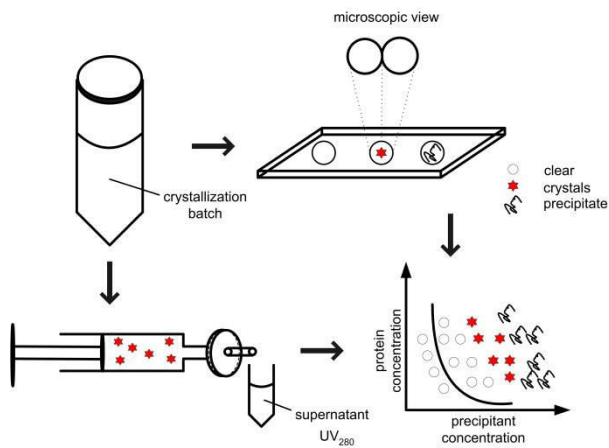


Figure 5.4: Schematic procedure of the millibatch method

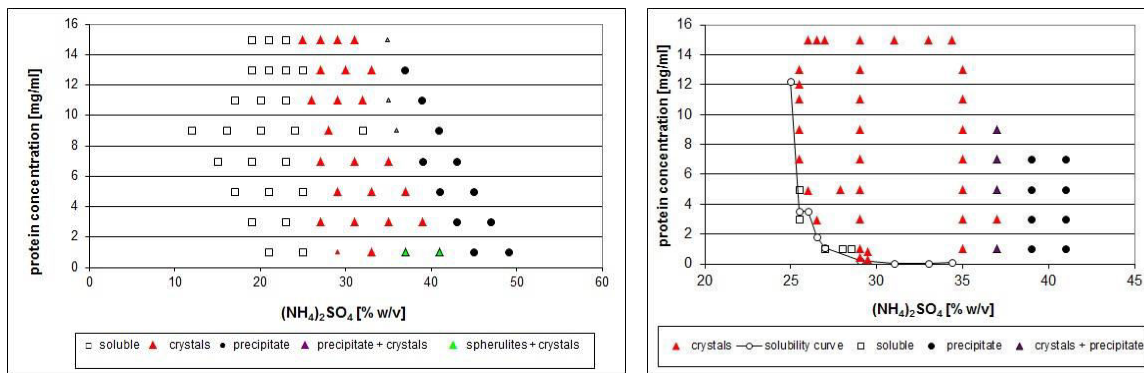


Figure 5.5: Phase diagrams generated with microbatch method to determine the relevant concentrations (left) and millibatch method with the associated solubility curve; adopted and adapted from Huettmann et al., 2015 (right). All batch crystallization experiments were investigated after 24 hours by microscopic analysis and in case of the millibatch method by UV₂₈₀ to determine the protein content in the supernatant. Experiments were performed at room temperature.

The generated phase diagrams fit very well and showed a large well-defined nucleation zone. The phase diagram generated with millibatch method also depicted the solubility limit after 24 hours crystallization and a small metastable zone. The metastable zone is in the region of 26-29 % ammonium sulfate and a protein concentration below 3 g/l, determined by two experiments above the solubility limit without the appearance of crystals.

5.4 Process design

Industrially applied crystallization methods are commonly batch crystallization processes using precipitants, cooling or evaporation to achieve nucleation (Giuletti et al., 2001; Hekmat et al., 2007; Kougoulus et al., 2006, Hubbuch et al., 2019). In addition, seeding is also frequently used either to overcome a nucleation hindrance or to avoid high degrees of supersaturation and spontaneous nucleation for a better control of crystal homogeneity and size (Barros Groß and Kind, 2017; Liu et al., 2010).

The degree of supersaturation plays a major role for nucleation as well as for crystal growth and currently new technologies were developed to investigate crystallization kinetics (Poplewska et al., 2018).

However, there is a challenge to find the optimal degree of supersaturation, given the fact that, according to a typical phase diagram, the optimum conditions for formation of crystalline nuclei are contrary to those needed for optimum conditions at the subsequent crystal growth phase. Thus, for nucleation, a high degree of supersaturation is needed for spontaneous formation of crystalline nuclei. Within the growth phase, for formation of large, ordered crystals, a slow growth rate requiring low to moderate levels of supersaturation is preferred (Bergfors, 2003).

In addition, crystallization is facilitated at high protein concentrations and low impurity contents, but in early process steps of biopharmaceutical productions the protein concentration is often rather low, and the impurity amount high (Skuori et al., 1995).

Impurities could also influence the phase diagram and can lead to loss of the nucleation zone (Skuori et al., 1995).

5.4.1 Crystallization of process intermediates maintaining the nucleation zone

Mechanical parameters like stirring speed (Kougoulus et al., 2006; Skuori et al., 1995) and impurities can diminish the nucleation zone, as well as ingredients in the matrix of the process intermediate can alter the solubility properties of the protein (Skuori et al., 1995; Hekmat et al., 2007). Hence, the working point, here the chosen precipitant and protein concentrations, of a crystallization process should be selected at a stable point of the nucleation zone with sufficient distance to the undersaturated and the precipitation zone to ensure process robustness. The solubility curve should be at a minimum to achieve optimal crystallization yields.

To investigate the crystallization behavior of process intermediates the crystallization process of interferon gamma was introduced at different process steps in ml scale. In Figure 2.6 a schematic process flow of the first purification steps of an established recombinant interferon gamma process using *E.coli* as host cell at Boehringer Ingelheim RCV GmbH & Co KG is shown.

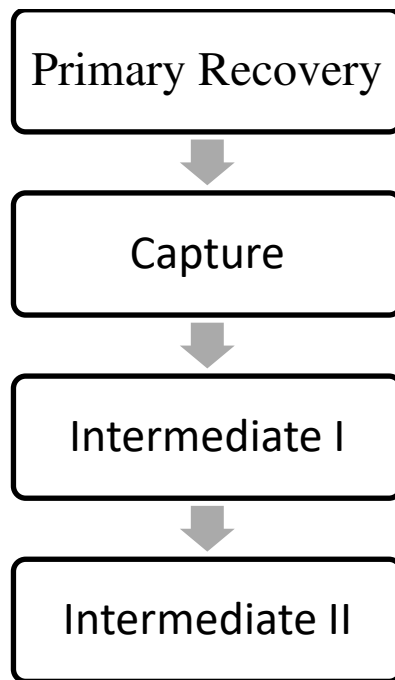


Figure 5.6: Schematic process flow of the first process steps of the interferon gamma purification process, established at Boehringer Ingelheim RCV GmbH & Co KG. Primary Recovery: cell breakage and clarification; Capture, Intermediate I and Intermediate II: First three chromatographic purification steps.

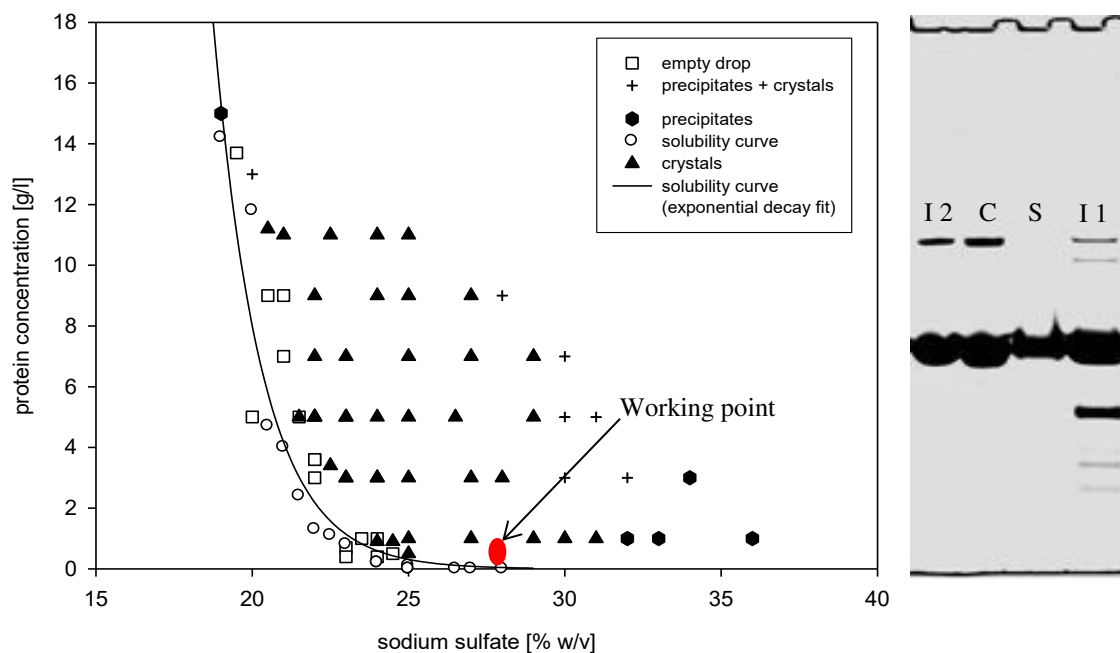


Figure 5.7: Phase diagram of interferon gamma and sodium sulfate with the depicted working point to crystallize the intermediate I Pool (27.5% sodium sulfate and ~ 0.5 g/l protein); adopted from Huettman et al., 2015 (left). Silver stained SDS-PAGE analysis (method provided by Boehringer Ingelheim RCV GmbH & Co KG, details not shown): I 2: Intermediate II Pool of the chromatographic process, C: dissolved crystals of the crystallized intermediate I pool, S: supernatant of the crystallized intermediate I pool, I 1: Intermediate I pool used as starting material of the crystallization process (right)

Crystallization of the intermediate I pool was achieved by batch crystallization using sodium sulfate as precipitant. Given that the pool concentration was below 1.5 g/l, and the dilution factor by addition of the precipitant will strongly decrease the protein concentration, the working point was selected at 27.5 % sodium sulfate resulting in a protein concentration of approximately 0.5 g/l. Crystallization process was carried out as described in Huettmann et al., 2015. The phase diagram and the SDS-Page analysis of the process are shown in Figure 2.7. The achieved purity by crystallization of the intermediate I pool was comparable to the intermediate II pool of the chromatographic process. The crystallization yield was 80 % whereas the chromatographic intermediate II step yield was 60 %. In both cases the process times were 15 hours. In this case the crystallization process could replace the intermediate II step without loss of purity and would have the benefit of a higher step yield at same process times. Additionally, the cost of goods could be reduced since no chromatographic resin is needed. The crystallization yield could be further enhanced by selecting a working point with a higher precipitant concentration.

5.4.2 Crystallization of process intermediates with loss of the nucleation zone

Impurities can strongly alter the phase diagram and can lead to a loss of the nucleation zone. Despite the loss of the nucleation zone, crystal growth must not be affected (Bergfors, 2003; Giuletti et al., 2001; Judge et al., 1998; Vuolanto et al., 2003). In such cases seeding techniques can close the gap between the loss of the nucleation reaction and crystal growth to achieve a successful crystallization process.

Seeding is a technique where prior produced crystals (micro-crystals or macro-crystals) are added to the crystallization batch. At an appropriate degree of supersaturation, the soluble protein will attach on the surface of the added crystals and crystal growth takes place (McPherson and Gavira, 2014; Pusey et al., 1986).

The capture pool (pool of the first chromatography step) of the interferon gamma process had also a protein concentration of < 1.5 g/l, hence the same working point as for the crystallization of the first intermediate pool (pool of the second chromatographic step) was chosen. The batch crystallization experiment resulted in amorphous precipitate instead of crystals. In a second attempt, addition of seed micro-crystals resulted in large single 3-dimensional crystals accompanied by some amorphous precipitates. Micro-crystal seed solutions were generated by crushing macro-crystals suspended in 31% sodium sulfate solution with an T25 Ultra Turrax, Ika Werke GmbH & Co KG, Staufen, Germany (1 min, 13500 rpm). The macro-crystal interferon gamma concentration in the solution is 0.1 mg/ml. The volume of the added micro-crystal seed solution for seeding is 6-8% of the final crystallization batch volume.

Seeding could replace the lost nucleation reaction resulting in successful crystallization, but also other solid forms like amorphous precipitates are still present as shown in Figure 2.8.

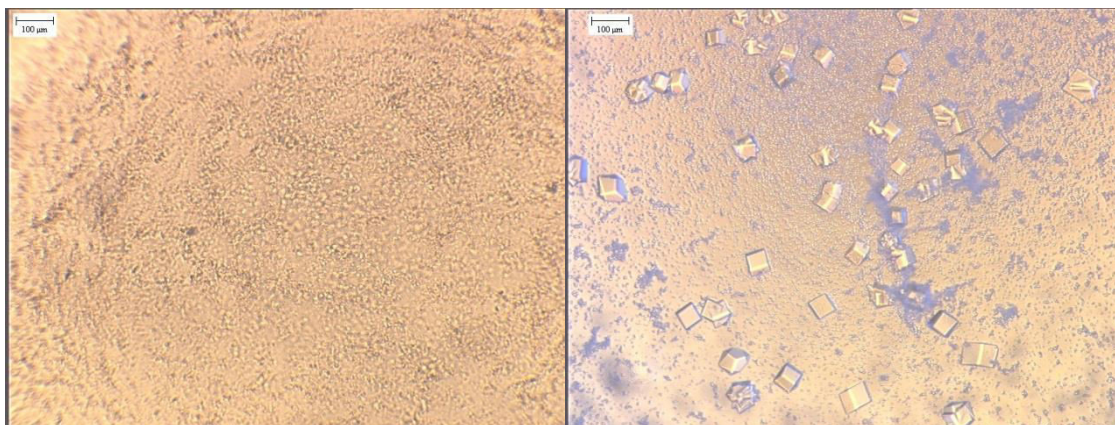


Figure 5.8: Microscopic images of crystallization experiments of the capture pool of the interferon gamma process after 15 hours. Batch process without seeding (left) and with seeding (right)

In case of crystallization of the crude homogenate the same effect was observed. Given that the concentration in the crude homogenate was below 1 g/l the operating point was chosen at a sodium sulfate concentration of 30 % resulting in a protein concentration of approximately 0.2 g/l. In this case, more amorphous precipitate was observed and the crystals size was smaller as shown in Figure 2.9.

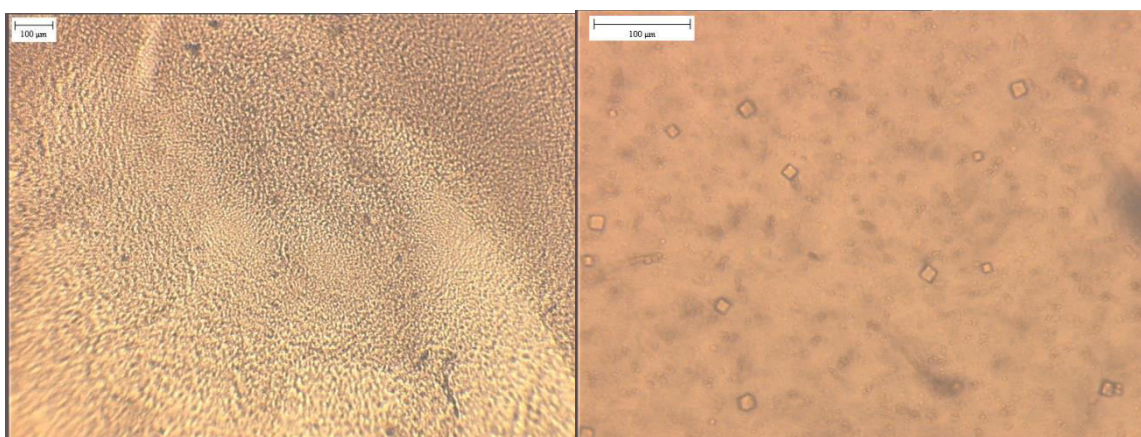


Figure 5.9: Microscopic images of batch crystallization of the crude homogenate of the interferon gamma process. After 15 hours. Batch crystallization without seeding (left) and with seeding (right)

The range of successful seeding was investigated for both process intermediates. In both cases interferon gamma could be crystallized with the help of seeding in the original crystallization zone predicted by phase diagrams. Hence, it could be said the phase diagrams of interferon gamma could predict crystallization conditions not only for pure protein solution, but also for impure protein solutions. The challenge is that not only crystals occur, but also other

structures, most likely host cell proteins, which precipitates in the same salt concentration range where interferon gamma crystallizes, resulting in low purities, when crystal harvest is performed by centrifugation. The purity could be increased by optimization of the harvest method resulting in a higher degree of separation of amorphous precipitate and crystals, e.g., filtration and sieving techniques.

Investigation of the different solid phases (amorphous precipitates and crystals of different sizes) was done for the crude homogenate using a working point for crystallization of 31 % ammonium sulfate and seeding instead of 31% sodium sulfate in 1ml scale. After crystallization the crystals and precipitates were harvested by centrifugation (20 min, 13.400 rpm), resuspended in 100 μ l 31 % ammonium sulfate solution and put as a layer on 1 ml 29 % sodium sulfate solution in an 1 ml Eppendorf tube. Centrifugation was carried out for 1.5 h at 3000 g using an Eppendorf centrifuge 5810R with swinging bucket and fractions were slowly taken from the bottom of the tube using a pipette. It could be shown that the grown crystals from the crude homogenate had a high purity. The amorphous precipitate and small crystals are accumulated in the top phases whereas the larger crystals are located in the middle and bottom phases shown in Figure 2.10.

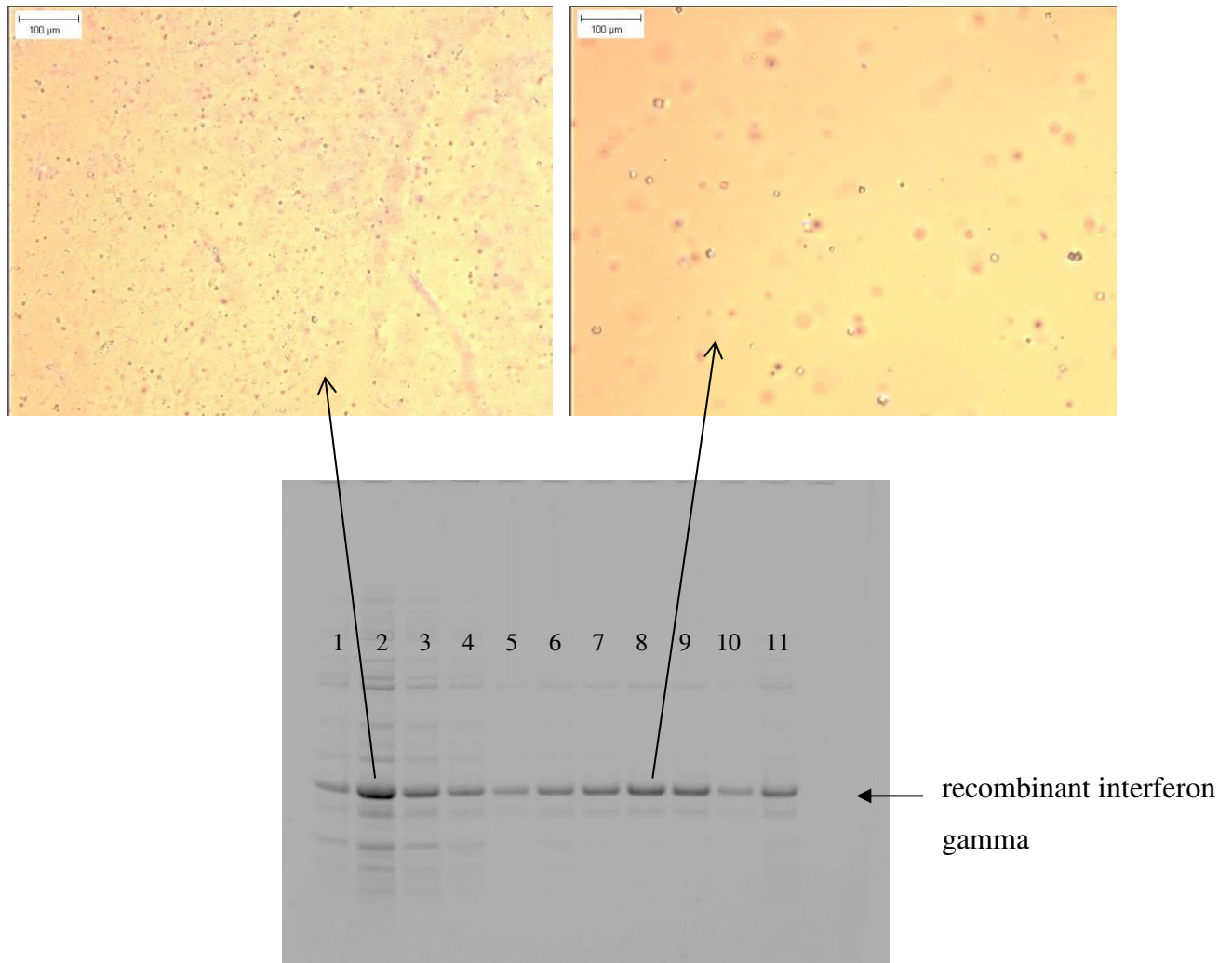


Figure 5.10: Microscopic analysis and coomassie blue stained SDS-PAGE analysis (method provided by Boehringer Ingelheim RCV GmbH & Co KG, details not shown) of the collected fractions after centrifugation. Lane1: top phase, lane 2-10 intermediate phases, lane 11: bottom phase

5.4.3 Overcome co-precipitation of impurities in crystallization processes

Co-precipitation of impurities during crystallization and how to overcome it is not often reported. Recrystallization is often used to reduce impurities (Liu et al., 2020, Meenan et al., 2002, Takakura et al., 2006). This technique may work well if only small amounts of certain impurities will co-precipitate with the target protein but will not work if the bulk of the impurities are co-precipitate.

In a first step of development the precipitation dependency of the impurities and the used crystallization agent should be investigated. In case of the crude homogenate of interferon gamma the majority of impurities precipitate at lower precipitant concentration as needed for crystallization. Hence, the precipitant addition was done in two steps, the first step to achieve

host cell precipitation and the second step to achieve crystallization conditions, as shown in Figure 2.11. The crystals were harvested by centrifugation and two times washed at a high precipitant concentration with the same volume as the crystallization batch volume for one hour under slightly shaking. After each wash step the crystals were harvested again by centrifugation and the supernatant was discarded.

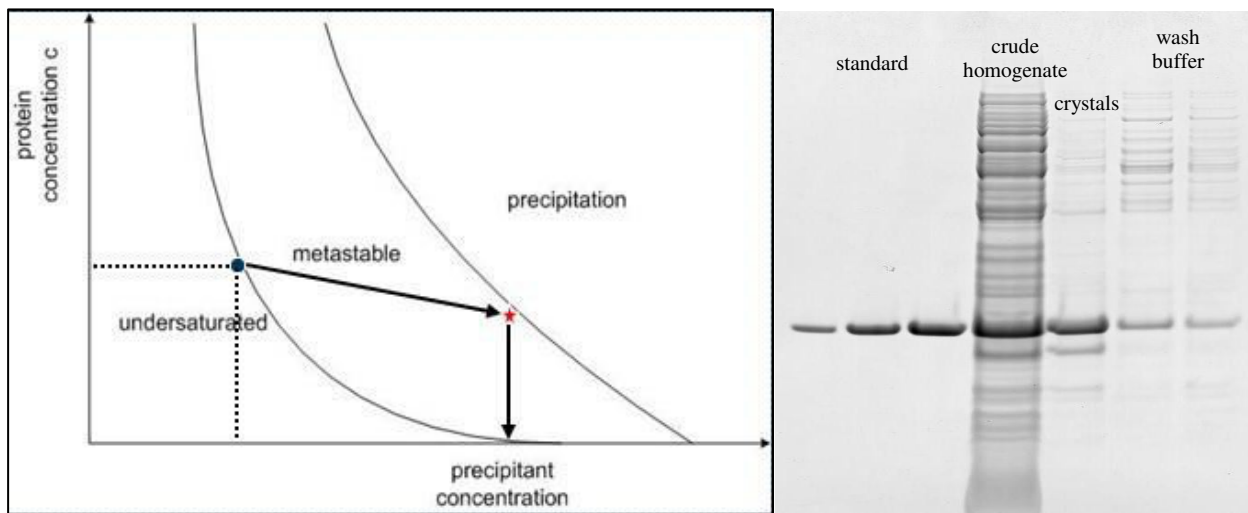


Figure 5.11: Schematic process of host cell precipitation followed by crystallization (left). (●): operating point for host cell precipitation, (★): operating point for subsequent crystallization of recombinant interferon gamma. Coomassie blue stained SDS-PAGE analysis (method provided by Boehringer Ingelheim RCV GmbH & Co KG, details not shown) of the subsequent crystallization.

In case of crystallization of the crude homogenate, the crystallization step yield and also the achieved purity were above 80 %, which was significant higher compared to the step yield of the chromatographic capture step of approximately 55 %.

The same procedure was used in case of the crystallization of the capture pool and again high yields and purities (~95 %) based on coomassie blue stained SDS-PAGE (method provided by Boehringer Ingelheim RCV GmbH & Co KG, details not shown) could be obtained. The crystallization step yield is more than twice of the step yield of the first intermediate step of ~40 %, but silver stained SDS-PAGE analysis revealed that the first intermediate step of the chromatography process achieved a higher purity. The dissolved crystals of the crystallized capture pool were further purified using the second intermediate column, as in this case the crystallization process replaces the first intermediate step. The results show that the additional upper and lower bands of the crystallization process were successfully depleted. The residual upper band could be also detected in the second intermediate pool (I 2) of the chromatographic process, even if it is significantly lower. (Figure 2.12).

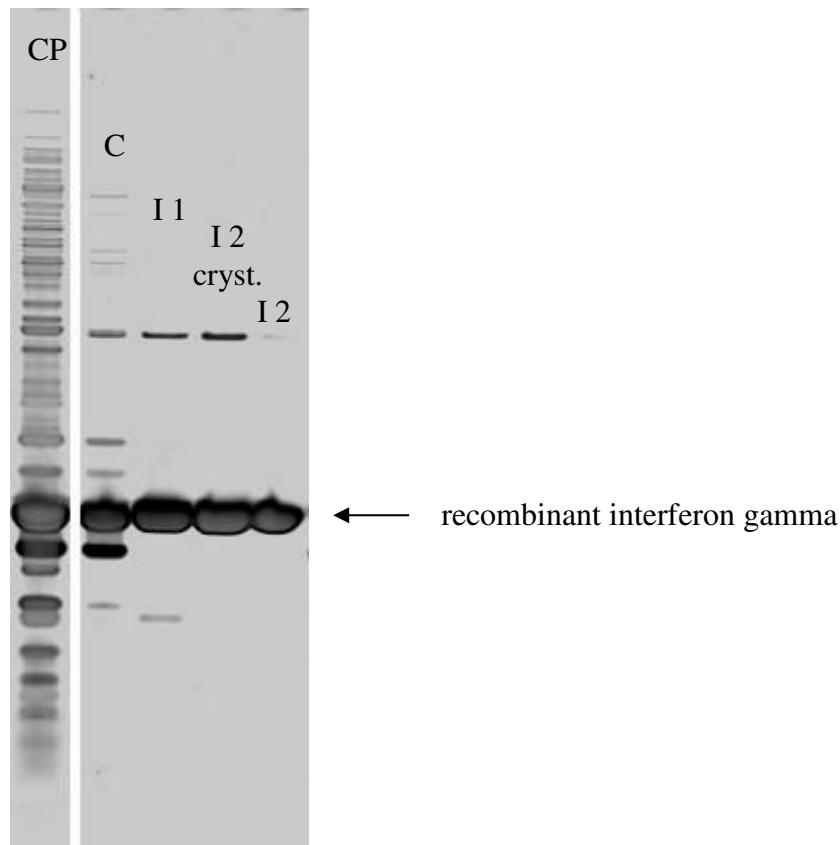


Figure 5.12: SDS-PAGE (silver stain) analysis (method provided by Boehringer Ingelheim RCV GmbH & Co KG, details not shown) of the crystallization process of the capture pool compared with the conventional process. CP: Capture Pool used for crystallization, C: dissolved crystals after crystallization of the capture pool, I 1: intermediate I pool of conventional process, I 2 cryst.: intermediate II pool generated of dissolved crystals as load, I 2: intermediate II pool of the conventional pool.

5.4.4 Optimization of pH and temperature

pH and temperature are strongly influenced by the solubility properties of the target protein and, hence, can alter the phase diagram. In addition, both parameters can also affect crystal growth behavior (Chayen, 2004; Wanka and Peukert, 2006). Dependency of the solubility of interferon gamma from temperature and pH are depicted in Figure 2.13. In both cases, the solubility could be strongly reduced. A reduction of the temperature below 15°C at 25 % ammonium sulfate decreases the solubility limit of 12.2 g/l at room temperature to below 2 g/l, but crystal growth is prolonged to 48 hours (instead of 5-20 h which was shown by Huettmann et al., 2015) and grown crystals have an unfavorable shape (needles).

A shift of pH in the basic range as well as in the acidic range also decreases the solubility of interferon gamma without altering the process time. The crystal shape of a cubic form was maintained in a pH range above 4.5 and below 9.5. Outside of this range heterogeneous crystal forms were detected (needles and cubic crystals). Temperature and pH shifts could be

used to further increase crystallization yields or reduce the needed amount of the used precipitate. In addition, these parameters can also have an influence on impurities in solution and can be used to achieve higher purities.

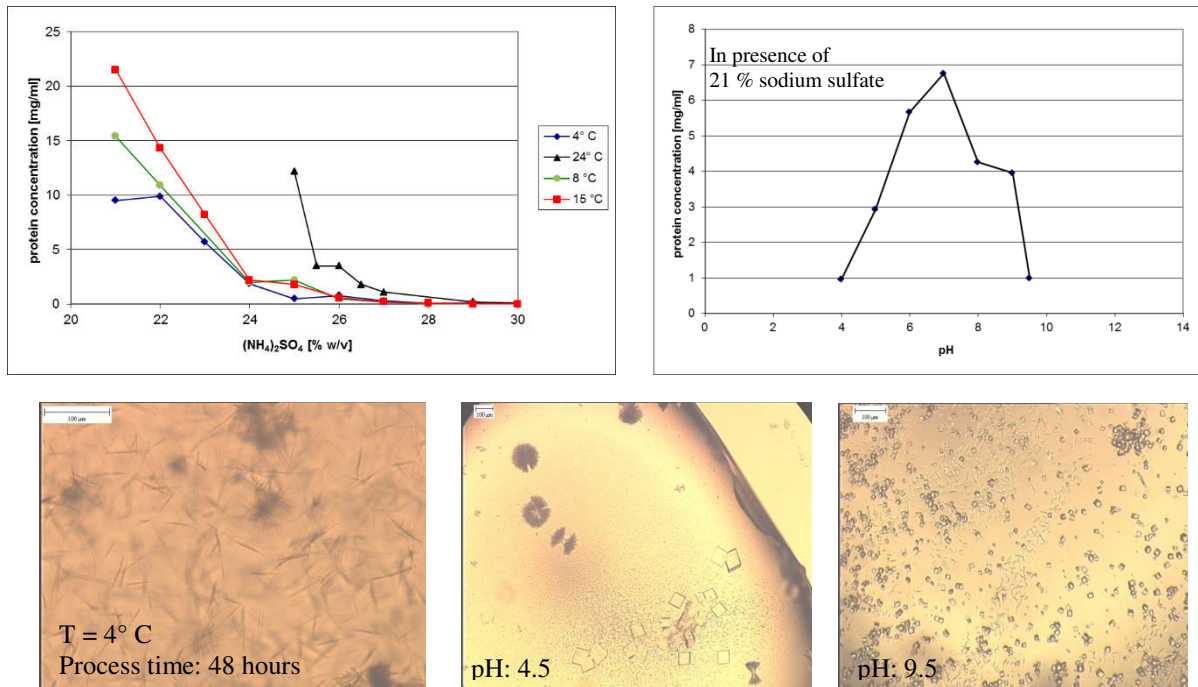


Figure 5.13: Temperature and pH dependency of the solubility of interferon gamma and the impact of crystal growth. Lowering of the temperature to 4 °C leads to elongated process times of 48 hours until crystals appear and alters the crystal habit to small needle crystals. pH values below 4.5 and above 9.5 resulted also in heterogeneous crystal morphology (needles and cubic crystals)

5.4.5 Control of the degree of supersaturation in the process by fed batch processes

Not only the degree of supersaturation but also the speed of supersaturation development has a strong impact on crystallization processes. A sudden rise of free energy can lead to precipitation instead of crystallization (Bergfors, 2003; McPherson, 2004). The use of fed batch processes instead of batch processes has some advantages like the control of the degree of supersaturation over time and the possibility to vary the speed of supersaturation development. This could be used to start at operating points just above the metastable zone to trigger nucleation followed by crystal growth in the metastable zone. This favors the growth of large crystals but is usually uneconomical since a lot of protein stays soluble at the end of a batch process. The adjustment of an appropriate feed rate of the precipitant would prevent the termination of growth by slowly increasing the precipitant concentration and would drive the crystallization process through the metastable zone until the solubility limit is rather zero. In

case of the single chain antibody, the solubility curve has a shallow progression and the solubility limit below the crystallization area is rather high. Also, the crystal growth is slow compared with interferon gamma where equilibrium is achieved in some hours. Introduction of a fed batch process significantly shortened the process times and increased the crystallization step yield. A batch crystallization process in a 150 ml scale using a stirred beaker glass as described in Huettmann et al., 2014 was started and terminated after 42 hours with ~50 % crystallization yield. The precipitant concentration was raised again as a second batch process and terminated after 24 hours again with ~50 % crystallization yield. In a last step a fed batch process was started rising the precipitant concentration slowly to 28 % sodium sulfate in 3.5 hours resulting in a crystallization step yield of nearly 100 % shown in Figure 2.14. The dilution caused by the fed batch process would result in a final protein concentration in the supernatant of 1 mg/ml if no crystallization would take place.

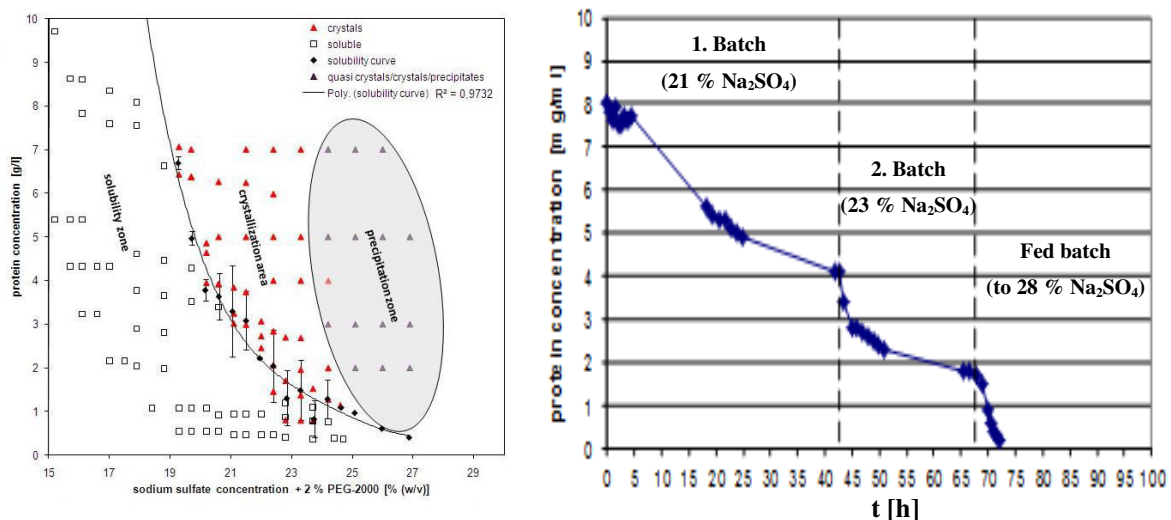


Figure 5.14: Phase diagram of the single chain antibody; adopted from Huettmann et al., 2014 (left) and crystallization times of batch and fed batch processes. The process times could be shortened significantly and the crystallization yield enhanced using a fed batch process.

5.5 Integrated Process

Process integration seems to be a powerful tool to combine two or more process steps in one step by maintaining the advantages of each single step, resulting in an economical process with enhanced selectivity (Huettmann et al., 2014). Given that in crystallization screens often high salt concentration and low concentration of polymers or high concentration of polymers

with low amounts of salts are combined to achieve successful conditions, often phase separation could be detected. In general, these phase separations are not of interest in the generation of crystals for X-ray analysis, but in case of industrial crystallization processes, phase separations are an additional process which has to be controlled (Kee et al., 2020; Pereira et al. 2020). Phase separations are aqueous two-phase systems (ATPS) and detailed described in literature. Especially their use to separate biomolecules is important, biomolecules will either accumulate in the top or in the bottom phase of such systems (Walter et al., 1972; Iqbal et al., 2016; Torres-Acosta et al., 2016). In case of the single chain antibody, successful crystallization conditions were achieved using high salt concentrations (sodium sulfate) and low amounts of polyethylene glycol 2000 as additive, resulting in 3-dimensional crystals and phase separation (Huettmann et al., 2014). The nucleation takes place in sodium sulfate rich phase or at the border to the polyethylene rich phase, but the crystal growth takes place in the polyethylene rich phase shown in Figure 2.15. Also, possible impurities will accumulate in one of the two phases, offering the chance, by adjusting the optimal ratio of polyethylene glycol and sodium sulfate, to achieve an additional separation of impurities and crystals.

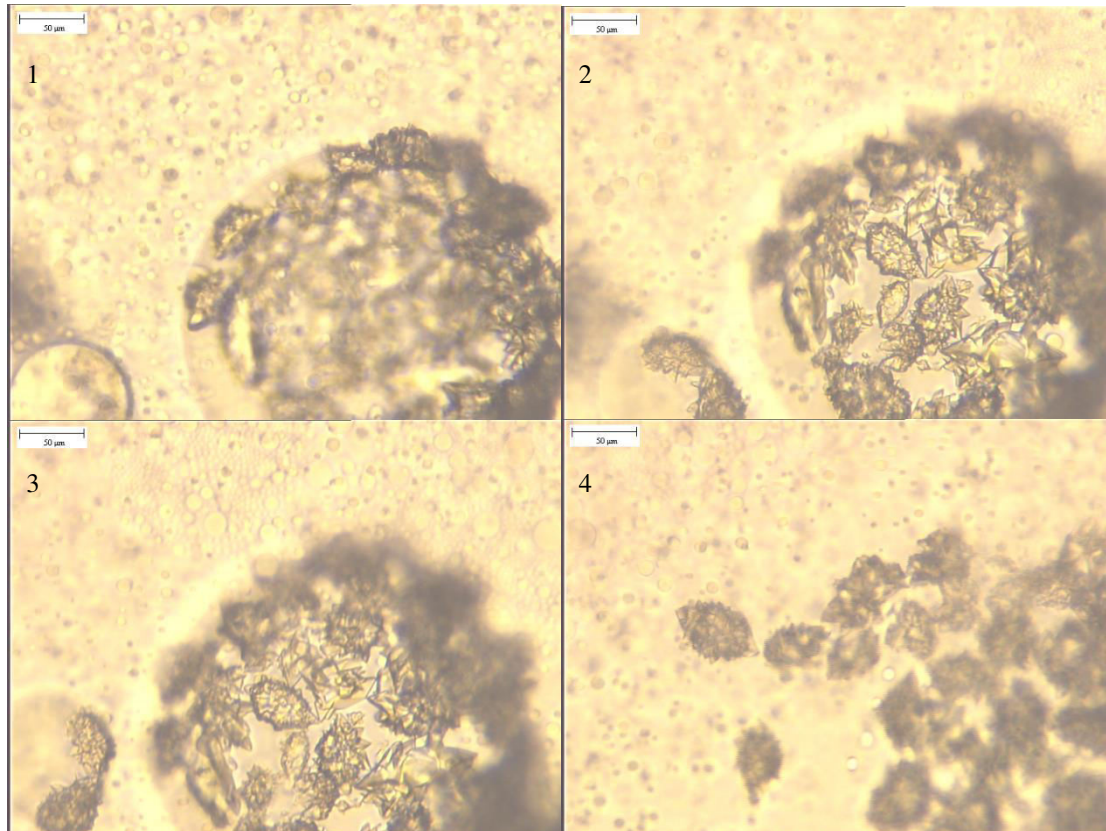


Figure 5.15: Accumulated crystals of the scFv in in the polyethylene glycol reach phase (1-3) and release of them in the surrounding salt rich phase (4); adopted from Huettmann et al., 2014.

5.6 Consideration for a Scale-up

Preparative crystallization processes are generally developed at small scale to reduce cost of goods and the limited amount of available product (Chayen, 2004; Filho et al., 2011). The successful scale up of mixing processes in stirred reactors is based on the similarity of reactor geometry and on the similarity of shear forces and flow fields. Important mixing parameters are the solids suspension to achieve the maximum contact area between solid and liquid phase, and controlled shear stress to avoid crystal breakage and secondary nucleation. Power input per volume and heat transfer are furthermore important (Kougoulus et al., 2006; Smejkal et al., 2013; Tait et al., 2009).

Given that it is not possible to keep all influencing forces and flow fields constant at both scales, only one parameter can be kept constant, the others will vary (Am Ende, 2010; Kougoulus et al., 2006; Prince and Smith, 2004). Hence a scale up could be either based on a constant solid suspension (homogeneity of suspension), constant tip speed (maximum shear stress), constant power input (power of mixing) or constant mixing time. The appropriate parameter for a scale up of a crystallization process has to be determined experimentally. A successful scale-up of crystallization processes of both proteins from 1 ml-scale to a stirred system in 100-200 ml scale were shown in Huettmann et al., 2014 and Huettmann et al., 2015.

6 Discussion

In this work an economical strategy to develop preparative crystallization processes for the purification of recombinant proteins was investigated. Given that crystallization has some benefits compared to conventional chromatographic separation techniques, since it combines unlimited scalability, very high selectivity, and low cost of goods, a general and practical approach to develop such processes is a high demand of the biopharmaceutical industry.

The different established techniques used to produce suitable crystals for X-ray analysis were investigated and adopted to meet requirements for development of an industrial crystallization process. Two recombinant proteins, interferon gamma and a single chain antibody, were successfully crystallized and crystal morphology was adjusted to achieve moderate 3-dimensional crystals in microliter scale. It could be demonstrated that the combination of vapor diffusion technique as initial screen, followed by microbatch technique as adjustment screen, is an appropriate strategy to find reproducible crystallization conditions and crystal morphology. As a third technique the millibatch method was established. This method closes the gap of unknown scalability because vapor diffusion and microbatch method are performed under conditions which are far from stirred tank crystallizations. Both methods are dedicated by an exorbitant surface volume ratio since they are performed in small droplets of only some microliters. The main area of the droplet surface is exposed either to air or oil, which is not the case in large scale. In addition, mechanical stress, which is caused by stirring in the tank, could not be considered in both methods. The millibatch method can partially mimic the large scale process since the surface volume ratio is in favor of the large scale process.

Furthermore, millibatch method is carried out in tubes with a more appropriate ratio of height and diameter (~3:1) than the droplets (~1:1). Mechanical stress was introduced by shaking of the tubes.

In a following step, phase diagrams with different precipitants were established. Phase diagrams are crucial for robust crystallization processes since they describe the interactions of the precipitant and the target protein. In case of interferon gamma three phase diagrams were generated depicting the undersaturated, metastable, nucleation and precipitation zone. The advantages and disadvantages of each phase diagram were discussed regarding the size of the nucleation and metastable zone, progression of the solubility curve and process times. It could be shown that ammonium phosphate is an inappropriate precipitant since the nucleation zone is rather small and crystallization time takes two days. In addition, the nucleation zone could

only be reached using a high amount of ammonium sulfate, which will lead to high dilutions of the protein solution resulting in low protein concentrations. In contrast, the use of ammonium sulfate or sodium sulfate as crystallization agents lead to phase diagrams with broad nucleation zones and short crystallization times (5 hours). Both precipitants have advantages, in case of sodium sulfate, a significant metastable zone could be detected in which optimal growth of large crystals is favored. In case of ammonium sulfate as precipitant, the dilution factor is reduced and the progression of the solubility curve is rather steep, which favors high crystallization yields already at moderate protein and precipitant concentration as shown in Figure 4.1.

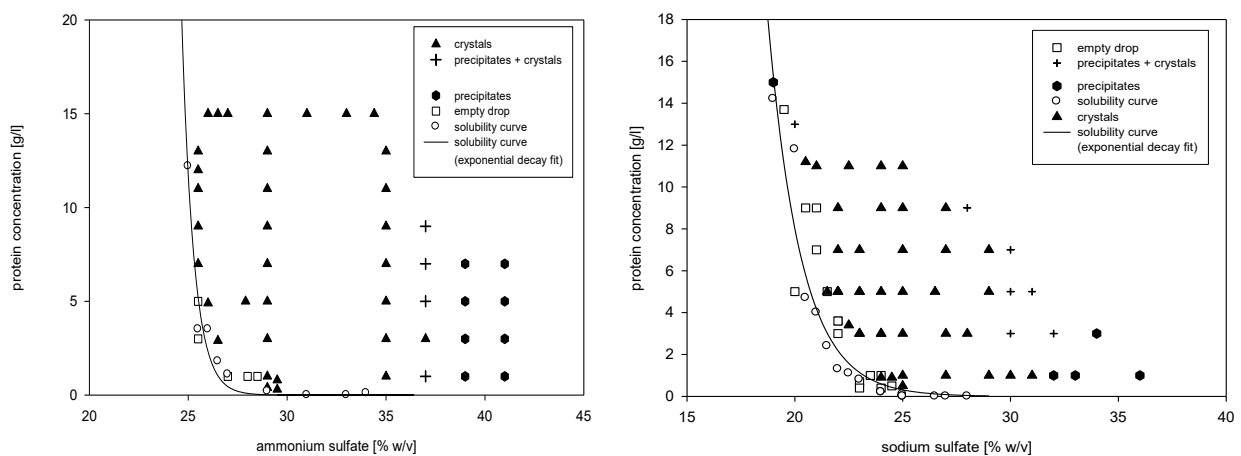


Figure 6.1: Phase diagrams of interferon gamma with ammonium sulfate (left) and sodium sulfate (right). In case of ammonium sulfate the steep progression of the solubility curve will assure high crystallization yields at moderate concentrations. In case of sodium sulfate a metastable zone between the solubility limit and the nucleation zone could be detected where optimal crystal growth can be achieved; adopted from Huettmann et al., 2015.

Based on the phase diagram different process designs and operating points were selected and investigated, also in impure solutions. In case of interferon, gamma crystallization could be performed in crude cell homogenate with support of seeding. Here, the crystallization area determined with the millibatch method was also confirmed by the seeding processes. A major challenge in crystallization of impure solutions was identified, the co-precipitation of host cell proteins. Investigation of the precipitation behavior of the host cell proteins in dependence of the crystallization agent revealed that the majority of impurities precipitate at lower amounts of crystallization agent than needed for crystallization conditions. In this case, the crystallization process was performed in two steps. In a first step, precipitant concentration was raised to a concentration before the solubility of the target protein was affected. After clarification of the precipitates the precipitant concentration in the supernatant was raised to

achieve crystallization conditions. The achieved crystallization yields were significantly higher than in the conventional interferon gamma process. In case of the crystallization of the crude homogenate and the second intermediate pool, the achieved purity was comparable or even higher than in the conventional process. In case of the crystallization of the capture pool, the achieved purity was lower than in the conventional process but could be compensated by the following purification step.

The change from batch processes to fed batch processes enabled the control of the degree of supersaturation as well as the speed to achieve supersaturation during the process. In case of the crystallization of the single chain antibody, the process time could be dramatically decreased, and the process was driven through a large metastable zone to a precipitant concentration where the solubility limit was close to zero.

Amplifying the phase diagrams by varying the pH and temperature show the potential to lower the needed amount of precipitant and can also alter the solubility properties of impurities. This can support to separate crystallization conditions of the target protein from conditions where impurities precipitate. It was also shown that variation of pH and temperature can alter growth behavior of the target protein and must be carefully checked regarding process times and crystal morphology.

Process integration was performed in the crystallization process of the single chain antibody. Due to the high content of sodium sulfate and the presence of polyethylene glycol an aqueous two-phase system was generated similar to the crystallization process. It could be shown that nucleation and growth of the scFv takes place in different phases. Nucleation takes place in the sodium rich phase and crystal growth in the polyethylene glycol rich phase.

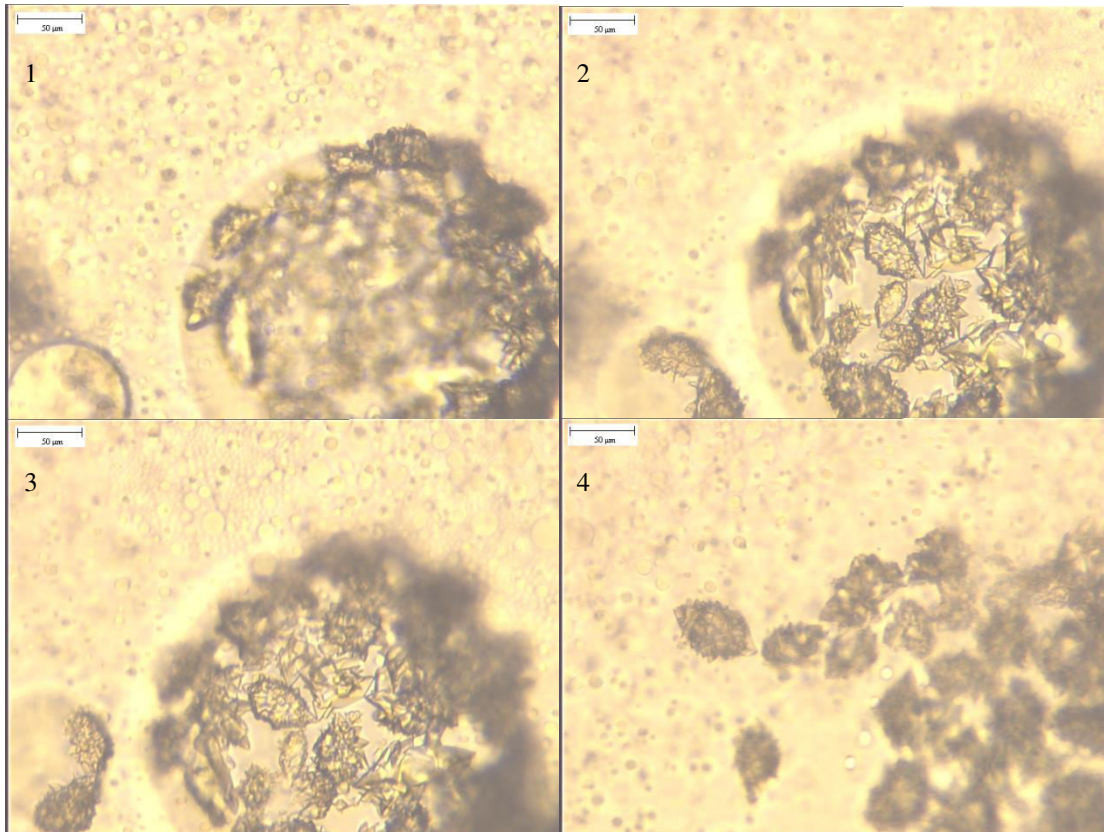


Figure 6.2: Accumulated crystals of the single chain antibody in in the polyethylene glycol reach phase (1-3) and release of them in the surrounding salt rich phase (4); adopted from Huetteman et al., 2014.

Varying of the concentration of sodium sulfate and polyethylene glycol can lead to accumulation of the soluble protein either in the top or bottom phase. Increasing of the polyethylene glycol content from 2 % to 9 % leads to a crystallization yield of nearly 100 %. Given that host cell proteins will also accumulate in the top or in the bottom phase, the separation of soluble impurities and protein as well as crystals can get further enhanced by optimal adjustment of the aqueous phase system.

7 Conclusion

In this work a general practical approach to develop industrial crystallization processes was to be generated and in summary it can be said that this was fulfilled:

- A systematical and practical approach to develop industrial crystallization process from screening of initial crystallization conditions in microliter scale to robust stirred crystallization processes in a several hundred milliliter scale was demonstrated using interferon gamma and a single chain antibody as model proteins.
-
- The importance of the selection of appropriate precipitants regarding crystal habit, crystallization yield, process time, and robustness was shown in the crystallization of interferon gamma.
- The key role of phase diagrams for process characterization and process knowledge was depicted and advantages and disadvantages of generated phase diagrams were discussed in detail. The reliability of the determined crystallization zone was also proven in the crystallization of impure solutions. In addition, the benefits and drawbacks of amplifying the generated phase diagrams by variation of pH and temperature were presented.
- The power of crystallization as purification step was demonstrated by achieving high yields and purities after crystallization of real process intermediates. Seeding technique was used in crystallization processes with loss of the nucleation zone. In addition, the advantages of fed batch processes compared to batch processes were shown by significantly shortened process times and enhanced crystallization yields.
- Process integration was identified as a promising tool to further improve the crystallization processes. Liquid-liquid extraction was integrated in the crystallization process of a single chain antibody. It was shown that nucleation and growth of crystals takes place in different phases. Optimal adjustment of the conditions can significantly increase the crystallization yield and furthermore can enhance separation of impurities and target protein in the phases.

8 References

- Affleck, R., Haynes, C. A., Clark, D. S., 1992. Solvent dielectric effects on protein dynamics. *Proceedings of the National Academy of Sciences*, 89(11), 5167-5170.
- Am Ende, D. J., 2010. *Manufacturing, Chemical Engineering in the Pharmaceutical Industry: R&D to Manufacturing*.
- Asherie, N., 2004. Protein crystallization and phase diagrams. *Methods*, 34(3), 266-272.
- Atha, D. H., Ingham, K. C., 1981. Mechanism of precipitation of proteins by polyethylene glycols. Analysis in terms of excluded volume. *Journal of Biological Chemistry*, 256(23), 12108-12117.
- Avrami, M., 1939. Kinetics of phase change. I General theory. *The Journal of chemical physics*, 7(12), 1103-1112.
- Barros Groß, M., Kind, M., 2017. Comparative study on seeded and unseeded bulk evaporative batch crystallization of tetragonal lysozyme. *Crystal growth & design*, 17(6), 3491-3501
- Barros Groß, M., Kind, M., 2018. From Microscale Phase Screening to Bulk Evaporative Crystallization of Proteins. *Journal of Crystal Growth* 498, 160-69
- Benvenuti, M., Mangani, S., 2007. Crystallization of soluble proteins in vapor diffusion for x-ray crystallography. *Nature protocols*, 2(7), 1633-1651.
- Breibeck, J., Rompel, A., 2019. Successful amphiphiles as the key to crystallization of membrane proteins: Bridging theory and practice. *Biochimica et Biophysica Acta-General Subjects*, 1863(2), 437-455.
- Bergfors, T., 2003. Seeds to crystals. *Journal of structural biology*. 142(1), 66-76
- Carbone, M. N., Etzel, M. R., 2006. Seeded isothermal batch crystallization of lysozyme. *Biotechnology and bioengineering*, 93(6), 1221-1224.
- Carugo, O., Argos, P., 1997. Protein—protein crystal-packing contacts. *Protein science*, 6(10), 2261-2263.
- Castro, F., Ferreira, A., Teixeira, J. A., Rocha, F., 2016. Protein Crystallization As a Process Step in a Novel Meso Oscillatory Flow Reactor: Study of Lysozyme Phase Behavior. *Crystal Growth & Design* 16(7), 3748-3755.
- Chayen, N. E., 2004. Turning protein crystallisation from an art into a science. *Current opinion in structural biology*, 14(5), 577-583.

- Chen, W., Li, X., Guo, M., Link, F. J., Ramli, S. S., Ouyang, J., Rosbottom, I., Heng, J. Y. Y., 2021. Biopurification of monoclonal antibody (mAb) through crystallization. *Separation and Purification Technology*, 263, 118358.
- Chernov, A. A., 2003. Protein crystals and their growth. *Journal of structural biology*, 142(1), 3-21.
- Chirgadze, D., 2001. *Protein crystallisation in action*. University of Cambridge.
- Cudney, R., Patel, S., Weisgraber, K., Newhouse, Y., McPherson, A., 1994. Screening and optimization strategies for macromolecular crystal growth. *Acta Crystallographica Section D: Biological Crystallography*, 50(4), 414-423.
- De Souza, F. P., Neto, A. A., Fossey, M. A., Neto, J. R., 2007. The effect of changes in the bulk dielectric constant on the DNA torsional properties. *Biopolymers: Original Research on Biomolecules*, 87(4), 244-248.
- D'Arcy, A., Mac Sweeney, A., Haber, A., 2004. Practical aspects of using the microbatch method in screening conditions for protein crystallization. *Methods*, 34(3), 323-328.
- DeLucas, L. J., Bray, T. L., Nagy, L., McCombs, D., Chernov, N., Hamrick, D., Chait, A., 2003. Efficient protein crystallization. *Journal of structural biology*, 142(1), 188-206.
- Duong-Ly, K. C., Gabelli, S. B., 2014. Salting out of proteins using ammonium sulfate precipitation. *Methods in enzymology*, 541, 85-94.
- Elkordy, A. A., Forbes, R. T., Barry, B. W., 2004. Stability of crystallised and spray-dried lysozyme. *International Journal of Pharmaceutics*, 278, 209–219
- Erdemir, D., Lee, A. Y., Myerson, A. S., 2009. Nucleation of crystals from solution: classical and two-step models. *Accounts of chemical research*, 42(5), 621-629.
- Etzel, M. R., 2006. Bulk protein crystallization—principles and methods. Editor(s): Shukla, A., Etzel M., Gadam S., *Process Scale Bioseparations for the Biopharmaceutical Industry*, 181-200.
- Filho, A., Hirata, G., Watanabe, É., Miranda, É., 2011. Precipitation and crystallization. *Comprehensive Biotechnology (Second Edition)*, 2(46), 651-663.
- Galkin, O., Vekilov, P. G., 2000. Control of protein crystal nucleation around the metastable liquid–liquid phase boundary. *Proceedings of the National Academy of Sciences*, 97(12), 6277-6281.
- Gavira, J. A., 2016. Current trends in protein crystallization. *Archives of biochemistry and biophysics*, 602, 3-11.
- George, A., Wilson, W. W., 1994. Predicting protein crystallization from a dilute solution property. *Acta Crystallographica Section D: Biological Crystallography*, 50(4), 361-365.

- Gilliland, G. L., 1988. A biological macromolecule crystallization database: a basis for a crystallization strategy. *Journal of crystal growth*, 90(1-3), 51-59.
- Giulietti, M., Seckler, M. M., Derenzo, S., Ré, M. I., Cekinski, E., 2001. Industrial crystallization and precipitation from solutions: state of the technique. *Brazilian Journal of Chemical Engineering*, 18(4), 423-440.
- Gottschalk, U., 2005. New and unknown challenges facing biomanufacturing: An editorial. *BioPharm international*, 18(3), 24-28.
- Haas, C., Drenth, J., 1999. Understanding protein crystallization on the basis of the phase diagram. *Journal of crystal growth*, 196(2-4), 388-394.
- Haidinger S.A., 2014. Scale-Up of Batch Protein Crystallization Processes for Industrial Application. Master Thesis, Institute of Bioprocess Science and Engineering, University of Natural Resources and Life Sciences, Vienna, Austria.
- Haire, L. F., Blow, D. M., 2001. A novel spin filter method for the measurement of solubility. *Journal of crystal growth*, 232(1-4), 17-20.
- Hebel, D., Ürdingen, M., Hekmat, D., Weuster-Botz, D., 2013. Development and scale up of high-yield crystallization processes of lysozyme and lipase using additives. *Crystal growth & design*, 13(6), 2499-2506.
- Hekmat, D., Hebel, D., Schmid, H., Weuster-Botz, D., 2007. Crystallization of lysozyme: From vapor diffusion experiments to batch crystallization in agitated ml-scale vessels *Process Biochemistry*, 42(12), 1649-1654.
- Hekmat, D., 2015a. Large-scale crystallization of proteins for purification and formulation. *Bioprocess and biosystems engineering*, 38(7), 1209-1231.
- Hekmat, D., Breitschwerdt P., Weuster-Botz, D., 2015b. Purification of Proteins from Solutions Containing Residual Host Cell Proteins via Preparative Crystallization. *Biotechnology Letters*, 37(9), 1791-1801.
- Hekmat, D., Huber, M., Lohse, C., Von Den Eichen, N., Weuster-Botz, D., 2017. Continuous Crystallization of Proteins in a Stirred Classified Product Removal Tank with a Tubular Reactor in Bypass. *Crystal Growth & Design* 17(8), 4162-4169.
- Hofmeister, F., 1888. On the understanding of the effect of salts. Second report. On regularities in the precipitating effect of salts and their relationship to their physiological behavior. *Nauyen-Schmiedebergs Archiv für Experimentelle Pathologie und Pharmakologie (Leipzig)*, 24, 247-260.
- Hubbich, J., Kind, M., Nirschl, H., 2019. Preparative Protein Crystallization. *Chemical Engineering & Technology* 42(11), 2275-2281.

- Huettmann, H., Berkemeyer, M., Buchinger, W., Jungbauer, A., 2014. Preparative crystallization of a single chain antibody using an aqueous two-phase system. *Biotechnology and Bioengineering*, 111(11), 2192-2199.
- Huettmann, H., Zich, S., Berkemeyer, M., Buchinger, W., Jungbauer, A., 2015. Design of industrial crystallization of interferon gamma: phase diagrams and solubility curves. *Chemical Engineering Science*, 126, 341-348.
- Iqbal, M., Tao, Y., Xie, S., Zhu, Y., Chen, D., Wang, X., Yuan, Z., 2016. Aqueous two-phase system (ATPS): an overview and advances in its applications. *Biological procedures online*, 18(1), 1-18.
- Jacobsen, C., Garside, J., Hoare, M., 1998. Nucleation and growth of microbial lipase crystals from clarified concentrated fermentation broths. *Biotechnology and bioengineering*, 57(6), 666-675.
- Jancarik, J. A. K. S., Kim, S. H., 1991. Sparse matrix sampling: a screening method for crystallization of proteins. *Journal of applied crystallography*, 24(4), 409-411.
- Jen, A., Merkle, H. P., 2001. Diamonds in the rough: protein crystals from a formulation perspective. *Pharmaceutical Research*, 18(11), 1483-1488.
- Judge, R. A., Johns, M. R., White, E. T., 1995. Protein purification by bulk crystallization: the recovery of ovalbumin. *Biotechnology and Bioengineering*, 48(4), 316-323.
- Judge, R. A., Forsythe, E. L., Pusey, M. L., 1998. The effect of protein impurities on lysozyme crystal growth. *Biotechnology and Bioengineering*, 59(6), 776-785.
- Judge, R. A., Jacobs, R. S., Frazier, T., Snell, E. H., Pusey, M. L., 1999. The effect of temperature and solution pH on the nucleation of tetragonal lysozyme crystals. *Biophysical journal*, 77(3), 1585-1593.
- Kantardjieff, K. A., Rupp, B., 2004. Protein isoelectric point as a predictor for increased crystallization screening efficiency. *Bioinformatics*, 20(14), 2162-2168.
- Kee, P. E., Ng, T.-C., Lan, J. C.-W., Ng, H.-S., 2020. Recent Development of Unconventional Aqueous Biphasic System: Characteristics, Mechanisms and Applications. *Critical Reviews in Biotechnology* 40(4), 555-569.
- Kelley, B., 2006. Designing a 10 ton antibody process: Is conventional chromatography limiting. In 232nd American Chemical Society National Meeting. Sept 1014, BIOT division, paper 133.
- Kim, Y., Babnigg, G., Jedrzejczak, R., Eschenfeldt, W. H., Li, H., Maltseva, N., Hatzos-Skintges, C., Gu, M., Makowska-Grzyska, M., Wu, R., An, H., Chhor, G., Joachimiak, A.,

2011. High-throughput protein purification and quality assessment for crystallization. *Methods*, 55(1), 12-28.
- Kirkwood, J., Hargreaves, D., O'Keefe, S., & Wilson, J., 2015. Analysis of crystallization data in the Protein Data Bank. *Acta Crystallographica Section F: Structural Biology Communications*, 71(10), 1228-1234.
- Klijn, M. E., Hubbuch, J., 2020. Time-Dependent Multi-Light-Source Image Classification Combined With Automated Multidimensional Protein Phase Diagram Construction for Protein Phase Behavior Analysis. *Journal of Pharmaceutical Science*, 109(1), 331-339.
- Klyushnichenko, V., 2003. Protein crystallization: from HTS to kilogram-scale. *Current Opinion in Drug Discovery and Development*, 6, 848–854.
- Kołodziej, M., Olbrycht, M., Poplewska, I., Piątkowski, W., Antos, D. Forced Convection Evaporation for Bulk Protein Crystallization. *Crystal Growth & Design* 18(9), 5194-5201.
- Kougoulos, E., Jones, A. G., Wood-Kaczmar, M. W., 2006. Process modelling tools for continuous and batch organic crystallization processes including application to scale-up. *Organic process research & development*, 10(4), 739-750.
- Lee, T. S., Vaghjiani, J. D., Lye, G. J., Turner, M. K., 2000. A systematic approach to the large-scale production of protein crystals. *Enzyme and Microbial Technology* 26, 582–592.
- Liu, J. J., Ma, C. Y., Hu, Y. D., Wang, X. Z., 2010. Effect of seed loading and cooling rate on crystal size and shape distributions in protein crystallization — A study using morphological population balance simulation. *Computers & Chemical Engineering*, 34(12), 1945-1952.
- Liu, Y., Hou, H., Li, J., Cheng, Q. D., Zhang, X., Zeng, X. B., Yin, D. C., 2020. Direct crystallization of proteins from impure sources. *Crystal Growth & Design*, 20(3), 1694-1705.
- Lomakin, A., Asherie, N., Benedek, G. B., 2003. Liquid-solid transition in nuclei of protein crystals. *Proceedings of the National Academy of Sciences*, 100(18), 10254-10257.
- Lorber, B., Skouri, M., Munch, J. P., Giegé, R., 1993. The influence of impurities on protein crystallization; the case of lysozyme. *Journal of crystal growth*, 128(1-4), 1203-1211.
- Low, D., O'Leary, R., Pujar, N. S., 2007. Future of antibody purification. *Journal of Chromatography, B Volume* 84(1), 48-63.
- Lu, J., Wang, X. J., Ching, C. B., 2002. Batch Crystallization of Soluble Proteins: Effect of Precipitant, Temperature and Additive. *Progress in Crystal Growth and Characterization of Materials*, 45(3), 195-205.

- Luft, J. R., Snell, E. H., DeTitta, G. T., 2011. Lessons from high-throughput protein crystallization screening: 10 years of practical experience. *Expert opinion on drug discovery*, 6(5), 465-480.
- Matthews, L. A., Duong, A., Prasad, A. A., Duncker, B. P., Guarné, A., 2009. Crystallization and preliminary X-ray diffraction analysis of motif N from *Saccharomyces cerevisiae* Dbf4. *Acta Crystallographica Section F: Structural Biology and Crystallization Communications*, 65(9), 890-894.
- McPherson, A., Koszelak, S., Axelrod, H., Day, J., Williams, R., Robinson, L., Cascio, D., 1986. An experiment regarding crystallization of soluble proteins in the presence of beta-octyl glucoside. *Journal of Biological Chemistry*, 261(4), 1969-1975.
- McPherson, A., 1999. Crystallization of biological macromolecules, 586.
- McPherson, A., 2004. Introduction to protein crystallization. *Methods*, 34(3), 254-265.
- McPherson, A., Cudney, B., 2014. Optimization of crystallization conditions for biological macromolecules. *Acta Crystallographica Section F: Structural biology communications*, 70(Pt 11), 1445–1467.
- McPherson, A., Gavira, J. A., 2014. Introduction to protein crystallization. *Acta Crystallographica Section F: Structural Biology Communications*, 70(1), 2-20.
- Meenan, P. A., Anderson, S.R., Klug, D.L., 2002. 3 - The influence of impurities and solvents on crystallization. Editor(s): Myerson, A. S., *Handbook of Industrial Crystallization (Second Edition)*.
- Mustafa, A. O., Derrick, J. P., Tiddy, G. J., Ford, R. C., 1998. A novel approach for the crystallization of soluble proteins using non-ionic surfactants. *Acta Crystallographica Section D: Biological Crystallography*, 54 (1), 154-157.
- Myerson, A.S., Toyokura, K., 1990. Crystallization as a separation process. *ACS Symposium Series Volume 438*, 419.
- Neugebauer, P., Khinast, J. G., 2015. "Continuous Crystallization of Proteins in a Tubular Plug-Flow Crystallizer. *Crystal Growth & Design* 15(3), 1089-1095.
- Neugebauer, J. M., 1990. [18] Detergents: An overview. *Methods in enzymology*, 182, 239-253.
- Obermair, Y., 2014. Protein Crystallization, Scale Up and Crystal Wash. Master Thesis, Department of Applied Life Science, University of Applied Sciences FH Campus Wien.
- Pechenov, S., Shenoy, B., Yang, M. X., Basu, S. K., Margolin, A. L., 2004. Injectable controlled release formulations incorporating protein crystals. *Journal of controlled release*, 96 (1), 149-158.

- Pereira, J. F.B, Freire, M. G., Coutinho, J. A. P., 2020. Aqueous Two-phase Systems: Towards Novel and More Disruptive Applications. *Fluid Phase Equilibria* 505, 112341.
- Peters, J., Minuth, T., Schröder, W., 2005. Implementation of a crystallization step into the purification process of a recombinant protein. *Protein expression and purification*, 39(1), 43-53.
- Poplewska, I., Łyskowski, A., Kołodziej, M., Szałański, P., Piątkowski, W., Antos, D., 2018. Determination of Protein Crystallization Kinetics by a Through-flow Small-angle X-ray Scattering Method. *Chemical Engineering Research & Design*, 141, 580-591
- Prince, K., Smith, M., 2004. Purification process scale-up. In *Protein Purification Protocols*, Humana Press, 244, 463-480.
- Privé, G. G., 2007. Detergents for the stabilization and crystallization of membrane proteins. *Methods*, 41(4), 388-397.
- Pu, S., Hadinoto, K., 2020. Continuous Crystallization as a Downstream Processing Step of Pharmaceutical Proteins: A Review. *Chemical Engineering Research & Design*, 160, 89-104.
- Pusey, M. L., Snyder, R. S., Naumann, R., 1986. Protein crystal growth. Growth kinetics for tetragonal lysozyme crystals. *Journal of Biological Chemistry*, 261(14), 6524-6529.
- Roque, A. C. A., Pina, A. S., Azevedo, A. M., Aires-Barros, R., Jungbauer, A., Di Profio, G., Heng, J. Y. Y., Haigh, J., Ottens, M., 2020. Anything but Conventional Chromatography Approaches in Bioseparation. *Biotechnology Journal*, 15(8):1900274
- Rupp, B., Wang, J., 2004. Predictive models for protein crystallization. *Methods*, 34(3), 390-407.
- Russo Krauss, I., Merlino, A., Vergara, A., Sica, F., 2013. An overview of biological macromolecule crystallization. *International journal of molecular sciences*, 14(6), 11643-11691.
- Saikumar, M. V., Glatz, C. E., Larson, M. A., 1998. Lysozyme crystal growth and nucleation kinetics. *Journal of crystal growth*, 187(2), 277-288.
- Saridakis, E., Chayen, N. E., 2009. Towards a 'universal' nucleant for protein crystallization. *Trends in biotechnology*, 27(2), 99-106.
- Schmidt, S., Havekost, D., Kaiser, K., Kauling, J., Henzler, H. J., 2005. Crystallization for the downstream processing of proteins. *Engineering in life sciences*, 5(3), 273-276.
- Shenoy, B., Wang, Y., Shan, W., Margolin, A. L., 2001. Stability of crystalline proteins. *Biotechnology and Bioengineering*, 73(5), 358-369.

- Skouri, M., Lorber, B., Giegé, R., Munch, J. P., Candau, J. S., 1995. Effect of macromolecular impurities on lysozyme solubility and crystallizability: dynamic light scattering, phase diagram, and crystal growth studies. *Journal of crystal growth*, 152(3), 209-220.
- Smejkal, B., Helk, B., Rondeau, J.-M., Anton, S., Wilke, A., Scheyerer, P., Fries, J., Hekmat, D., Weuster-Botz, D., 2013a. Protein Crystallization in Stirred Systems-scale-up via the Maximum Local Energy Dissipation. *Biotechnology and Bioengineering* 110(7), 1956-1963
- Smejkal, B., Agrawal, N. J., Helk, B., Schulz, H., Giffard, M., Mechelke, M., Ortner, F., Heckmeier, P., Trout, B. L., Hekmat, D., 2013b. Fast and Scalable Purification of a Therapeutic Full-length Antibody Based on Process Crystallization. *Biotechnology and Bioengineering*, 110(9), 2452-2461.
- Tait, S., White, E.T., Litster, J.D., 2009. "A Study on Nucleation for Protein Crystallization in Mixed Vessels. *Crystal Growth & Design* 9(5), 2198-2206.
- Takakura, T., Ito, T., Yagi, S., Notsu, Y., Itakura, T., Nakamura, T., Inagaki, K., Esaki, N., Hoffman, R.M., Takimoto, A., 2006. High-level expression and bulk crystallization of recombinant l-methionine [γ]-lyase, an anticancer agent. *Applied Microbiology and Biotechnology*, 70(2), 183-192.
- Thömmes, J., Etzel, M., 2007. Alternatives to chromatographic separations. *Biotechnology progress*, 23(1), 42-45.
- Torres-Acosta, M. A., Mayolo-Deloya, K., González-Valdez, J., Rito-Palomares, M., 2019. Aqueous Two-Phase Systems at Large Scale: Challenges and Opportunities. *Biotechnology journal*, 14(1), 1800117.
- Vekilov, P. G., 2010. Nucleation. *Crystal growth & design*, 10(12), 5007-5019.
- Von Hippel, P. H., Wong, K. Y., 1964. Neutral salts: the generality of their effects on the stability of macromolecular conformations. *Science*, 145(3632), 577-580.
- Vuolanto, A., Uotila, S., Leisola, M., Visuri, K., 2003. Solubility and crystallization of xylose isomerase from *Streptomyces rubiginosus*. *Journal of crystal growth*, 257 (3-4), 403-411.
- Walter H., Sasakawa, S., Albertsson, P-A., 1972. Cross-partition of proteins. Effect of ionic composition and concentration, *Biochemistry* 11(21), 3880–3883.
- Wanka, J., Peukert, W., 2006. The meaning of the second osmotic virial coefficient for the protein crystallization. *Chemie Ingenieur Technik*, 78(3), 273-278.
- Watson, A. A., Christou, C. M., O'Callaghan, C. A., 2011. Expression, purification and crystallization of the human UL16-binding protein ULBP1. *Protein Expression and Purification*, 79(1), 44-48.

- Zang Y, Kammerer B, Eisenkolb M, Lohr K, Kiefer H., 2011. Towards protein crystallization as a process step in downstream processing of therapeutic antibodies: Screening and optimization at microbatch scale. *PloS ONE*, 6(9), e25282
- Zhou, H. X., Pang, X., 2018. Electrostatic interactions in protein structure, folding, binding, and condensation. *Chemical reviews*, 118(4), 1691-1741.

9 Publications

Publication I:

Huettmann, H., Berkemeyer, M., Buchinger, W., Jungbauer, A., 2014. Preparative crystallization of a single chain antibody using an aqueous two-phase system. Published in *Biotechnology and Bioengineering*, 111(11), 2192-2199.

DOI: [10.1002/bit.25287](https://doi.org/10.1002/bit.25287)

Contribution to the publication:

Hauke Hüttmann designed, conducted and evaluated the experiments. Hauke Hüttmann drafted the manuscript and revised it together with Prof. Alois Jungbauer.

Publication II:

Huettmann, H., Zich, S., Berkemeyer, M., Buchinger, W., Jungbauer, A., 2015. Design of industrial crystallization of interferon gamma: phase diagrams and solubility curves. Published in *Chemical Engineering Science*, 126, 341-348.

DOI: [10.1016/j.ces.2014.12.018](https://doi.org/10.1016/j.ces.2014.12.018)

Contribution to the publication:

Hauke Hüttmann has jointly designed the experiments with his colleagues. Hauke Hüttmann conducted and evaluated the experiments,, except the establishment of solubility curves for sodium chloride, di-ammonium hydrogen phosphate and PEG-4000, these were conducted and evaluated by Susanne Zich. Hauke Hüttmann drafted the manuscript and revised it together with Susanne Zich and Prof. Jungbauer.

Publication I

Preparative Crystallization of a Single Chain Antibody Using an Aqueous Two-Phase System

Hauke Huettmann,¹ Matthias Berkemeyer,¹ Wolfgang Buchinger,¹ Alois Jungbauer²

¹Boehringer Ingelheim RCV GmbH & CoKG, Dr. Boehringer Gasse 5-11, Vienna A-1121, Austria

²Department of Biotechnology, University of Natural Resources and Life Sciences, Vienna, Muthgasse 18, Vienna 1190, Austria; telephone: +43 1 47654 6226; fax: +43 1 3697615; e-mail: alois.jungbauer@boku.ac.at

ABSTRACT: A simultaneous crystallization and aqueous two-phase extraction of a single chain antibody was developed, demonstrating process integration. The process conditions were designed to form an aqueous two-phase system, and to favor crystallization, using sodium sulfate and PEG-2000. At sufficiently high concentrations of PEG, a second phase was generated in which the protein crystallization occurred simultaneously. The single chain antibody crystals were partitioned to the top, polyethylene glycol-rich phase. The crystal nucleation took place in the sodium sulfate-rich phase and at the phase boundary, whereas crystal growth was progressing mainly in the polyethylene glycol-rich phase. The crystals in the polyethylene glycol-rich phase grew to a size of $>50\ \mu\text{m}$. Additionally, polyethylene glycol acted as an anti-solvent, thus, it influenced the crystallization yield. A phase diagram with an undersaturation zone, crystallization area, and amorphous precipitation zone was established. Only small differences in polyethylene glycol concentration caused significant shifts of the crystallization yield. An increase of the polyethylene glycol content from 2% (w/v) to 4% (w/v) increased the yield from approximately 63–87%, respectively. Our results show that crystallization in aqueous two-phase systems is an opportunity to foster process integration.

Biotechnol. Bioeng. 2014;111: 2192–2199.

© 2014 Wiley Periodicals, Inc.

KEYWORDS: recombinant protein; industrial crystallization; aqueous two-phase extraction; phase diagram; single chain antibody

Introduction

Bulk crystallization and aqueous two-phase extraction can be integrated into a single process, and may be an alternative for the purification of therapeutic proteins, such as single chain antibodies. Small molecule pharmaceuticals and industrial enzymes are routinely purified by crystallization (Myerson and Toyokura, 1990), but the purification of biopharmaceuticals is rarely applied on the industrial scale, with the exception of a few well-known examples, such as insulin.

Indeed, the crystallization of proteins has gained a reputation for being an exacting and difficult task (McPherson, 1990). This is due, in part, to the many solution parameters that must be taken into account, such as pH, temperature, buffer type and concentration, effects of different precipitants, and effects of impurities (Lorber et al., 1993; McPherson, 1999). Some examples for bulk crystallization or crystallization of proteins from impure solutions are the crystallizations of lipase (Jacobsen et al., 1997; Lee et al., 2000), lysozyme (Judge et al., 1998; Lorber et al., 1993), ovalbumin (Judge et al., 1995), L-methionine γ -lyase (Takakura et al., 2006), an aprotinin variant (Peters et al., 2004), and an intact monoclonal IgG₄ (Zang et al., 2011).

Protein crystals are also stable (Shenoy et al., 2001), and, therefore, an excellent intermediate form for storage. Crystallization also represents an alternative formulation (Basu et al., 2004; Govardhan et al., 2005) to costly lyophilization procedures (Webb et al., 2002). Optimized bulk crystallization can provide high yield and purity, considerable volume reduction, short process times, nearly unlimited scalability, and low cost of goods, due to inexpensive chemicals (Etsel, 2006). Some proposals for a

Abbreviations: ATPS, aqueous two-phase system; PEG-2000, polyethylene glycol, with an average molecular weight of 2000 Da; w/v, weight per volume; MW, molecular weight; HEPES, 2-[4-(2-Hydroxyethyl)-1-piperazinyl]-ethanesulfonic acid; w/w, weight per weight; PEG, polyethylene glycol; A, point on the binodal curve depicting the total composition of an immiscible solution; B, point on the binodal curve depicting the composition of the bottom phase; T, point on the binodal curve depicting the composition of the top phase; K, partition coefficient; G, partition ratio; c, c_p, protein concentration; V, volume; t, top phase; b, bottom phase; X, amount of phase forming component; ρ , density of solution [g/mL]; 0, concentration of a particular component in the total system.

Correspondence to: A. Jungbauer

Received 25 January 2014; Revision received 28 March 2014; Accepted 5 May 2014

Accepted manuscript online 2 June 2014;

Article first published online 8 September 2014 in Wiley Online Library (<http://onlinelibrary.wiley.com/doi/10.1002/bit.25287/abstract>).

DOI 10.1002/bit.25287

general approach to generate a bulk crystallization process have been described (Lee et al., 2000; Schmidt et al., 2004; Zang et al., 2011).

Liquid–liquid extraction, using an aqueous two-phase system in particular, is also an effective, alternative purification technique to chromatography (Azevedo et al., 2009; Rosa et al., 2010). Two-phase systems occur when two polymers, one polymer, and one kosmotropic salt, or two salts, one chaotropic salt and one kosmotropic salt, are mixed together at appropriate concentrations or at a particular temperature. The two-phases are mostly composed of water (60–80%), and the formation of the distinct phases is affected by pH, temperature, and ionic strength.

Aqueous two-phase systems provide mild conditions, which are more appropriate to partitioning biomolecules than conventional water-organic solvent systems (Philipson et al., 1960; Walter et al., 1972). The interfacial tension between both phases is much lower than in the water-organic solvent systems, hence, the integrity of the molecules and their special activity is maintained (Kim and Rha, 2000a,b; Wu et al., 1996). Since these phase components are inert towards biological materials, they can easily be employed to partition biomolecules. The partitioning coefficient (K) is a characteristic used to evaluate the partitioning of the protein in the phases.

The basis of partitioning depends upon surface properties of the particles and molecules, which include size, charge, and hydrophobicity (Walter and Johansson, 1994). The small droplets, which are generated in a stirred-phase system, also produce short distances and large surface areas, facilitating mass transfer of biomolecules. The most salient feature of the two-phase system is its high water content, which, when complemented with suitable buffers and salts, provides a suitable milieu for biological materials, and can easily be scaled-up (Cascone et al., 1991; Kroner et al., 1982; Veide et al., 1983) to produce high yields (Fauquex et al., 1985; Kula et al., 1981).

Here, we have investigated a combined extraction and crystallization process of a single chain antibody. The aqueous two-phase system was generated using polyethylene glycol as an additive to improve crystal shape in a salt-induced crystallization process. This process consisted of crystallization with concurrent extraction. The dissolved protein was first partitioned into the separated phases at a distinct ratio, then, during the crystallization, when the protein undergoes a state-change from liquid to solid, partitioning in the single phases changed. The results from this study show how an integrated process of crystallization and aqueous two-phase extraction can be implemented and optimized to produce greater purity and yield of protein crystals, appropriate for industrial uses.

Materials and Methods

All methods were carried out at room temperature.

Reagents

Polyethylene glycol was purchased from MERCK-Schuchardt, Hohenbrunn, Germany. Sodium sulfate (anhydrous),

ammonium acetate, sodium chloride, sodium acetate trihydrate, and HEPES were purchased from Merck KGaA, Darmstadt, Germany. The single chain antibody was provided by Boehringer Ingelheim RCV GmbH & Co KG. Water was purified using a euRO 20 DI reverse osmosis system, obtained from SG Water, Barsbüttel, Germany.

Determination of the Binodal Curve and Tie-Lines

Determination of the binodal curve was carried out using the cloud point method. Five tubes of different PEG concentrations (10, 20, 30, 40, and 50% (w/w)) and five tubes of different sodium sulfate concentrations (25, 22.5, 20, 18, 16% (w/w)) were prepared. The tubes containing PEG were titrated with a 27.8% (w/w) sodium sulfate solution and the tubes containing sodium sulfate with a 46% (w/w) PEG solution until the appearance of turbidity. After clouding, water was added until turbidity disappeared. The amount of added solutions and water was gravimetrically determined. The associated concentrations of PEG and sodium sulfate at these points were calculated and plotted.

Each tie line could be divided in two segments: one segment is the distance between the point on the binodal curve depicting the composition of the top phase (T) and the point depicting the total composition of the immiscible solution (A), and the other segment is the distance between point A and the point on the binodal curve depicting the composition of the bottom phase (B). The ratio of segments was calculated, as follows:

$$\frac{V_t \rho_t}{V_b \rho_b} = \frac{AB}{AT} \quad (1)$$

where V and ρ are the volume and the density of the top (t) or bottom (b) phase. The density was measured using a density meter, DMA 4500, from Anton Paar (Graz, Austria). The phase volumes were visually determined using the scale of the plastic tubes. Knowing the total compositions of the solutions and the associated ratios of segments, the tie-lines were graphically determined.

To verify the compositions of the top and bottom phases, the PEG concentration of the top phase and the salt concentration of the bottom phase were measured, respectively. The PEG-2000 concentrations were measured using a programmable DV-II + viscosimeter from Brookfield (Stuttgart, Germany), and the sodium sulfate concentrations were measured by conductivity, using an inoLab pH/Cond 720 from WTW (Weilheim, Germany). The associated compositions of sodium sulfate and PEG-2000 in the poor phases could be calculated with the following equation:

$$\frac{V_t \rho_t}{V_b \rho_b} = \frac{X_b - X_0}{X_0 - X_t} \quad (2)$$

where X denotes the concentration of the particular component in the phases (t:top, b: bottom) or in the total system (0).

Determination of the Crystallization Phase Diagram

A protein stock solution (40 g/L) was mixed with different amounts of a precipitant stock solution containing 33.6% (w/v) sodium sulfate, 0.09 M ammonium sulfate, and 0.1 M HEPES pH 7.0, 50% (w/v) PEG-2000 and distilled water in 1.5 mL Eppendorf tubes. The PEG-2000 concentration was held constant in all trials at 2% (w/v). Twenty 1 mL batches with different protein and precipitant concentrations were prepared as initial conditions. The batches were incubated at room temperature with gentle mixing for 20 h. After incubation, samples were investigated for crystals, precipitates, or other structures by light microscopy. The batches were centrifuged using a Minispin Eppendorf centrifuge (20 min; 13,400 rpm), filtered (0.22 μ m), and protein concentrations in the filtrates were measured by UV spectroscopy at 280 nm using a Power Wave HT plate reader from Bio-Tek (Bad Friedrichshall, Germany).

Next, precipitant stock solution and PEG-2000 was used to raise the concentration of the precipitant in the filtrates, and the new batches were incubated and analyzed in the same manner as the prior batches. This procedure was carried out three to four times. Protein concentrations in the initial batches and in the filtrates were plotted against the associated precipitant concentrations. In this way, a two dimensional graph was generated, depicting solubility, crystallization, and precipitation area of the protein in relation to the precipitant concentration.

Partitioning of a Single Chain Antibody

Two sets of experiments with total compositions above the binodal curve were performed in the same manner as described in the section about the determination of the binodal curves, using similar solutions of the determination of the phase diagram. The produced solutions were weighed, incubated for half an hour, and centrifuged at 1,000g for 30 min, using an Eppendorf centrifuge 5810R with a swinging bucket of the type A-4-6-2. The protein concentrations in both phases were spectrometrically measured. The partition coefficient K was calculated with the following equation:

$$K = \frac{c_{P,t}}{c_{P,b}} \quad (3)$$

where c_p is the protein concentration in the top phase (t) or bottom (b) phase. The natural logarithms of the different partition coefficients were plotted against the differences of PEG-2000 and sodium sulfate contents between the phases. The contents of these components were calculated, as follows:

$$X \left[\frac{W}{W} \right] = X \left[\frac{W}{V} \right] \cdot \rho \quad (4)$$

where X is the amount of phase-forming components in percent of weight per weight (w/w) or percent of weight per volume (w/v), and ρ is the density of the solution. Here, ρ is

calculated by dividing the weight of the solution by the respective volume, which was 10 mL in all experiments. The partition ratio G , which is the ratio of the whole amount of protein in the phases, is defined by:

$$G = K \frac{V_t}{V_b} \quad (5)$$

with V being the volume of the top phase (t) and bottom (b) phase.

Results and Discussion

Crystallization Phase Diagrams

Developing an industrial crystallization process requires crystals of moderate size and uniformity. Therefore, fragile, needle crystals or thin plates are undesired because they tend to break at increased shear stress, which is generated in stirred-tank reactors, and leads to heterogeneity in size. Furthermore, a large nucleation zone is desired, with sufficient distance to unfavorable zones, such as the precipitation area.

Another important factor for crystallization is the solubility curve slope, which indicates the end of the crystallization process, and thus, appoints the crystallization yield. Solubility curves with a steep slope are favorable because it allows a high yield at the beginning of the crystallization zone. Crystallization conditions of a single chain antibody were found using sodium sulfate as precipitant, resulting in thin needle crystals. Addition of small amounts of PEG-2000 led to a more appropriate shape of the crystals, which changed from needles to a more compact, bipyramidal form, shown in Figure 1. Theoretically the partition coefficient would further increase with increasing molecular mass of PEG with the risk of reduction of solubility and further increase of viscosity. Therefore we refrained from further screening of larger PEG molecules.

A phase diagram was generated to get information about the crystallization area. The single chain antibody was crystallized with sodium sulfate as precipitant, and PEG-2000 as additive.

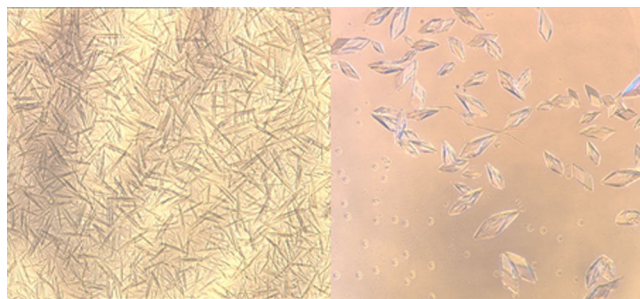


Figure 1. Single chain antibody, crystallized without (left) and with PEG-2000 (right). Crystallization without PEG-2000 resulted in small, thin needles. Crystallization with PEG-2000 resulted in three dimensional, medium-sized crystals.

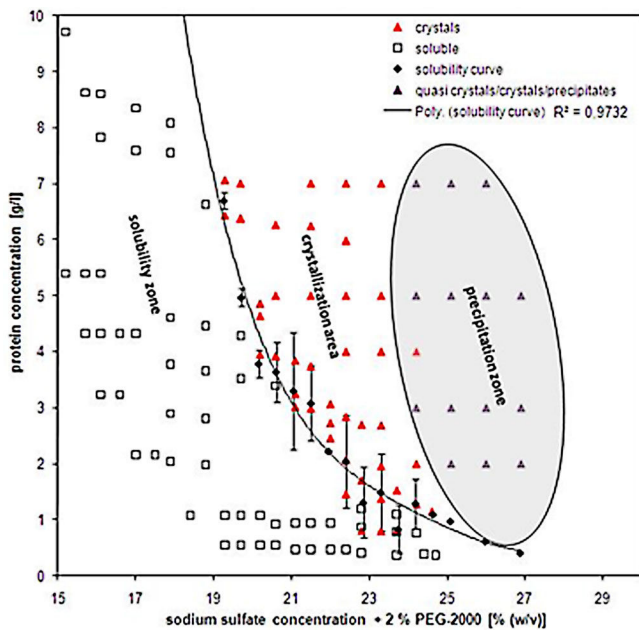


Figure 2. Phase diagram of the single chain antibody and sodium sulfate with 2% (w/v) PEG-2000 as additive. The solubility curve was fitted using a polynomial regression. The protein is soluble to the left of the solubility curve. On the right side of the solubility curve, a sufficient, large crystallization area is depicted. The unfavorable precipitation zone is marked in gray.

Figure 2 shows the deduced phase diagram with the solubility curve, the crystallization area, and the zonal border between the crystallization area and precipitation zone. The protein could be crystallized at sodium sulfate concentrations in the range between 19.5% (w/v) to 24.5% (w/v); hence, the crystallization area was large and appropriate to develop preparative crystallization processes. At sodium sulfate concentrations above 24.5% (w/v), the crystal quality decreased. Crystals at these high salt concentrations were characterized by blurred edges and large, thin agglomerates, furthermore amorphous precipitates were observed.

The solubility curve in this case is flat, and plateaus at values of 1 g/L at the end of the crystallization area. In order to achieve high crystallization yield, the starting protein concentration must be sufficiently high. Crystallization has to be accomplished at salt concentrations above 22% (w/v) and below 24% (w/v) to achieve phase transition, without inducing precipitation.

Determination of the Binodal Curve and Tie-Lines

The generated, binodal curve had a steep slope at high polymer concentrations, which flattens with increasing salt concentrations. Hence, as expected, the binodal curve has a concave pattern.

The highest, miscible salt concentration at high polymer concentration was determined at 1.28% (w/w) sodium sulfate and 45.5% (w/w) PEG-2000. The highest miscible polymer

concentration at high salt concentration was determined at 0.092% (w/w) PEG-2000 and 16.94% (w/w) sodium sulfate. Therefore, mixing PEG-2000 with sodium sulfate at compositions above the binodal curve resulted in PEG-2000-rich phases, with salt concentrations equal or above 1.28% (w/w) sodium sulfate, whereas the PEG-2000 concentration in salt-rich phases could be easily depleted below 1% (w/w).

Tie-lines are commonly parallel; however, here, the tie-lines are not completely parallel. This effect may have been caused, on the one hand, by the inaccuracy of the cloud point method, which was used to determine the binodal curve (primarily in regions with high PEG-2000 or sodium sulfate content), and, on the other hand, by small changes in temperature or differences in the molecular weight distribution of PEG-2000 by which tie-lines close to the critical point could be strong influenced.

The calculated PEG-2000 contents, based on viscosity measurements, in the top phases were higher, as expected, than the graphically determined tie-lines. The determination of higher PEG-2000 concentrations resulted in higher inaccuracies, due to the exponential devolution of the calibration curve. Figure 3 shows the binodal curve and tie-lines. The differences of the graphically determined and measured contents of PEG-2000 and sodium sulfate are shown in Table I.

Partitioning of the Solved Single Chain Antibody

The natural logarithms of the partition coefficients were plotted as a function of the differences between the sodium sulfate concentrations of the phases (Fig. 4B). The dissolved single chain antibody was enriched in the bottom phase at a critical concentration difference of sodium sulfate between the phases. Increasing the sodium sulfate concentration in the trials with constant PEG-2000 concentrations, the partition of the single chain antibody shifted in favor to the top phase.

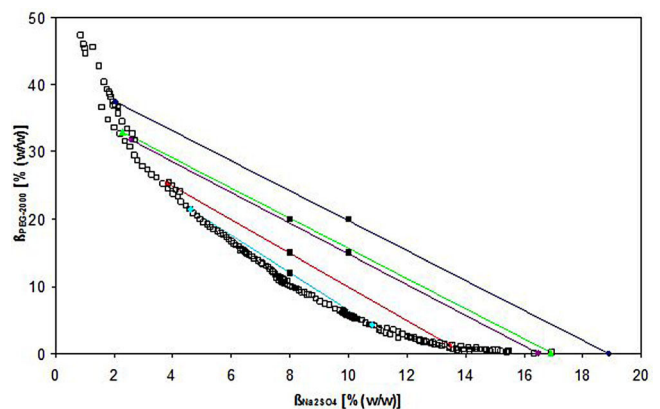


Figure 3. Equilibrium diagram of PEG-2000 and sodium sulfate at room temperature.

Table I. Graphically determined composition of PEG-2000 and sodium sulfate in top and bottom phases.

| Total composition [Peg/Na ₂ SO ₄] [% (w/w)] | PEG-2000 top phase (graphically determined) [% (w/w)] | PEG-2000 top phase (determined by viscosity) [% (w/w)] | Na ₂ SO ₄ bottom phase (graphically determined) [% (w/w)] | Na ₂ SO ₄ bottom phase (determined by conductivity) [% (w/w)] |
|--|---|--|---|---|
| 20/10 | 37.5 | 39.7 | 18.9 | 18.9 |
| 20/8 | 33 | 38.5 | 16.9 | 16 |
| 15/10 | 31.7 | 35.2 | 16.5 | 15.7 |
| 15/8 | 25.4 | 29.3 | 13.5 | 13.5 |
| 12/8 | 21.5 | 22.2 | 10.8 | 9.3 |

At sodium sulfate concentration differences above the critical concentration difference, the single chain antibody enriched in the top phase. Hence, crystallization at different sodium sulfate concentration influenced the partition of the solved single chain antibody in the phases, and could be used to separate the single chain antibody from other impurities like host cell proteins and DNA by only adjusting the sodium sulfate concentration. If most of the impurities accumulate in the bottom phase, it is advisable to increase the sodium

sulfate concentration to enrich the single chain antibody in the top phase; whereas, if most of the impurities accumulate in the top phase, the sodium sulfate concentration could be lowered to enrich the single chain antibody in the bottom phase.

It is also possible to influence the partitioning of the single chain antibody in the phases by controlling the PEG-2000 concentration. At a critical PEG-2000 concentration difference of approximately 36.8% (w/w), the single chain antibody was enriched in the bottom phase; whereas, concentration differences above the critical concentration difference resulted in higher concentrations of the single chain antibody in the top phase. The devolution of the partitioning coefficient against the PEG-2000 concentration differences is flat for concentration differences at 34.5% (w/w), but becomes steeper with increasing PEG-2000 concentration difference between the phases.

At a concentration difference of 42.9% (w/w), the whole amount of protein was in the top phase. Therefore, controlling the PEG-2000 concentration is a strong tool to influence the partitioning of the single chain antibody in the phases. Figure 4A shows the results of the single chain antibody partitioning at different PEG-2000 concentration differences between the phases. At higher values the whole amount of protein is accumulated in the top phase.

The different partitions of a solute in ATPS are characterized by the partition ratio, or *G* value. Since the phase volumes could be very different, the partition ratio is important to calculate the mass balance of the single chain antibody. *G* values achieved by varying the sodium sulfate concentration at a constant PEG-2000 content are shown in Table II, and *G* values achieved by varying the PEG-2000 concentration at a defined sodium sulfate concentration are shown in Table III.

The *G* values achieved by varying the sodium sulfate concentration are very low compared with the values achieved by varying the PEG-2000 concentration. Only a little amount of PEG-2000 (2% (w/v)) and large amounts of sodium sulfate, in the range of 21–26% (w/v), are used in these batches, hence, the top phase volumes are only approximately 0.5 mL, whereas the bottom phase volumes are 9.5 mL. Although the partitioning coefficient achieved values above 1, the partition ratio remained below 0.1. Therefore, the majority of the single chain antibody (>90%)

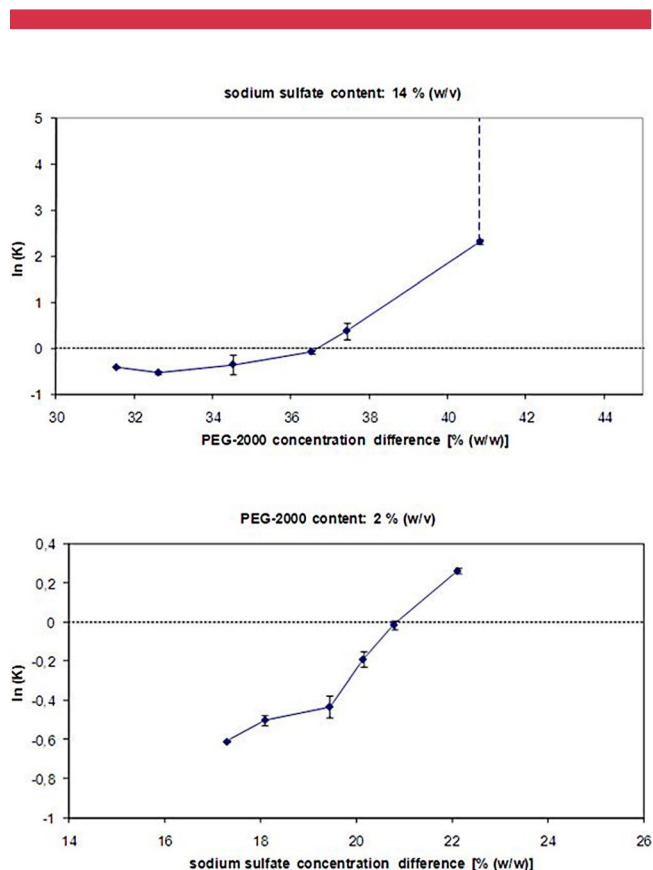


Figure 4. Partitioning coefficient of the single chain antibody as a function of differences in (A) PEG-2000 and (B) sodium sulfate concentrations between the phases. The dotted line depicts the state in which the target protein concentration of both phases is the same.

Table II. Overview of partition coefficients and ratios, according to sodium sulfate concentration difference.

| Sodium sulfate concentration difference [% (w/w)] | Total amount of sodium sulfate [% (w/v)] | Partition ratio <i>G</i> | Partition coefficient <i>K</i> | Natural logarithm of <i>K</i> |
|---|--|--------------------------|--------------------------------|-------------------------------|
| 22.13 | 26 | 0.079 | 1.3 | 0.261 |
| 20.8 | 25 | 0.057 | 0.99 | -0.015 |
| 20.15 | 24 | 0.040 | 0.83 | -0.192 |
| 19.45 | 23 | 0.036 | 0.65 | -0.432 |
| 18.1 | 22 | 0.029 | 0.61 | -0.500 |
| 17.3 | 21 | 0.029 | 0.54 | -0.611 |

Table III. Overview of partition coefficients and ratios according to PEG-2000 concentration difference.

| PEG-2000 concentration difference [% (w/w)] | total amount of PEG-2000 [% (w/v)] | partition ratio G | partition coefficient K | natural logarithm of K |
|---|------------------------------------|-------------------|-------------------------|------------------------|
| 42.92 | 20 | — | — | — |
| 40.82 | 18 | 8.519 | 10 | 2.303 |
| 37.42 | 16 | 1.146 | 1.46 | 0.37 |
| 36.52 | 14 | 0.616 | 0.92 | -0.079 |
| 34.52 | 12 | 0.380 | 0.71 | -0.359 |
| 32.62 | 10 | 0.251 | 0.59 | -0.534 |
| 31.55 | 9 | 0.255 | 0.66 | -0.422 |

remained in the bottom phase, independent of the sodium sulfate content.

The variation of PEG-2000 in the batches at constant sodium sulfate concentration (14% (w/v)) caused differing the partition ratios over a wide range. At a PEG-2000 concentration difference of approximately 37% (w/w), the single chain antibody accumulated in the bottom phase, whereas, at higher concentration differences, the single chain antibody accumulated in the top phase. At very high PEG-2000 concentration differences (>42% (w/w)), the whole amount of the single chain antibody was in the top phase. The amount of the single chain antibody in the bottom phase could be enriched to

approximately 80% by lowering the PEG-2000 concentration caused a corresponding concentration difference between the phases in the range of 31.6 onto 32.6% (w/w). Therefore, controlling the content ratios of sodium sulfate and PEG-2000 could be used to enrich either the concentration of the single chain antibody or the total amount of the single chain antibody in a distinct phase.

Crystallization of the Single Chain Antibody in an Aqueous Two-Phase System

Based on the crystallization phase diagram of the single chain antibody (Fig. 2), further investigation of the single chain antibody crystallization in aqueous two-phase systems was done. Only experiments using sodium sulfate, as opposed to PEG-2000, as precipitant, without additives, resulted in crystals. Hence, it was assumed that, in crystallization experiments using an aqueous two-phase system, nucleation takes place in the sodium sulfate-rich, bottom phase. However, each time crystals appeared, they accumulated in the PEG-2000-rich phase. Therefore, crystal growth must primarily take place in the top phase, with lower single chain antibody concentration (Table II).

The nucleation of the single chain antibody causes a concentration decrease of the solved single chain antibody in the sodium sulfate rich phase, whereas the crystal growth causes a concentration decrease of the dissolved single chain

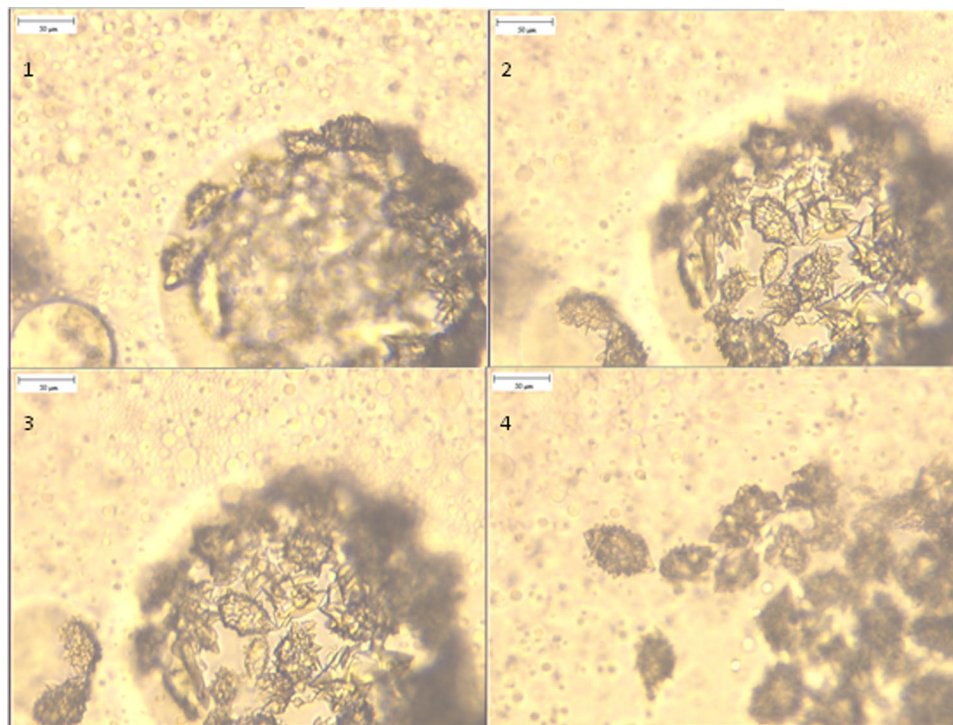


Figure 5. Accumulated crystals in a PEG-2000-rich droplet, and release of them into the surrounding sodium sulfate-rich phase (1–4).

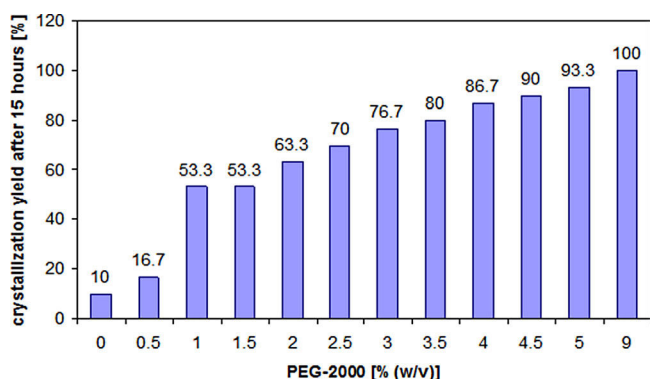


Figure 6. Influence of PEG-2000 concentration on crystallization yield in the top phase.

antibody in the PEG-2000 rich phase. Hence, an imbalance of the protein partition equilibrium in the phases occurs for which it must be compensated by mass transfer of the single chain antibody from one phase to the other, according to the partition coefficient. In the following, and due to a stirred system, large droplets of the PEG-2000-rich phase, packed full of crystals, were generated.

The dense packaging of crystals in the PEG-2000-rich phase resulted in high crystal agglomerates, which are grown together. The enlargement of the droplets, caused by crystal growth and the accumulation of crystals, resulted in a more energetically unfavorable state of the droplets, and additionally increased their sensitivity to shear forces. Therefore, the droplets tended to burst, releasing the crystals into the circumfluent sodium sulfate-rich phase, shown in Figure 5.

The property of the crystals that accumulate in the PEG-2000-rich top phase offers an option to harvest the crystals. At the end of the crystallization, the stirrer is stopped, and

after phase separation, the large bottom phase, containing no crystals, is drained. Then, the small, crystal-rich, top phase can easily be filtered.

Influence of PEG-2000 on Crystallization Yield

PEG-2000 acts simultaneously as inducer for the extraction process and former of crystal shape, but also as anti-solvent. Therefore, with increasing content of PEG-2000, the solubility of the protein will decrease. Experiments were carried out with 22% (w/v) sodium sulfate and a total protein concentration of 3 g/L. The PEG-2000 concentration was in the range of 0–9% (w/v).

Figure 6 shows yield of the crystallization process after 15 hours, depending on the PEG-2000 content in the batches. Crystallization yield increases with increasing content of PEG-2000. At a PEG-2000 content of 9% (w/v), no more protein could be detected in the supernatant; hence, the crystallization yield was nearly 100%. However, the quality of crystal shape declined with increasing PEG-2000 concentration, represented by decreased crystal sizes and blurred edges. Therefore, an increase of PEG-2000 has a direct influence on the crystallization phase diagram, and achieves high crystallization yields, even at low sodium sulfate concentrations.

Scale-Up

A scale-up experiment was carried out to proof the accuracy and appropriation of bulk crystallization in an aqueous two-phase system. About 27.5 mL of protein stock solution ($c = 40$ g/L) was added to a mixture of 147 mL precipitant stock solution, containing 33.6% (w/v) sodium sulfate, 0.09 M ammonium sulfate, 0.1 M HEPES, pH 7.0, 8.8 mL stock solution of 50% (w/v) PEG-2000, and 36.7 mL deionized water in a 250 mL glass beaker. The total volume was 220 mL, the protein concentration in the batch was 5 g/L, the sodium sulfate concentration was 22.5% (w/v), and the



Figure 7. Bulk crystallization in an aqueous two-phase system, stirred (left) and unstirred (right), with phase separation.

PEG-2000 concentration was 2% (w/v). The stirrer speed was 200 rpm.

Figure 7 shows the stirred crystal suspension after 20 h. The white flocks are the droplets of the PEG-2000-rich phase, densely packed with crystals. In the upper region of the beaker, the stirring was not sufficient, thus, crystals could be adsorbed at the glass wall. If stirring was stopped, the two-phases dispersed, and the crystals accumulated in the small top phase, exception the crystals, which were adsorbed at the glass wall.

Conclusion

This study demonstrates that it is possible to generate a process where a sufficient concentration of PEG-2000 in salt induces protein crystallization, and causes an extraction process, which takes place simultaneously. This additional extraction process offers new possibilities to increase the efficiency and economy of crystallization processes, and is an opportunity for process integration.

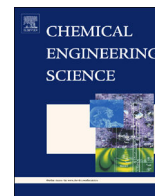
The content of PEG-2000 has an effect on crystallization yield, since it also acts as anti-solvent. Higher PEG-2000 content in the crystallization batches strongly increased crystallization yields. The ability of the crystals to accumulate in the top phase facilitates the crystal harvest, since the top phase is much smaller than the bottom phase. Therefore, in a first step, the bottom phase could be drained very quickly without filtration, and in a second step, only the small top phase has to be filtrated. Based on these facts, it should be possible to develop a process, comprising conditions, which enables nucleation in a phase of higher purity, followed by shifting the PEG-2000 or sodium sulfate content to conditions, which favor higher purity in the phase where crystal growth takes place.

We conclude that this process has a high potential, and that combined extraction and crystallization processes can be effective protein purification tools in downstream operations.

References

- Azevedo AM, Rosa PAJ, Ferreira IF, Aires-Barros MR. 2009. Chromatography-free recovery of biopharmaceuticals through aqueous two-phase processing. *Trends Biotechnol* 27(4):240–247.
- Basu SK, Govardhan CP, Jung CW, Margolin AL. 2004. Protein crystals for the delivery of biopharmaceuticals. *Expert Opin Biol Ther* 4(3):301–317.
- Cascone O, Andrews BA, Asenjo JA. 1991. Partitioning and purification of thaumatin in aqueous two-phase systems. *Enzyme Microb Technol* 13:629–635.
- Etzel M. 2006. Bulk protein crystallization—Principles and methods. In: Shukla A, Etzel M, Gadam S, editor. *Process scale bioseparations for the biopharmaceutical industry*. Boca Raton, FL: Taylor & Francis. p 575.
- Fauquex P-F, Husted H, Kula MR. 1985. Phase equilibration in agitated vessels during extractive enzyme recovery. *J Chem Technol Biotechnol* 35:51–59.
- Govardhan C, Khalaf N, Jung CW, Simeone B, Higbie A, Qu S, Chemmalil L, Pechenov S, Basu SK, Margolin AL. 2005. Novel long-acting crystal formulation of human growth hormone. *Pharm Res* 22(9):1461–1470.
- Jacobsen C, Garside J, Hoare M. 1997. Nucleation and growth of microbial lipase crystals from clarified concentrated fermentation broths. *Biotechnol Bioeng* 57(6):666–675.
- Judge RA, Forsythe EL, Pusey ML. 1998. The effect of protein impurities on lysozyme crystal growth. *Biotechnol Bioeng* 59(6):776–785.
- Judge RA, John MR, White ET. 1995. Protein purification by bulk crystallization: The recovery of ovalbumin. *Biotechnol Bioeng* 48:316–323.
- Kim C-W, Rha C. 2000a. Interfacial tension of polyethylene glycol/potassium phosphate aqueous two-phase systems. *Phys Chem Liq* 38(1):25–34.
- Kim C-W, Rha C. 2000b. Phase separation of polyethylene glycol/salt aqueous two-phase systems. *Phys Chem Liq* 38(2):181–191.
- Kroner KH, Schutte H, Stach W, Kula MR. 1982. Evaluation of crude dextran as phase-forming polymer for the extraction of enzymes in aqueous two-phase systems in large scale. *J Chem Tech Biotechnol* 32:130–137.
- Kula MR, Kroner KH, Husted H, Schutte H. 1981. Technical aspects of extractive enzyme purification, *Ann N Y Acad Sci* 369:341–354.
- Lee TS, Vaghjiani JD, Lye GJ, Turner MK. 2000. A systematic approach to the large-scale production of protein crystals. *Enzyme Microb Technol* 26:582–592.
- Lorber B, Skouri M, Munch J-P, Giegé R. 1993. The influence of impurities on protein crystallization; the case of lysozyme. *J Crystal Growth* 128:1203–1211.
- McPherson A. 1990. Current approaches to macromolecular crystallization. *Eur J Biochem* 189:1–23.
- McPherson A. 1999. *Crystallization of Biological Macromolecules*. New York, NY: Cold Spring Harbor Laboratory Press. p 586.
- Myerson AS, Toyokura K. 1990. *Crystallization as a separation process*. Washington, DC: ACS Symposium Series Vol. 438, p 419.
- Peters J, Minuth T, Schröder W. 2004. Implementation of a crystallization step into a purification process of a recombinant protein. *Protein Expr Purif* 39:43–53.
- Philipson L, Albertsson P-A, Frick G. 1960. The purification and concentration of viruses by aqueous polymer phase systems. *Virology* 11(3):553–571.
- Rosa PAJ, Ferreira IF, Azevedo AM, Aires-Barros MR. 2010. Aqueous two-phase systems: A viable platform in the manufacturing of biopharmaceuticals. *J Chromatogr A* 1217(16):2296–2305.
- Schmidt S, Havekost D, Kaiser K, Kauling J, Henzler HJ. 2004. Kristallisation für die Aufarbeitung von Proteinen. *Chem Ing Tech* 76(6):819–822.
- Shenoy B, Wang Y, Shan W, Margolin AL. 2001. Stability of crystalline proteins. *Biotechnol Bioeng* 73(5):358–369.
- Takakura T, Ito T, Yagi S, Notsu Y, Itakura T, Nakamura T, Inagaki K, Esaki N, Hoffman RM, Takimoto A. 2006. High level expression and bulk crystallization of recombinant L-methionine γ -lyase, an anticancer agent. *Appl Microbiol Biotechnol* 70:183–192.
- Veide A, Smeds A-L, Enfors S-O. 1983. A Process for large-scale isolation of β -galactosidase from *E. coli* in an aqueous two-phase system. *Biotechnol Bioeng* 25:1789–1800.
- Walter H, Johansson G. 1994. Preface. *Methods Enzymol* 228:xv–xvi.
- Walter H, Sasakawa S, Albertsson P-A. 1972. Cross-partition of proteins. Effect of ionic composition and concentration *Biochem* 11(21):3880–3883.
- Webb SD, Webb JN, Hughes TG, Sesin DF, Kincaid AC. 2002. Freezing bulk-scale biopharmaceuticals using common techniques—And the magnitude of freeze-concentration. *BioPharm Int* 15(5):22–34.
- Wu Y-T, Zhu Z-Q, Mei L-H. 1996. Interfacial tension of poly (ethylen glycol) + salt + water systems. *J Chem Eng Data* 41(5):1032–1035.
- Zang Y, Kammerer B, Eisenkolb M, Lohr K, Kiefer H. 2011. Towards protein crystallization as a process step in downstream processing of therapeutic antibodies: Screening and optimization at microbatch scale. *PLoS ONE* 6(9):e25282.

Publication II



Design of industrial crystallization of interferon gamma: Phase diagrams and solubility curves



Hauke Huettmann^b, Susanne Zich^a, Matthias Berkemeyer^b, Wolfgang Buchinger^b, Alois Jungbauer^{a,*}

^a Department of Biotechnology, University of Natural Resources and Life Sciences, Vienna, Vienna, Muthgasse 18, Vienna 1190, Austria

^b Boehringer Ingelheim RCV GmbH & Co KG, Dr. Boehringer Gasse 5-11, A-1121 Vienna, Austria

HIGHLIGHTS

- Kind of precipitant highly influences the economics of crystallization processes.
- Phase diagrams are the key factor to design robust crystallization processes for industrial applications.
- Homogeneous nucleation is the driving force of the crystallization of rhINF- γ .
- Formation of uniform crystals takes place by Ostwald ripening instead of growth out of the liquid phase.

ARTICLE INFO

Article history:

Received 26 May 2014

Received in revised form

17 November 2014

Accepted 5 December 2014

Available online 15 December 2014

Keywords:

Phase diagram

Solubility curve

Cytokine

Crystallization

Biopharmaceutical

ABSTRACT

Phase diagrams and solubility curves for engineering of crystallization for interferon gamma have been developed by small scale precipitation and crystallization experiments. A scale up was carried out to proof the accuracy and the suitability of the created phase diagram with sodium sulfate for bulk crystallization. To provide nucleation and a high yield the operating point was chosen at a protein concentration of 6 mg/mL and a sodium sulfate concentration of 25% [w/v]. Crystallization was completed within 5 h with a yield of > 95%. The double logarithmic plot of crystallized fraction versus time yielded in an overall kinetic crystallization constant of $5.79 \times 10^{-2} \text{ min}^{-1}$. Regular cubic crystals can be observed which contradicts the low Avrami coefficient. The Avrami coefficient of 1 is interpreted that nucleation takes place throughout the entire crystallization process and larger crystals are formed by Ostwald ripening instead of growth out of the liquid phase. The established process with its conditions is suited for industrial protein crystallization.

© 2014 Elsevier Ltd. All rights reserved.

1. Introduction

Phase diagrams and solubility curves are the basis for engineering of crystallization processes. Batch crystallization has the potential to become an efficient recovery and concentration process in manufacturing of biopharmaceuticals (Przybycien et al., 2004). Development of crystallization conditions for a protein suitable for bioprocessing is still difficult and requires knowledge about the thermodynamic properties

of the protein solution. Crystals should be formed in a reasonable time less than 24 h, relatively pure and with a size, shape and mechanical strength that they can be easily separated from the mother liquid. This is different to the search of crystallization conditions for structural biology purposes. The high demand in crystallization conditions suited for bioprocessing may have discouraged a lot of engineers to apply batch crystallization as a recovery process. For the structural biology applications these criteria except crystal size and purity are not important. High throughput techniques (HTP-techniques) for crystallization became a powerful tool for finding optimal conditions (Joachimski, 2009). Such techniques provide crystallization conditions, but do not provide phase diagrams, which are important to optimize and engineer crystallization conditions.

Crystals for structure analysis differ from those for bulk crystallization. For structure analysis large single crystals without grid irregularities and high packing quality, which diffract highly, are required, but no phase diagrams and induction kinetics. All kinds of chemicals and additives can be used for generating crystals and

Abbreviations: rhINF- γ , recombinant human Interferon gamma; PEG 4000, Polyethylene glycol 4000; HCP, host cell proteins; HTP-techniques, high throughput techniques; UV₂₈₀, ultraviolet light with a wavelength of 280 nm

* Corresponding author. Tel.: +43 1 47654 6226; fax: +43 1 47654 6675.

E-mail addresses: hhuettman@gmx.de (H. Huettmann),

susanne.zich@boku.ac.at (S. Zich),

matthias.berkemeyer@boehringer-ingenheim.com (M. Berkemeyer),

wolfgang.buchinger@boehringer-ingenheim.com (W. Buchinger),

alois.jungbauer@boku.ac.at (A. Jungbauer).

<http://dx.doi.org/10.1016/j.ces.2014.12.018>

0009-2509/© 2014 Elsevier Ltd. All rights reserved.

optimizing their structure (Mueller et al., 2007; Peters et al., 2005). Excipient, costs, yield and scalability are not relevant and growth kinetics could take months. A method published for successful crystallization of rhINF- γ for structure analysis lasts one week and additionally a harmful additive, benzamidine, a serin proteinase inhibitor, had to be used (Landar et al., 2000). For bulk crystallization the objectives of the process are different. Precipitants must be inexpensive, the compounds should be of pharmaceutical grade, the growth kinetics should be fast, within several hours, the crystallization yield must be high and the protein must not lose its potency after crystals are redissolved (Jacobsen et al., 1997). Crystal grid irregularities and a large single crystal shape are not as important as purity and scalability of the process (Peters et al., 2005). For that reason the crystallization time, solubility and precipitation range of the target protein is important, when implementing it into a purification process, e.g. as a purification or formulation step. But complete phase diagrams for prediction of crystallization are rarely available. A general strategy to implement protein crystallization into a purification process was proposed as follows (Lee et al., 2000; Schmidt et al., 2004): (a) screening for appropriated crystallization conditions with vapor diffusion techniques and pure protein (purity > 95%), (b) optimization of the conditions (addition of additives, exchange of buffers, etc.), (c) generating a phase diagram of protein and precipitant concentration with microbatch method, (d) amplifying of the phase diagram with other parameters like temperature and pH, (e) fitting of the phase diagram range with or without the help of seeding for contaminated protein solutions and (f) finally scale up to pilot or large scale process. The number of such implemented processes is rare (Przybycien, 1998). Only a few reports have been published so far about bulk protein crystallization (Hekmat et al., 2007). Some examples for that or crystallization of protein from impure solutions are the crystallization of lipase (Jacobsen et al., 1998), lysozyme (Lorber et al., 1993; Judge et al., 1998), ovalbumin (Judge et al., 1995), L-methionine γ -lyase (Takakura et al., 2006), insulin (Schlichtkrull, 1956) and an aprotinin variant (Peters et al., 2005). We present a systematic approach to establish a crystallization step of a biopharmaceutical relevant protein, recombinant Interferon gamma (rhINF- γ) as a purification step. The human interferon gamma is a cytokine produced by activated T-cells and natural killer cells. The active form is a 45 kDa heterodimer, which contains a 20 kDa and a 25 kDa glycopeptide. It exhibits pleiotropic biological activities (Dijkmans and Billiau, 1988) and is particularly used in clinics for treatment of visceral leishmaniasis and chronic granulomatous.

In order to evaluate precipitants to be adequate for preparative batch crystallization solubility curves of rhINF- γ were determined to find the point in time, when the solubility reach the equilibrium and how this can affect the establishment of the phase diagram and further the protein crystallization. The obtained phase diagrams with different precipitants will be compared and discussed. Based on the generated phase diagrams, a favorable operating point for batch crystallization was selected and the crystallization was performed as 150 mL batch crystallization.

2. Materials and methods

2.1. rhINF- γ

rhINF- γ was produced in *Escherichia coli* (not glycosylated) and obtained from the pilot plant at Boehringer Ingelheim RCV GmbH & Co KG, Vienna, Austria.

2.2. Chemicals

Acetic acid, ammonium acetate, ammonium phosphate dibasic, hydrochloric acid, Polyethylenglycol 4000, sodium acetate tri-hydrate,

sodium chloride, sodium hydroxide and sodium sulfate were purchased by Merck KGaA, Darmstadt, Germany. Ammonium sulfate was obtained from Mallinckrodt Baker Inc., New Jersey, USA.

2.3. Generating of protein stock solutions by ultra- and diafiltration

Ultra- and diafiltration of rhINF- γ was performed using Amicon Ultra-15 Centrifugal Filter Units with Ultracel-3 membranes from Millipore GmbH, Vienna, Austria. Ultrafiltration was performed by centrifuging the filter units several times at 5000 rcf for 10 min (Centrifuge 5810R from Eppendorf AG, Hamburg, Germany) until a protein concentration of approximately 40 mg/mL was achieved. Diafiltration was performed by adding the same volume of diafiltration buffer (0.1 M ammonium acetate pH: 6.0), followed by a twofold concentration. This procedure was repeated seven times.

2.4. Buffer preparation

All buffers were prepared with water deionised and purified using an ultra-pure water system (SG Water, Barsbüttel, Germany) or a Millipore Milli-Q system (Millipore Corp., Bedford, MA, USA). The pH of these buffers was adjusted with hydrochloric acid, sodium hydroxide or acetic acid.

2.5. Determination of protein concentration

Protein concentration was determined by UV absorption at a wavelength of 280 nm using a Genios Pro TM UV plate reader from Tecan Crailsheim, Germany. An extinction coefficient $\epsilon_{0.1\%}$ of 0.75 for rhINF- γ was used for calculation of the protein concentration.

2.6. Determination of solubility curves

A constant volume of rhINF- γ stock solution with a concentration of 40 g/L was mixed in 1.5 mL tubes (Eppendorf tube, Eppendorf, Hamburg, Germany) with different volumes of the adequate precipitant stock solution (40% [w/v] PEG 4000, 30% [w/v] sodium chloride, 30% [w/v] di-ammonium hydrogen phosphate, 50% ammonium sulfate, 37.5% [w/v] sodium sulfate) resulting in different salt and protein concentrations. After mixing, the solutions were incubated for 1–4 days using an end over end mixer (Stuart SB 3 Blood Tube Rotator Mixer, Bibby Scientific Limited, Stone, Staffordshire, UK) with 20 rpm at room temperature. Formed precipitates were separated by centrifugation of the samples at 16,110g at 25 °C for 30 min (Centrifuge 5415R, Eppendorf AG, Hamburg, Germany). The supernatant was removed and protein concentration measured by UV₂₈₀. The initial and obtained protein concentrations were plotted against the belonging salt concentrations to get the solubility curves.

2.7. Determination of phase diagrams

The protein stock solution was mixed with different amounts of the precipitant stock solution and distilled water respectively in 1.5 mL tubes (Eppendorf tube, Eppendorf, Hamburg, Germany) to get the desired protein and precipitant concentrations. 1 mL batches with different protein and precipitant concentrations were generated as initial conditions. The batches were incubated at room temperature with gently mixing (Assistent 348 Roller, Karl Hecht GmbH & Co KG, Sondheim, Germany) for 20 h, in case of using di-ammonium hydrogen phosphate as precipitant for 4 days. After incubation samples are investigated for crystals, precipitates or other structures by light microscopy (Labovert FS microscope, Leitz, IL, USA). The batches are centrifuged (20 min; 13,400 rpm; MiniSpin centrifuge, Eppendorf AG, Hamburg, Germany), filtrated (0.22 μ m) and measured

by UV₂₈₀. The filtered supernatant was used again and the precipitant concentration in the filtrates was raised by adding precipitant stock solution. The new batches were incubated and analyzed in the same manner as the batches before. This procedure was carried out three up to four times. In this way the phase properties of a wide range of precipitant and protein concentrations could be empirically determined. A phase diagram was assembled by depicting undersaturation, crystallization and precipitation area of the protein in relation to the precipitant concentration.

3. Theory

Crystallization processes consist of two major mechanisms: nucleation (formation of the solid phase) and crystal growth. Both mechanisms were studied and described in the past for small molecules and also for proteins using kinetically and thermodynamically based models (Dixit et al., 2001; Galkin and Vekilov, 1999; Lindenberg and Mazotti, 2009; Vetter et al., 2013). Nowadays population balance models are used to predict and optimize crystallization processes (Aoun et al., 1999; Basu et al., 2004; Kougoules et al., 2005; Leyssens et al., 2011; Shi et al., 2005). However, in all cases nucleation is assumed as the formation of single nuclei of a critical size at a more or less constant supersaturation followed by crystal growth out of the liquid phase causing a strong decrease of the supersaturation until solubility equilibrium is reached.

In our case we observed a strong decrease of the supersaturation directly at the start of the nucleation reaction resulted in an irregular shaped microcrystalline precipitate with dense and less dense regions. Crystal growth of single 3-dimensional crystals has primarily happened on the expense of the microcrystalline precipitate than from the liquid phase. Due to the fast phase transition process, the irregular shape and agglomeration behavior of the microcrystalline precipitate and growing crystals caused by hydrophobic surface patches (Fig. 5B) a determination of particle sizes and also of nucleation and growth rates could not be accurately performed. Therefore a simpler model was used to describe the crystallization kinetics and to depict that the nucleation was the driving force, which causing the main drop of protein concentration in the liquid phase whereas 3-dimensional crystal growth has happened from the nucleated material.

The crystallization kinetics can be described by an exponential function using the Avrami equation (Avrami, 1939)

$$X_t = 1 - e^{-Kt^n} \quad (1)$$

where X_t is the fraction of protein crystallized after time t , K is the crystallization rate constant and n is the Avrami exponent. The Avrami exponent consists of two terms:

$$n = N + qC \quad (2)$$

where N is the nucleation and is either 0 if all crystals are nucleated simultaneously at the beginning of the growth process or 1 if nuclei are formed at a constant rate. C is the dimensionality of crystal growth and is 1, 2 or 3-dimensional and q describes the time dependence of growth: $q = 1$ for linear growth and $q = 0.5$ for diffusion limited growth.

The Avrami equation can be transformed in following equation:

$$X_t = \frac{C_t}{C_0 - C_s} = 1 - e^{-Kt^n} \quad (3)$$

where C_0 represents the initial protein concentration, C_t is the protein concentration in the crystalline phase at time t and C_s is the protein concentration at the solubility limit.

The protein concentration in the crystalline phase at time t can be calculated from following equation:

$$C_t = C_0 - C_{sup,t} \quad (4)$$

where $C_{sup,t}$ represents the protein concentration in the supernatant at time t .

The double logarithmic form of Eq. (3) results in

$$\ln\left(-\ln\left(\frac{C_t}{C_0 - C_s}\right)\right) = \ln K + n \ln t \quad (5)$$

Plotting of $\ln(-\ln((C_t)/(C_0 - C_s)))$ vs. $\ln t$ will result in a straight line with a slope of n and an intercept of $\ln K$. For comparison of crystallization rates of processes with different crystal morphology or nucleation properties, it makes sense to use a modified form, n -independent crystallization rate (Khanna and Taylor, 1988)

$$K' = K^{(1/n)} \quad (6)$$

4. Results and discussion

4.1. Determination of solubility curves

For the determination of the solubility curves of rhINF- γ the protein solution was mixed with different precipitant solutions and incubated up to 4 days. Then the mixture was centrifuged and the supernatant was measured by UV₂₈₀. The measured protein concentrations were plotted against the precipitant concentration for every incubation period, to show if the equilibrium of dissolution process is reached. The results for two different precipitants are shown in Fig. 1 as an example.

Experiments carried out with PEG 4000 as precipitant showed that the equilibrium was reached after the first day, because the remaining protein concentration in the supernatant did not change in the subsequent days (Fig. 1A). In the case of sodium chloride the used salt concentrations were too high to reach equilibrium, in all experiments the whole protein was precipitated. But it is clearly seen that it needs 4 days to precipitate the whole protein (Fig. 1B). With these examples it was shown that the velocity to reach a solubility limit depends on the precipitant used. In the next part of this article the effect of the velocity of equilibrium achievement on phase diagrams is described.

4.2. Effects of different precipitants on phase diagrams

Phase diagrams give information about the relevant range of precipitant and protein concentration. They depict the undersaturation, metastable, crystallization and precipitation zone. The solubility curve marks the equilibrium of protein in solid and liquid states. Hence it depicts the amount of protein, which will stay in solution at the end of a crystallization process and can be used to calculate the crystallization yield for different operating points.

In Fig. 2 the phase diagrams of rhINF- γ with two precipitants, after different incubation periods, are shown. The comparison of different phase diagrams depicts the advantages and disadvantages with regard to industrial use. The problem to get a suitable phase diagram for industrial processes is the determination of crystallization kinetics and phase equilibrium (Moretti et al., 2000). Precipitants like salts or polymers will have different impact on protein solubility and time to reach equilibrium could vary from hours to days (Ries-Kautt and Ducruix, 1989). A prediction of time needed to reach equilibrium for different precipitants is therefore difficult and has to be determined experimentally.

The first investigated precipitant was di-ammonium hydrogen phosphate and the equilibrium was reached after 4 days (Fig. 2A). The time to reach the solubility equilibrium also correlates with the time to get crystals. This was the point of time where crystals have appeared and no further growth was observed, hence solubility equilibrium seemed to be reached. The phase diagram

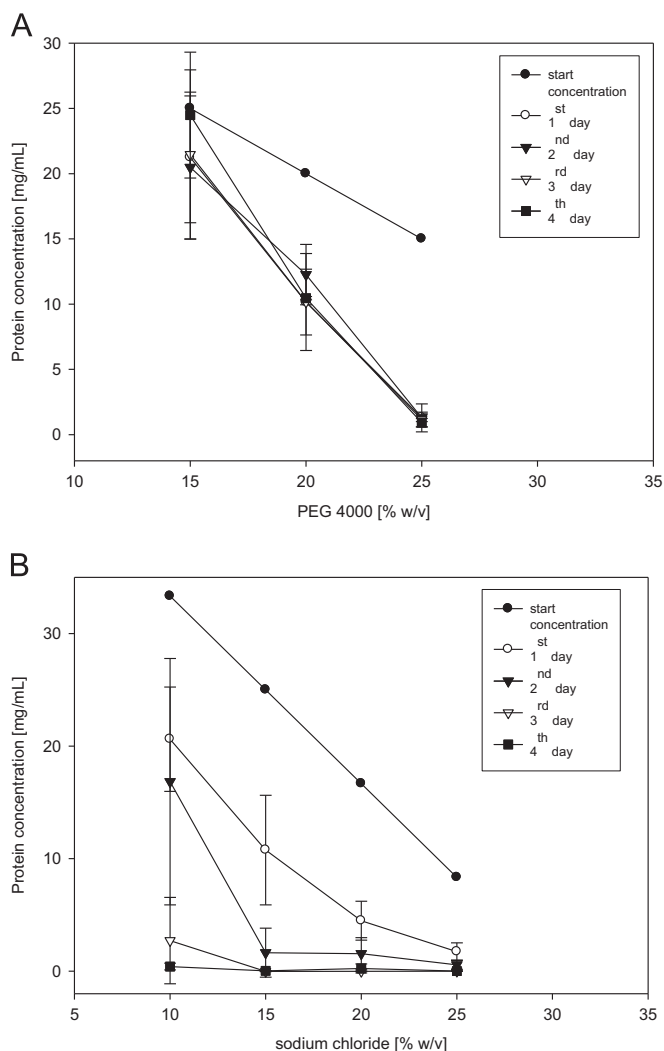


Fig. 1. Solubility of rhINF- γ in 0.1 M ammonium acetate buffer pH 6.0 at different (A) PEG 4000 concentrations and (B) sodium chloride concentrations. (●) Protein initial protein concentration, (○) remaining protein concentration after 1 day, (Δ) remaining protein concentration after 2 days, and (■) remaining protein concentration after 3 days.

indicates that di-ammonium hydrogen phosphate is not a suitable precipitant for industrial bulk crystallization, because the time to reach the solubility equilibrium and to get crystals is not economical and the area, where crystals grow is not clearly separated from where precipitates are formed.

In contrast sodium sulfate is a suitable precipitant (Fig. 2B), because the equilibrium was reached very fast. Solubility equilibrium and formation of crystals was attained within a few hours. In the phase diagram a broad nucleation area can be found clearly separated from the area of precipitation. This is one criterion why sodium sulfate can be used as a precipitant for industrial bulk crystallization. Another advantage is the low solubility after adding the precipitant. Thus a high yield can be expected, because less protein remains in solution after crystallization equilibrium has been reached.

Crystallization of a protein involves reduction of the solubility of the protein. This can be achieved by elimination of the surface charges of a protein (due to counter ions) or reduction of the circumfluent solvation layer of the protein. The solvation layer will be reduced by kosmotrope ions like sulfate and phosphate and increased by chaotrope ions like ammonium. The surface charge of a protein can be reduced by appropriate counter ions. Chaotrope anions and kosmotrope cations can easily form inner sphere ion

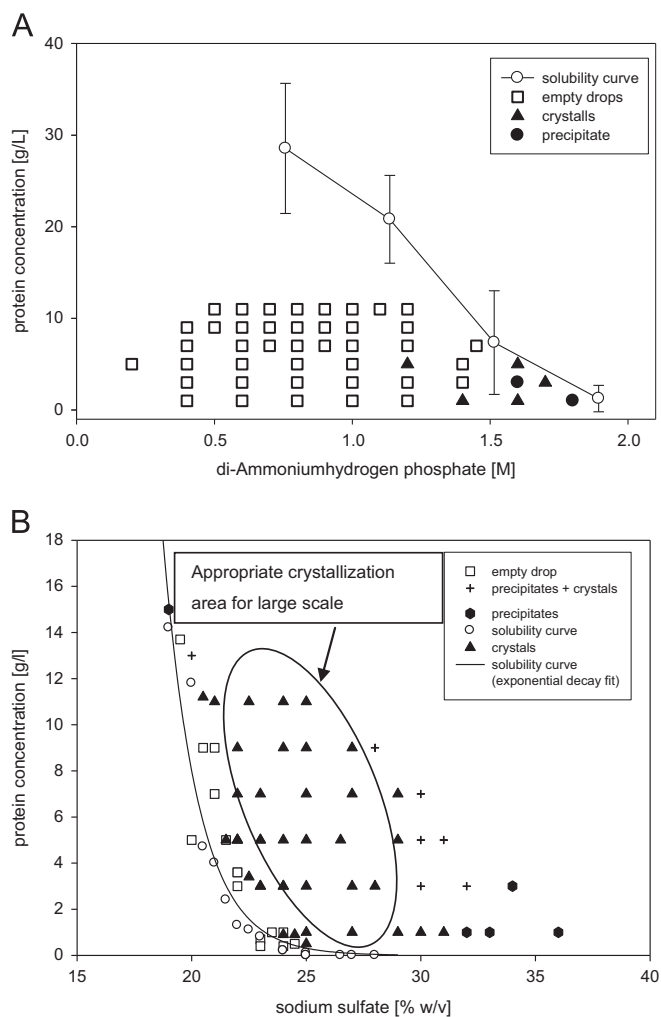


Fig. 2. Comparison between phase diagram and solubility curve of rhINF- γ in 0.1 M ammonium acetate buffer pH 6.0 with (A) di-ammonium hydrogen phosphate and (B) sodium sulfate. The stable crystallization area appropriate for industrial crystallization processes is surrounded. (○) Solubility curve, (●) amorphous precipitate, (▲) crystals, (□) empty drops, and (–) fitted solubility curve.

pairs with the positive (chaotrope) and negative (kosmotrope) charges of proteins and reduce the surface net charge of a protein (Collins, 2004). In case of the use of sodium chloride as precipitant, the strong decrease of the solubility of rhINF- γ is achieved due to the direct binding of the weakly hydrated chloride ions to the positive charges of the protein. The effect of different ions on the solubility of proteins are described in the Hofmeister series (Hofmeister, 1888) and is mainly dominated by anions (Yang, 2009). The order of such ions can also be reverse depending of the pI of the protein and the chosen pH (Ries-Kautt and Ducruix, 1997; Retailleau et al., 1997). The pI of rhINF- γ is above pH 9.0 and hence the net surface charge is positive at pH values below the pI . In case of the crystallization with di-ammonium hydrogen phosphate the pH was between 8.0 and 8.3 and for all other used precipitants approximately pH 6.0 resulting in a positive net surface charge of the protein in all experiments.

Knowing from crystallization experiments at different pH values using sodium sulfate the remaining soluble protein concentration was highest at neutral pH and decreasing with acidic and basic pH values. Hence in case of the use of di-ammonium hydrogen phosphate (pH 8.0–8.3) the pH is closer to the pI than in the other experiments and the solubility of the protein was strongly reduced. Apart from this the cubic crystal form was maintained in the range of pH 5.0–9.0, at lower or higher pH values single needles and

cluster of needles was also detected (data not shown). At pH values of 4.0 and 9.5 only amorphous precipitate was detected.

Given that the net surface charge of rhINF- γ was in all experiments positive the anions of the used salts could have directly interacted with the protein, but the positive charges on proteins (derivatives of ammonium) are weakly hydrated in opposite to the used anions in the crystallization solution (sulfate and phosphate), this circumstance hindered the formation of inner sphere ion pairs. Nevertheless due to the high amount of the used precipitants salt bridges could be build between the sulfate or phosphate ions and the protein (Chakrabarti, 1993). Hence sulfate or phosphate ions could be involved in the crystal binding sites and influenced the crystal morphology, resulting in rod shaped crystals in case of bound phosphate ions and cubic shaped crystals in case of bound sulfate ions.

The successfully used precipitants for crystallization of rhINF- γ dissociated in ammonium (chaotrope), sodium (kosmotrope), sulfate (kosmotrope) and phosphate (kosmotrope) ions.

The strength of sodium sulfate and di-ammonium hydrogen phosphate to reduce the solubility of rhINF- γ seems to be comparable. In both cases crystallization has been started at a salt concentration of approximately 1.5 M. Phosphate is a more kosmotrope anion than sulfate compared with their Jones–Dole viscosity B coefficients (0.59 for phosphate and 0.208 for sulfate), but sodium is more kosmotrope than ammonium (0.086 for sodium and -0.007 for ammonium) (Krestov, 1991; Robinson et al., 1981). The strength of ammonium sulfate to reduce the solubility of rhINF- γ is much lower compared with di-ammonium hydrogen phosphate and sodium sulfate. Crystallization was induced at a salt concentration of approximately 2.3 M. It is assumed that the chaotrope cation (ammonium) increased the solubility of rhINF- γ resulting in an increased concentration of ammonium sulfate compared with sodium sulfate and also counteract against the higher kosmotrope impact of the phosphate ion resulting in comparable crystallization slot of di-ammonium hydrogen phosphate and sodium sulfate.

Phase diagrams using ammonium sulfate or sodium chloride as precipitants were also generated for lysozyme (Cheng et al., 2006; Tam et al., 2011; Watanabe et al., 2009) and ovalbumin (Tam et al., 2011). Generally the time to reach equilibrium was set to 24 h for experiments at room temperature and 96 h for experiments at lower temperatures. But time to reach equilibrium depends on the initial salt concentration (Cheng et al., 2006). A study of precipitation kinetics reveals that higher initial salt concentrations cause an extended need of time to reach equilibrium. In case of lysozyme and high ammonium sulfate concentrations equilibrium was not reached after 96 h. Experiments to determine solubility equilibrium using vapor diffusion method refer to typical times to reach equilibrium of less than 3 days depending on kind of protein and precipitant (Talreja et al., 2010).

4.3. Process design

On the base of phase diagrams appropriated precipitant concentrations and corresponding crystallization yields and sizes could be depicted for different protein concentrations. Detailed and reliable phase diagrams are a requisite for optimal process design, enabling process control either in open or closed loop control applications. Different control mechanism considering either product, temperature or precipitant or both concentrations combined with population balance models was investigated for batch and semi-batch crystallization processes for small molecules (Fujiwara et al., 2005; Nagy et al., 2008; Nagy, 2009). Also combined antisolvent addition and temperature gradient crystallization was investigated (Lindenberg et al., 2009). A good overview of the development of control and design of crystallization processes are described by Nagy and Braatz (2012).

Here we compare the phase diagrams achieved with ammonium and sodium sulfate. In the phase diagram using sodium sulfate as precipitant (the three zones) undersaturation, crystallization and precipitation are clearly depicted (Fig. 3A). Furthermore the crystallization zone could be subdivided into a metastable and a nucleation zone. The borderline between metastable and nucleation zone is more diffuse than really well-defined, in this region nucleation could occur caused by different circumstances, e.g. vibrations, small shifts in temperature or small foreign particles. Generally nucleation must not occur in the metastable zone, but already existing crystals could grow inside this zone.

The occurrence of crystals and precipitates in the intermediate range of the nucleation and precipitation zone is caused by concentration differences until the protein solution and the precipitant solution are totally mixed. Therefore there are regions with different degrees of supersaturation, which can forward the formation of crystal seeds as well as the formation of precipitates.

Using ammonium sulfate as precipitant resulted in a phase diagram, which shows the three expected zones undersaturation, crystallization and precipitation, but a significant metastable zone could not be detected (Fig. 4A). The nucleation zone is larger compared to the nucleation zone of the phase diagram with sodium sulfate. Both precipitants ensure a stable crystallization process because the operating point could be in the nucleation zone with sufficient distance to the undersaturation and precipitation zone. An advantage of ammonium sulfate is the steep solubility, so that high yields could be achieved at low salt concentrations. The absence of a significant metastable zone ensures that nucleation takes place as soon as the operating point is just above the undersaturation zone. Therefore crystallization at salt concentrations of 30–35% [w/v] and protein concentrations of 0.5–15 g/L would result in yields of nearly 100%. In the case of using sodium sulfate as precipitant, the advantage is the opportunity to control the crystal size. Choosing operating points above the metastable zone or seeding inside the zone will result in different crystal sizes. The more distant the

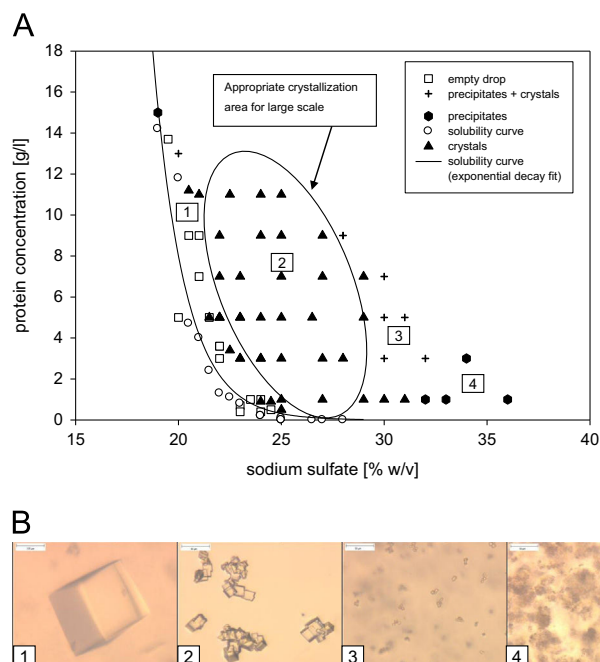


Fig. 3. (A) Phase diagram and solubility curve of rhINF- γ in 0.1 M ammonium acetate buffer pH 6.0 with sodium sulfate. The stable crystallization area is surrounded. (○) Solubility curve, (●) amorphous precipitate, (▲) crystals, (□) empty drops, (—) fitted solubility curve. (B) Microscopic images of crystals grown in different phases. From left to right: 1. metastable phase, 2. nucleation zone, 3. interphase between crystallization and precipitation zone, and 4. precipitation zone.

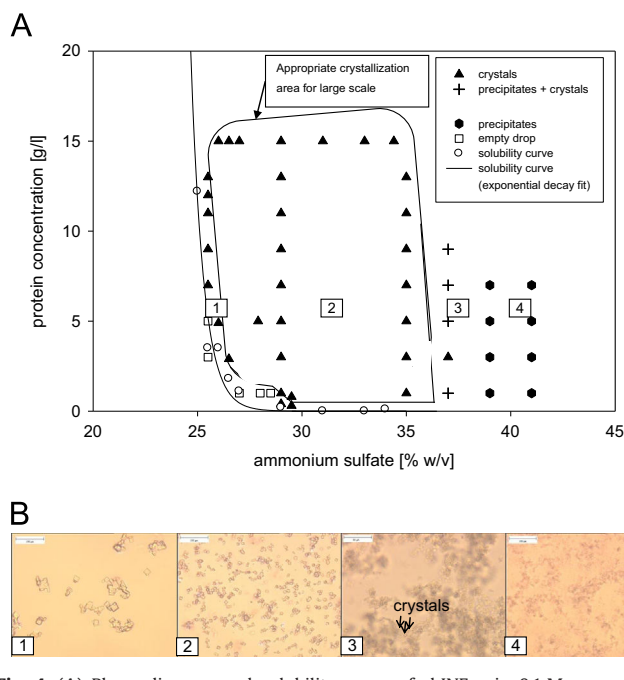


Fig. 4. (A) Phase diagram and solubility curve of rhINF- γ in 0.1 M ammonium acetate buffer pH 6.0 with ammonium sulfate. The stable crystallization area is surrounded. (\circ) Solubility curve, (\bullet) amorphous precipitate, (\blacktriangle) crystals, (\square) empty drops, ($-$) fitted solubility curve. (B) Microscopic images of crystals grown in different areas. From left to right: 1. at the beginning of the nucleation zone, 2. directly in the nucleation zone, 3. interphase between crystallization and precipitation zone, 4. precipitation zone.

operating point is from the metastable zone the higher the supersaturation and the smaller the crystal size will be (Mersmann et al., 2000). But operating points above the metastable zones also means that a part of the protein will stay soluble caused by the shallow progression of the solubility curve in this area, hence a crystallization yield of nearly 100% could only be reached for salt concentrations above 25% [w/v]. The crystal size will also decrease if the salt concentration or the protein concentration respectively is raised. The power of this effect depends on the type of salt. Figs. 3B and 4B show crystals grown at different salt concentrations.

Protein crystals grown in sodium sulfate (20.5% [w/v]) at an initial protein concentration of 11 g/L achieved sizes of 150 μm , whereas protein crystals grown at an initial protein concentration of 5 g/L and 22% [w/v] ammonium sulfate achieved only sizes of 20 μm . Further increase of the sodium sulfate concentration at the same protein concentration yielded in crystal sizes of 8 μm (25% [w/v]) and 5 μm (29% [w/v]). The crystallization yields changed with increased precipitant concentration from 57% (20.5% [w/v] sodium sulfate) to nearly 100% ($\geq 25\%$ [w/v] sodium sulfate). Crystals grown in ammonium sulfate (26% [w/v]) and an initial protein concentration of 5 g/L have achieved sizes of 20 μm . An increase of the ammonium sulfate concentration at the same initial protein concentration yielded in crystal sizes of 8 μm (30% [w/v]) and 5 μm (35% [w/v]). The belonging crystallization yields were 30% for an ammonium sulfate concentration of 26% [w/v] and nearly 100% for ammonium concentrations of or above 30% [w/v]. Tables 1 and 2 show the crystallization yields and related crystal sizes at different operating points for sodium sulfate and ammonium sulfate.

The use of ammonium sulfate has also the advantage of a lower dilution of the protein solution resulting in reduced buffer consumption and higher protein concentrations. Ammonium sulfate has a higher solubility compared with sodium sulfate and therefore a higher stock solution concentration can be generated (approximately 4 M ammonium sulfate versus 2.6 M sodium sulfate stock solutions).

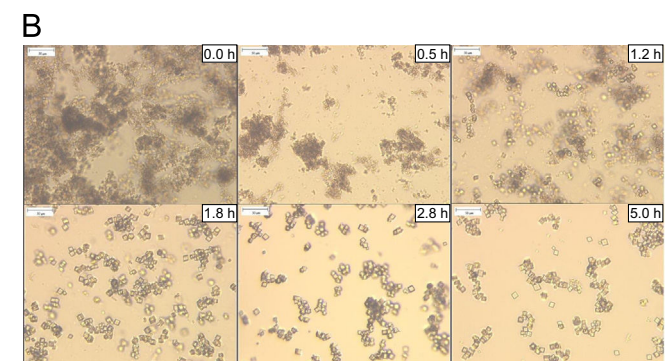
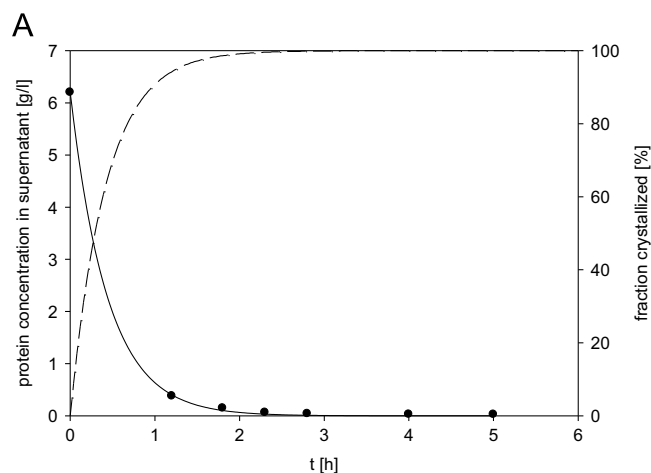


Fig. 5. (A) Devolution of the protein concentration in the liquid phase during bulk crystallization (\bullet), the data was fitted with an exponential decay ($-$) and the associated rhINF- γ crystallization isotherm based on the fitted function of the protein measurement (UV₂₈₀) in the liquid phase ($- -$). (B) Microscopic images of rhINF- γ crystals during the associated bulk crystallization in 0.1 M ammonium acetate buffer pH 6.0 and 25% [w/v] sodium sulfate as precipitant.

Table 1

List of operating points and the corresponding crystal sizes and yields for rhINF- γ with sodium sulfate as precipitant.

| Precipitant | Precipitant concentration [% w/v] | Protein concentration [mg/mL] | Crystal size [μm] | Crystallization yield [%] |
|----------------|-----------------------------------|-------------------------------|--------------------------------|---------------------------|
| Sodium sulfate | 20.5 | 11 | 150 | 57 |
| Sodium sulfate | 22.0 | 5 | 20 | 74 |
| Sodium sulfate | 25.0 | 5 | 8 | > 95 |
| Sodium sulfate | 29.0 | 5 | 5 | > 99 |

4.4. Scale up experiment

A scale up was carried out to proof the accuracy and the suitability of the created phase diagram with sodium sulfate for bulk crystallization. To provide nucleation and a high yield the operating point was chosen at a protein concentration of 6 mg/mL and a sodium sulfate concentration of 25% [w/v]. 25 mL protein stock solution of a concentration of 37 g/L was added to 125 mL sodium sulfate stock solution of a concentration of 30% [w/v] in a 200 mL glass beaker. The stirrer speed was 200 rpm. By adding the protein solution turbidity appeared immediately. A microscopic view directly after the addition detected the solid phase as cloudy precipitate. After 1 h less than 1 mg/mL remained in the liquid

Table 2
List of operating points and the corresponding crystal sizes and yields for rhINF- γ with ammonium sulfate as precipitant.

| Precipitant | Precipitant concentration [% w/v] | Protein concentration [mg/mL] | Crystal size [μm] | Crystallization yield [%] |
|------------------|-----------------------------------|-------------------------------|--------------------------------|---------------------------|
| Ammonium sulfate | 26.0 | 5 | 20 | 30 |
| Ammonium sulfate | 30.0 | 5 | 8 | > 99 |
| Ammonium sulfate | 35.0 | 5 | 5 | > 99 |

phase. Further samples taken over time showed a continued reduction of precipitate and an enhanced formation of crystals. After 1 h the first crystals could be clearly detected and after 5 h no more precipitate was observed and the solubility equilibrium was achieved. We assume that the process of crystallization was driven by a strong nucleation resulting in a microcrystalline precipitate, followed by a fast Ostwald ripening process resulting in single 3-dimensional crystals grown on the expense of the microcrystalline precipitate (Ostwald, 1900). At the start of the crystallization the supersaturation ratio was very high (theoretically ~ 200) and most of the protein nucleated as clusters of microcrystalline precipitates. These microcrystalline precipitates were of irregular shape with dense and less dense regions and their formation was kinetically favored compared with single 3-dimensional crystals. The microcrystalline precipitate had a high surface to volume ratio resulting in a high surface energy. This is thermodynamically unfavorable and molecules of the surface were tend to detach, especially since the high start supersaturation ratio was tenfold reduced after the formation of the microcrystalline precipitate. The dense structures of the microcrystalline precipitate had an advantage compared with the less dense regions since their surface to volume ratio was lower and as a result they attached more molecules at their surfaces as detached from their surface. If a critical size of such a microcrystalline particle is reached it will directly dissolve. Hence the less dense microcrystalline structures were dissolved and the dense structures had grown to the final single 3-dimensional crystals (Ng et al., 1996; Vetter et al., 2013).

The final average crystal size was 10 μm and the crystallization yield was 96%. Fig. 5A shows the decrease of the protein concentration in the liquid phase measured by UV₂₈₀. This curve was fitted by an exponential decay. In Fig. 5B the associated progression of crystal formation is depicted. After 5 h regular cubic crystals with uniform size are formed. The microscopic picture supports the assumption that the protein precipitate has been converted into crystals.

Fig. 6 shows the double-logarithmic plot of $-\ln[1-X_t]$ versus t for the crystallization of rhINF- γ at room temperature. The overall crystallization rate constant K and the Avrami exponent n can be derived from the intercept and the slope of the straight line (see Eq. (5)). The fraction crystallized as a function of time was calculated from the fitted data of residual protein in solution (Fig. 5A) using Eq. (4). Crystallization directly started after addition of sodium sulfate without any induction or lag phase, which is often detected in the crystallization of polymers (Chen et al., 2013; Dibildox-Alvarado and Toro-Vazquez, 1998). The half-time crystallization value, $\tau_{1/2}$, is 0.3 h and depicts the time when 50% of the protein is crystallized.

The overall crystallization rate constant (K) is $5.79 \pm 0.05 \times 10^{-2} \text{ min}^{-n}$ and the Avrami exponent is 1. The Avrami exponent reflects the details of nucleation and growth mechanism and the obtained value would suggest that nucleation takes place

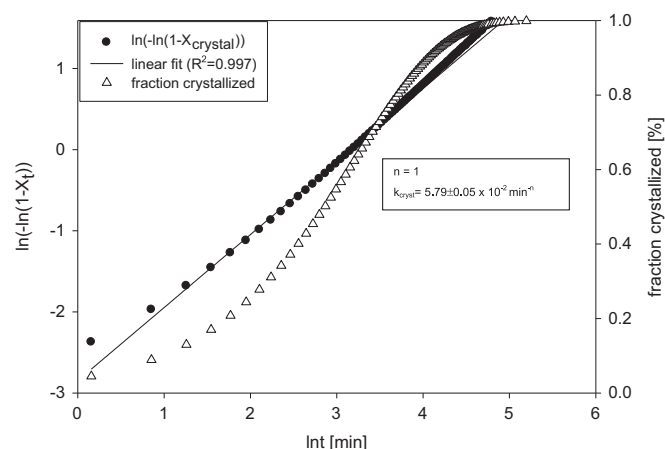


Fig. 6. Graphical determination of the overall crystal growth rate k_{cryst} and the Avrami exponent n . (●) Double-logarithmic plot of $-\ln[1-X_t]$, (Δ) crystallized fraction of rhINF- γ over the time, (–) straight line fit value ($R^2=0.997$).

instantaneous at the beginning of the crystallization process ($N=0$) with a 1-dimensional crystal growth ($C=1$). However, investigation of the crystallization process by microscopic view and protein measurement in the supernatant (Fig. 5) reveal that at the start of crystallization a lot of nuclei forms instantaneously, seen as a dark cloud of solid material, containing more than 90% of the protein. Subsequently these nuclei disappear and 3-dimensional crystals occur. The transformation of the solid material from precipitate to 3-dimensional crystals is not represented by the Avrami exponent since the calculation is based on the remaining protein amount in the supernatant during the crystallization. Changes in the solid phase are not considered. Due to the fact that more than 90% of the crystallizable material is crystallized immediately as nuclei the nucleation rate is the driving force (homogeneous) in the Avrami equation and growth can be neglected resulting in an Avrami exponent of 1 ($N=1$ and $C=0$). Here the modified overall crystallization rate (K') is equal to the overall crystallization rate of $5.79 \pm 0.05 \times 10^{-2} \text{ min}^{-1}$ at 25 °C since $n=1$ and is in the same magnitude of crystallization rates known from oils or fats at similar temperature (Chen et al., 2013; Dibildox-Alvarado and Toro-Vazquez, 1998). Determined crystallization growth rates of canavilin are in the range of $0.56\text{--}0.7 \times 10^{-3} \text{ min}^{-1}$ and for lysozyme in the range of $1.9 \times 10^{-3} \text{ min}^{-1}$ and are one order of magnitude slower (Baird et al., 2013; Carbone and Etzel, 2006). The crystallization kinetics strongly depends on parameters like supersaturation, temperature and the net charge of the protein (Schmit and Dill, 2012).

5. Conclusion

With the general equilibration and kinetic information it can be predicted if a precipitant is suitable for industrial bulk crystallization. The time, which is necessary to reach the solubility equilibrium, is as important as the remaining protein concentration in the liquid phase or the amount of precipitant required for nucleation. So the protein should have a low solubility (high yield), which could be reached fast (within 24 h) with the precipitant of choice. It could be shown that if the equilibrium between solid and soluble protein was quickly reached, also the formation of crystals could be seen within hours. But not only the solubility curve is essential for the decision to select a certain precipitant in a crystallization process, also the phase diagram is important. Small nucleation zones are critical in industrial scale because only a minimal change in buffer preparation can lead to precipitation

instead of crystallization. Appropriate precipitants yield phase diagrams with a broad nucleation range, high crystallization yields and moderate crystal sizes. The decision criteria to select appropriate precipitants for industrial crystallization of rhINF- γ were shown. Phase diagrams were established and compared regarding advantages and disadvantages. Two appropriate precipitants for bulk crystallization of rhINF- γ could be characterized. As last step, a scale up experiment was successfully carried out to proof the accuracy and the appropriation of phase diagrams for bulk crystallization.

References

- Aoun, M., Plasari, E., David, R., Villiermaux, J., 1999. A simultaneous determination of nucleation and growth rates from batch spontaneous precipitation. *Chem. Eng. Sci.* 54, 1161–1180.
- Avrami, M., 1939. Kinetics of phase change. I General theory. *J. Chem. Phys.* 7 (12), 1103–1112.
- Baird, J.K., McFeeters, R.L., Caraballo, K.G., 2013. Specific rate of protein crystallization determined by the Guggenheim method. *Int. J. Thermophys.* (Retrieved from).
- Basu, S.K., Govardhan, C.P., Jung, C.W., Margolin, A.L., 2004. Protein crystals for the delivery of biopharmaceuticals. *Expert Opin. Biol. Ther.* 4, 301–317.
- Carbone, M.N., Etzel, M.R., 2006. Seeded isothermal batch crystallization of lysozyme. *Biotechnol. Bioeng.* 93 (6), 1221–1224.
- Chakrabarti, P., 1993. Anion binding sites in protein structure. *J. Mol. Biol.* 234 (2), 463–482.
- Chen, F., Zhang, H., Sun, X., Wang, X., Xu, X., 2013. Effects of ultrasonic parameters on the crystallization behavior of palm oil. *J. Am. Oil Chem. Soc.* 90 (7), 941–949.
- Cheng, Y.C., Lobo, R.F., Sandler, S.I., Lenhoff, A.M., 2006. Kinetics and equilibria of lysozyme precipitation and crystallization in concentrated ammonium sulfate solutions. *Biotechnol. Bioeng.* 94 (1), 177–188.
- Collins, K.D., 2004. Ions from the Hofmeister series and osmolytes: effects on proteins. *Methods* 34, 300–311.
- Dibildox-Alvarado, E., Toro-Vazquez, J.F., 1998. Evaluation of tripalmitin crystallization in sesame oil through a modified Avrami equation. *J. Am. Oil Chem. Soc.* 75 (1), 73–76.
- Dijkmans, R., Billiau, A., 1988. Interferon γ : a master key in the immune system. *Curr. Opin. Immunol.* 1 (2), 269–274.
- Dixit, N.M., Kulkarni, A.M., Zukoski, C.F., 2001. Comparison of experimental estimates and model predictions of protein crystal nucleation rates. *Colloids Surf. A: Physicochem. Eng. Asp.* 190, 47–60.
- Fujiwara, M., Nagy, Z.K., Chew, J.W., Braatz, R.D., 2005. First-principles and direct design approaches for the control of pharmaceutical crystallization. *J. Process Control* 15, 493–504.
- Galkin, O., Vekilov, P.G., 1999. Direct determination of the nucleation rates of protein crystals. *J. Phys. Chem. B* 103 (49), 10965–10971.
- Hekmat, D., Hebel, D., Schmid, H., Weuster-Botz, D., 2007. Crystallization of lysozyme: from vapor diffusion experiments to batch crystallization in agitated ml-scale vessels. *Process Biochem.* 42 (12), 1649–1654.
- Hofmeister, F., 1888. Zur Lehre von der Wirkung der Salze. *Naunyn-Schmiedeberg's Archiv für Experimentelle Pathologie und Pharmakologie (Leipzig)* 24, 247–260.
- Jacobsen, C., Garside, J., Hoare, M., 1998. Nucleation and growth of microbial lipase crystals from clarified concentrated fermentation broth. *Biotechnol. Bioeng.* 57 (6), 666–675.
- Jacobsen, C., Hoare, M., Dunnill, P., 1997. Characterization of protein crystallization for process development and design. In: Shamlou, P.A. (Ed.), *The 1997 Jubilee Research Event: a Two-Day symposium held at the East Midlands conference centre, Nottingham, 8–9 April 1997. Rugby, Warwickshire [England]: Institution of Chemical Engineers. UK Institution of Chemical Engineers, Rugby, UK*, pp. 805–808.
- Joachimski, A., 2009. High-throughput crystallography for structural genomics. *Curr. Opin. Struct. Biol.* 19 (5), 573–584.
- Judge, R.A., Forsythe, E.L., Pusey, M.L., 1998. The effect of protein impurities on lysozyme crystal growth. *Biotechnol. Bioeng.* 59 (6), 776–785.
- Judge, R.A., Johns, M.R., White, E.T., 1995. Protein purification by bulk crystallization: the recovery of ovalbumin. *Biotechnol. Bioeng.* 48 (4), 316–323.
- Khanna, Y.P., Taylor, T.J., 1988. Comments and recommendations on the use of the Avrami equation for physico-chemical kinetics. *Polymer Eng. Sci.* 28 (16), 1042–1045.
- Kougoulos, E., Jones, A.G., Jennings, K.H., Wood-Kaczmar, M.W., 2005. Use of focused beam reflectance measurement (FBRM) and process video imaging (PVI) in a modified mixed suspension mixed product removal (MSMPR) cooling crystallizer. *J. Cryst. Growth* 273, 529–534.
- Krestov, G.A., 1991. *Thermodynamics of Solvation: Solution and Dissolution, Ions and Solvents, Structure and Energetics*. Ellis Horwood Ltd., New York, US.
- Landar, A., Curry, B., Parker, M.H., DiGiacomo, R., Indelicato, S.R., Nagabhushan, T.L., Rizzi, G., Walter, M.R., 2000. Design, characterization, and structure of a biologically active single-chain mutant of human rhINF- γ . *J. Mol. Biol.* 299 (1), 169–179.
- Lee, T.S., Vaghjani, J.D., Lye, G.L., Turner, M.K., 2000. A systematic approach to the large-scale production of protein crystals. *Enzyme Microb. Technol.* 26 (8), 582–592.
- Leyssens, T., Baudry, C., Escudero Hernandez, M.L., 2011. Optimization of a crystallization by online FBRM analysis of needle-shaped crystals. *Org. Process Res. Dev.* 15 (2), 413–426.
- Lindenberg, C., Krättli, M., Cornel, J., Mazotti, M., 2009. Design and optimization of a combined cooling/antisolvent crystallization process. *Cryst. Growth Des.* 9 (2), 1124–1136.
- Lindenberg, C., Mazotti, M., 2009. Effect of temperature on the nucleation kinetics of L-glutamic acid. *J. Cryst. Growth* 311, 1178–1184.
- Lorber, B., Skouri, M., Munch, J.P., Giegé, R., 1993. The influence of impurities on protein crystallization; the case of lysozyme. *J. Cryst. Growth* 128 (1), 1203–1211.
- Mersmann, A., Heyer, C., Schubert, H., 2000. How to influence the median crystal size of precipitates. In: Sen Gupta, B., Ibrahim, S. (Eds.), *Mixing and Crystallization*. Kluwer Academic Publishers, Dordrecht, Netherlands, pp. 243–255.
- Moretti, J.J., Sandler, S.I., Lenhoff, A.M., 2000. Phase equilibria in the lysozyme–ammonium sulfate–water system. *Biotechnol. Bioeng.* 70 (5), 498–506.
- Mueller, M., Jenni, S., Ban, N., 2007. Strategies for crystallization and structure determination of very large macromolecular assemblies. *Curr. Opin. Struct. Biol.* 17, 572–579.
- Nagy, Z.K., 2009. Model based robust control approach for batch crystallization product design. *Comput. Chem. Eng.* 33 (10), 1685–1691.
- Nagy, Z.K., Braatz, R.D., 2012. Advances and new directions in crystallization control. *Annu. Rev. Chem. Biomol. Eng.* 3, 55–75.
- Nagy, Z.K., Chew, J.W., Fujiwara, M., Braatz, R.D., 2008. Comparative performance of concentration and temperature. *J. Process Control* 18, 399–407.
- Ng, J.D., Lorber, B., Witz, J., Theobald-Dietrich, A., Kern, D., Giegé, R., 1996. The crystallization of biological macromolecules from precipitates: evidence for Ostwald ripening. *J. Cryst. Growth* 168 (1–4), 50–62.
- Ostwald, W., 1900. Über die vermeintliche Isomerie des roten und gelben Quecksilberoxyds und die Oberflächenspannung fester Körper. *Z. Phys. Chem.* 34, 495–503.
- Peters, J., Minuth, T., Schröder, W., 2005. Implementation of a crystallization step into the purification process of a recombinant protein. *Protein Expr. Purif.* 39 (1), 43–53.
- Przybycien, T.M., 1998. Protein–protein interactions as a means of purification. *Curr. Opin. Biotechnol.* 9 (2), 164–170.
- Przybycien, T.M., Pujar, N.S., Steele, L.M., 2004. Alternative bioseparation operations: life beyond packed-bed chromatography. *Curr. Opin. Biotechnol.* 15 (5), 469–478.
- Retailleau, P., Ries-Kautt, M.M., Ducruix, A.F., 1997. No salting-in of lysozyme chloride observed at low ionic strength over a large range of pH. *Biophys. J.* 73, 2156–2163.
- Ries-Kautt, M.M., Ducruix, A.F., 1997. Inferences drawn from physicochemical studies of crystallogenesis and precrystalline state. *Methods Enzymol.* 276, 23–59.
- Ries-Kautt, M.M., Ducruix, A.F., 1989. Relative effectiveness of various ions on the solubility and crystal growth of lysozyme. *J. Biol. Chem.* 264 (2), 745–748.
- Robinson Jr., J.B., Strottmann, J.M., Stellwagen, E., 1981. Prediction of neutral salt elution profiles for affinity chromatography. *Proc. Natl. Acad. Sci.* 78, 2287–2291.
- Schlichtkrull, J., 1956. Insulin crystals. II. Shape of rhomboidal zinc-insulin crystals in relation to species and crystallization media. *Acta Chem. Scand.* 10, 1459–1464.
- Schmidt, S., Havekost, D., Kaiser, K., Kauling, J., Henzler, H.J., 2004. Kristallisation für die Aufarbeitung von Proteinen. *Chem. Ing. Tech.* 76 (6), 819–822.
- Schmit, J.D., Dill, K., 2012. Growth rates of protein crystals. *J. Am. Chem. Soc.* 134 (9), 3934–3937.
- Shi, D., Mhaskar, P., El-Farra, N., Christofides, P.D., 2005. Predictive control of size distribution in protein crystallization. *Nanotechnology* 16, 562–574.
- Takakura, T., Ito, T., Yagi, S., Notsu, Y., Itakura, T., Nakamura, T., Inagaki, K., Esaki, N., Hoffman, R.M., Takimoto, A., 2006. High-level expression and bulk crystallization of recombinant L-methionin γ -lyase, an anticancer agent. *Appl. Microbiol. Biotechnol.* 70 (2), 183–192.
- Talreja, S., Perry, S.L., Guha, S., Bhamidi, V., Zukoski, C.F., Kenis, P.J.A., 2010. Determination of the phase diagram for soluble and membrane proteins. *J. Phys. Chem. B* 114 (13), 4432–4441.
- Tam, S.K., Chan, H.C., Ng, K.M., 2011. Design of protein crystallization processes guided by phase diagrams. *Ind. Eng. Chem. Res.* 50 (13), 8163–8175.
- Vetter, T., Iggland, M., Ochsnein, D.R., Häseler, F.S., Mazotti, M., 2013. Modelling nucleation, growth, and Ostwald ripening in crystallization processes: a comparison between population balance and kinetic rate equation. *Cryst. Growth Des.* 13 (11), 4890–4905.
- Watanabe, E.O., Popova, E., Miranda, E.A., Maurer, G., Pessôa Filho, P., de, A., 2009. Phase equilibria for salt-induced lysozyme precipitation: effect of salt type and temperature. *Fluid Phase Equilib.* 281 (1), 32–39.
- Yang, Z., 2009. Hofmeister Effects: an explanation for the impact of ionic liquids on biocatalysis. *J. Biotechnol.* 144 (1), 12–22.